THE BOUNDARY-LAYER FLOW-FIELD REGIME OVER NAIROBI

BY

FRANKLIN J. OPIJAH

A thesis submitted in part fulfilment for the degree of master of science in Meteorology at the University of Nairobi

January, 1992

This thesis is my original work and has not been presented for a degree in any other university

_____   20/1/93

F. J. Opijah

This thesis has been submitted for examination with the approval of university supervisors:

_____ 21/1/93

Prof. John K. Ng'ang'a

_____ 22/1/1993

Prof. Andrew E. Okeyo

Department of Meteorology,

University of Nairobi,

P. O. Box 30197,

NAIROBI, KENYA.

" *The wind blows to the south*

    and turns to the north;

round and round it goes,

    ever returning on its course"

" *And when the south wind blows,*

    you say, 'it's going to be hot,'

      and it is"

        (Eccl. 1.6; St. Luke 12.55; NIV)

On interpreting the signs of the times

To my parents who have often encouraged me
to work with dedication and diligence,
to revere God always,
and to live in harmony with my fellow man

Table of Contents

List of Figures

List of Tables

List Of Acronyms

AMSL = Above Mean Sea Level

EAST = East African Standard Time

LT. = Local Time

PBL = Planetary Boundary Layer

RH = Relative Humidity

SBL = Surface Boundary Layer

List of Symbols

A: Surface albedo

C: Constant of Proportionality in nocturnal boundary
      layer depth computation

 Cp: Specific heat capacity at constant pressure
     (=1004J/kg/K)

c_1, c_2 : Empirical constants in daytime boundary layer model
         (Respectively, 0.2 and 5.0)

C_s: Soil volumetric thermal capacity (MJ/m^3K)

e, e_s: Vapour pressure; saturation vapour pressure (mb)

f: Coriolis parameter $(\cong 3.81 \times 10^{-6}s^{-1})$

g: gravitational acceleration $(= 9.81ms^{-2})$

H: Boundary layer thickness (m) at grid point

h,ha: terrain height (AMSL) at grid point;
          referance point

ijk: Cartesian co-ordinate system unit vectors; grid point

k: Slope factor; station

K_{HS}: Thermal diffusivity of soil (m^2s^{-1})

L: Monin-Obukhov Scale length (m)

L_N: Net long wave radiation (Wm^{-2})

L_v Latent heat of vapourization $(= 2.296 \times 10^6J/kg)$

p, P_0: pressure; standard pressure (1000mb)

Q_E : Moisture Heat Flux (Wm^{-2})

Q_g: Ground Heat Flux (Wm^{-2})

Q_H: Sensible Heat .Flux (Wm^{-2})

R_d: Dry gas specific constant (= 287.1 J/kg/K)

R_N: Net radiation (Wm^{-2})

RH:Relative humidity (%)

S_g: Global radiation (W/m^2)

S_N: Net solar radiation (W/m^2)

t: time

T_a: Air Temperature at screen height (K)

T: Absolute temperature (K)

T_s: Soil temperature (K)

T_*: Turbulent temperature scale (0.08K)

U_*: Friction wind velocity (m/s)

u, v, w: component velocities

U,V:Wind velocity vector

W_k:Weighting function for station k

X,X_i: Variable; i^{th} variable

X_{ijk}: Variable at grid point

x,y,z: Cartesian co-ordinates

z_a: Anemometer height (10m)

z_o: Surface roughness length over land (m)

Γ_d: Dry adiabatic lapse rate (9.8K/km)

γ :Gradient of air temperature above the inversion layer (K/km)

Δ: Finite differencing

Δt: time step (s)

ε_a; ε_s: Atmosphere and sky emissivity; surface emissivity

Θ: Potential temperature (K); Direction of wind (degrees)

$\overline{(\Theta w)}_o$ surface kinematic heat flux (m/s)

$\varkappa$: Ratio of dry gas constant to specific heat capacity

at constant pressure (0.286);

Von Karman Constant (0.41)

λ: Thermal Conduction in soils (W/mK)

π: =3.14159

ρ_a: Air Density (1.21 kgm^{-3})

σ: Stefan-Boltzmann's constant (5.74 $\times$ 10^{-8} W/m^{2}K^4)

τ: Stress function

ϕ: Inversion Strength above the Mixed Layer (K/km)

Ω: Earth's rotation frequency (7.292 $\times$ 10^{-5}s^{-1})

Abstract

Logarithmic wind profile equations account for the aerodynamics within the lower atmosphere. This paper employs logarithmic equations in various forms while incorporating changes in atmospheric stability to simulate the spatial and temporal structure of both the planetary boundary layer depth and the field of flow within it. Turbulent fluxes of sensible heat and momentum as a result of the impact of the synoptic flow on the frictionally active surface are assumed to be the only means of modifying the mixing heights. Cumulus convection, moisture flux, and the associated effects of latent heat change are ignored. As a case study, the procedure is designed to investigate diurnal/nocturnal and seasonal changes by modelling using monthly time averages over a year's period, 1986, in Nairobi. To this end, a three-dimensional simple Eulerian model is attained in the analyses.

Results show a reasonable resemblance between the nocturnal-diurnal and seasonal cycles of the computed mixing heights and the observed surface weather parameters, particularly wind speed and insolation. Seasonal variations were noticed for the estimated mixing heights during daytime only. The inversion strengths of 12 ± 7 were comparable with those at the sinking arm of the Hadley cell of the general circulation. The inversion strengths however vary seasonally with the highest values in the period from June to August, and the lowest in the rainy months of April and October. The elevated inversions, though, are not responsible in determining the model depths of the planetary

boundary layer owing to the lofty heights at which they occur. The inversions are substantially influenced by the upper level trade wind regime in addition to surface processes. Low ground heat storage, being just 10% to 0.5% of the global radiation, is due to the nature of the soil within the region. Horizontal and vertical variations in the wind field seem to be a consequence of the influence of the large forests, altered surface fabric, urbanisation and terrain undulations as they alter the synoptic flow.

Chapter One

1.0 **Introduction**

The need to understand processes within the lowest atmosphere
is enhanced when the region under consideration is a fast
growing urban area with a rapid rate of population growth.
Many disciplines apply principles derived from atmospheric
dynamics in, and the depth of, the lowest layer of the
atmosphere under direct influence of the underlying surface.
This region, referred to variously as the planetary or
atmospheric boundary layer, or mixing layer, is the zone
within which the surface eddy fluxes of momentum, sensible
heat and moisture are significant (for example, Pasquill and
Smith, 1983). The potential of pollution transport/diffusion
and wind energy generation is mainly governed by wind field
characteristics within the boundary layer -the flow course
and strength between the ground surface and the top of the
boundary layer.

In recent times, emphasis in studies on atmospheric
circulation has been placed on the influence of local
features whose impact on small-scale circulation patterns is
quite important especially in the tropics (see for instance,
Ramsey, 1966; Sherman, 1978). The flow is affected, not only
by the sun's differential insolation and the resulting
difference in pressure patterns (Oke 1987), but also by the
changing atmospheric stability, terrain elevations,
vegetation, urbanisation and hydrological features (Sutton,
1953; Lettau, 1969; Harris, 1979; Fujita and Wakimoto, 1982;
Pielke, 1984). Further, a thorough knowledge of temporal and

spatial patterns of the boundary layer thickness, which is man's zone of activity (Brown, 1974), is imperative in improving modelling processes within the boundary layer.

1.1 **Statement of the Problem**

Planetary boundary layer depth variations in both space and time depend upon changes in the dynamical parameters and the physical features at the surface. The boundary layer may either be stationary or disturbed. Whereas stationary boundary layers are dominated by the trade wind regime, disturbed boundary layers respond rapidly to large scale forcing (Abu Bakr, 1988). The height of the layer is usually marked by a capping inversion which curtails upward motion (Tennekes, 1973), though sometimes no clearly marked top exists. External synoptic fields may contribute to the formation of the capping inversion - for instance, the pattern of the upper level trade wind regime, or large scale subsidence (Oke, 1987). However, the presence of convective clouds and convergence zones may interfere with the depth of the boundary layer so that the "buffer-effect" is reduced and upward propagation of fluxes proceeds to higher levels (Pasquill and Smith, 1983). Such a boundary layer then ceases to be stationary. The same effect results from the presence of very high and rough orographic features, urban heat islands, and as occurs outside the tropics, frontal convergence (Pasquill and Smith, 1983). In stationary boundary layers, the presence of low level cloud cover reduces sensible heat flux at the surface and suppresses the depth of the boundary layer (Oke, 1987).

As contrasted to boundary layer models in laboratories,

the planetary boundary layer is influenced by the rotation of the earth (Zilitinkevich, 1972). Usually, the mixing layer height is generated by the evolving growth as fluxes are exchanged between lower and upper levels in the layer resulting from the encounter of the atmospheric flow with a rough and rigid surface characterised by topographic, hydrological and anthropogenic features; occasionally radiative, condensational and evaporative processes modify the thermal structure within the layer, and consequently its depth (Harris, 1979). Free and forced convection then play a part in the development of the layer. Thermal mixing during the day increases from morning according to the daytime cycle of sensible heat flux and wind speed (Oke, 1973). The mixing intensifies thereby raising the mixing height whose growth rate is highest in the late morning hours. On the other hand, decreasing sensible heat flux at the surface leads to a decrease in the nocturnal planetary boundary layer depth to a minimum in the morning; forced convection in the turbulent layer transfers the quantities from low to higher levels (Oke, 1987). Buoyancy is ignored in the development of neutral boundary layers, with turbulent energy used in the boundary layer growth obtained from instabilities within the surface layer and the wind direction shear in the Ekman layer (Pasquill and Smith, 1983).

Coupling between the surface and the rest of the boundary layer as turbulent air below meets undisturbed air above, varies diurnally - being more effective during the day than night - and causes the commonly observed diurnal cycle of wind speed (Oke, 1987). The coupling follows the surface heat budget pattern whereby the wind speed at the surface increases to a maximum in the late afternoon - when the

faster moving air above transports momentum downwards more easily - before dropping after sunset. At this time, the growth of the surface based inversion cuts off the heat supply from the surface and subsequently the depth of the mixing height in a relaxation process (Oke, 1987 and Deardoff, 1972). Just after sunset, the effect of convective mixing is suppressed and the nighttime height of the planetary boundary layer is determined by the surface friction, geostrophic wind and radiational cooling during the night (Garrat, 1982). In effect, the general daily cycle of the wind speed is similar to that of the depth of the planetary boundary layer, though not identical. The same pattern is noticeable in the seasonal cycle of the wind speed and mixing heights. Wind direction follows the position of the sun both diurnally and seasonally.

Small-scale regions, in the absence of surface roughness elements, could be expected to have more or less uniform flow in space, both in magnitude and direction. This is however altered by the existing roughness features in such a way that the measured surface wind field reflects local, and not necessarily synoptic, conditions. Urbanisation has been known to induce heat island effects which alter the flow field for areas in proximity to it (Vukovich et al, 1976; Okoola, 1980; Hjemfelt, 1982). It is generally accepted that heat islands create low pressure zones which by consensus alter the flow direction such that it is towards the heat island. Moreover, the arrangement of buildings within a city favours channelling and canyon effects (Oke, 1987), complicating the situation further.

Terrain modifies the flow both laterally and vertically.

Orographic barriers deviate the flow, causing the originally
straight flow to meander around the obstacle and overflow it
(Sherman, 1978). This pattern is not just confined to the
position of the barrier but extends to regions far away both
horizontally and vertically, the extent of which is dependent
on the strength of the initial flow and the size of the
barrier (Long, 1952; Kasahara, 1966). In the vertical, the
effect extends in decreasing magnitude up to the top of the
planetary boundary layer (Endlich et al,1982). These is also
observed for valleys and escarpments where drainage flow is
experienced. Another of the most pronounced surface effects
on horizontal flow arises from the presence of dense
vegetation cover (Oke, 1973; Abu Bakr, 1988). The net effect
is a decrease in the wind speed from the frictional shielding
of the trees, which is reflected in the flow above the
vegetation within the surface boundary layer for all
stability conditions. All surface roughness elements cause a
friction drag on the flow, altering its cause and decreasing
its strength.

1.2 **The Objective**

The major purpose of this work is to simulate the flow field
within the planetary boundary layer by utilising a minimum
number of stations. With mainly surface observatories and a
limited number of upper air data stations, numerical analyses
are performed basing on the expected dynamical behaviour of
the wind field within the boundary layer. As a case study
that utilises only a year's data, the model algorithm is
designed to investigate short term changes within the
climatologically observed variations over a small scale

region - Nairobi and its neighbourhood.

The aims and objectives of this Study will therefore be divided into three parts as follows:

1. Analysis of the surface wind-field regime within the region thereby determining the mean temporal pattern of the flow.

2. Simulation of the depth of the planetary boundary layer over the area so as to give its diurnal and seasonal patterns, and the spatial structure.

3. Extension of the surface observations of the wind field into three dimensions using an objective approach to investigate the spatial regime: the depth of the mixing layer marking the upper limit of the rectangular block.

It is to be expected that studies which use the actual observed data give a more realistic situation in modelling than would be the case where purely predicted values were used.

1.3 **Aspects of Practical Application of Study**

The depth of the planetary boundary layer and the flow within it have many applications in day to day life. Primarily, being the region within which vertical mixing is mainly confined (Harris, 1979), the boundary layer depth relates to pollution concentration in an area and the impact on air quality associated with it. A shallow depth implies that most pollutants are confined to very low levels close to the surface with the imminent danger on life and materials due to poor vertical mixing. If at the same time the wind speeds are pretty low, pollution episodes may result (Gord, 1956). Poor vertical propagation, though, limits the chances of

precipitation scavenging and cases of acid rain (Junge, 1963). The converse is true for a large depth of the boundary layer. Wind speeds increase the rate of removal of pollutants from an area, subsequently decreasing concentration levels. At the same time, strong winds quickly diffuse or transport pollutants to new areas. Very strong winds rapidly transfer pollutants to regions at long distances remote from their sources. Slow moving to stationary winds conversely minimises the transportation or diffusion of pollutants. The direction of flow determines the direction of transport.

As they are natural processes, the flow field and mixing heights are not easily controlled by artificial methods. A knowledge of their characteristics can however be helpful in reducing air pollution in many ways. For instance, industries that emit toxic chemicals can be restricted to operate only within the period that results in minimal surface concentrations - periods with the best vertical atmospheric overturning and diffusive dilution. Alternatively, such industries can ,in the initial planning, be placed in areas where harmful emissions are not likely to infiltrate residential areas. This would best be located on the lee-ward side of inhabited regions. Nevertheless, wind direction varies diurnally in continuous fashion. By knowing the direction that accounts for the strongest flow, the region likely to be most adversely affected is identified. Secondly, knowledge of the mixing heights and their diurnal variation would suggest optimal heights of factory chimneys which if located in the surface boundary layer - a fraction of the planetary boundary layer - would lead to high concentrations at the surface (Pasquill and Smith, 1983).

A second area in which boundary layer flow modelling is

of profound importance is in the study of wind power. The potential for energy generation is determined by considering the wind strength within an area (Ludwig and Byrd, 1980; Oludhe, 1987). Due to lack of data at potential sites of wind power generation, data used is obtained from established meteorological observatories. Such stations are placed in particular areas for definite applications, for example in airports for aviation and at agricultural research institutes for agricultural purposes. Usually such areas are located far from potential sites of wind turbines. Since it would be expensive to place instrumented towers at every potential wind power site for a period of as long as one year or more, stations that are already in operation can be used to estimate the history of winds at any site (Endlich, 1982). The boundary layer depth which determines many wind characteristics at the surface is important in such analyses, as the vertical structure of the wind field is necessary for the purpose of determining the height at which wind turbines are to be located.

Planetary boundary layer modelling and the inherent wind field within it find applications in weather prediction using numerical techniques. Surface friction and heat flux may be of little importance when considering short-range prediction of synoptic scale disturbances, but become important when longer scales are considered, or when improved accuracy is desired in short-range forecasting (Haltiner and Williams, 1980). Bulk parameterisation of fluxes within the surface layer is done using measurements at only a single height which is then used to define the entire boundary layer processes (Paulson, 1970).

Certainly, flow in the boundary layer is important in the fields of architecture, general comfort and many other disciplines. This study provides a greater insight into the wind field structure in the boundary layer over Nairobi which can be useful for practical applications as mentioned above.

1.4 **Literature Review**

Although accurate solutions of the wind field could be computed using classical formulae such as the Navier-Stokes equations, numerical solutions of the full equations is not feasible, prompting the use of simpler objective analyses which minimise computational costs.

Sherman (1978), in attempting to include the effects of terrain on the field of flow for use in pollution models, devised a procedure for constructing three dimensional mass-consistent wind fields, a method based on variational calculus. The method involves the solution of the Lagrange multiplier. The multiplier, weighted at grid points using three-point first forward (or backward) finite differences with regard to the location of topographic barriers, was calculated from a system of linear equations for each grid point, applying the equation of mass continuity to minimise divergence. The entire system was solved simultaneously using successive over relaxation. A difference form of the weighted Lagrange multiplier was then added to a mean wind field obtained from a spatially sparse wind field data set interpolated and extrapolated at grid points in a Eulerian model volume. Ludwig and Byrd (1980) applied the same argument, with the mass-conservative flow field obtained using eigenvectors of a covariance matrix. The approach by Sherman (1978) was extended by Goodin et al (1980) to include

varying grid spacing in the vertical direction and time-variations in the depth of the boundary layer with a divergence reduction algorithm. Endlich et al (1982), by the stringent condition of mass-consistency and by imposing the condition of minimising the difference between the observed and adjusted values proposed by Sherman, further modified the methodology thereby using second degree partial derivatives computed by relaxation with the inclusion of the effects of terrain. This was achieved with the use of a terrain following sigma co-ordinate system based on the general variation of the mixing layer height with terrain proposed by Bhumralker et al (1980).

Values of the Lagrange multiplier are most significant in areas where the vertical topographic scale is comparable to the horizontal scale, but vanishes for regions that have more or less uniform terrain. The effects of terrain may be reflected at regions remote from topographic barriers (Bhumralker, 1980). In this regard, the spatially sparse interpolated horizontal flow field may be assumed to adequately represent the actual situation (Sherman, 1978). Whereas the horizontal components of velocity can be obtained by resolving the wind field into zonal and meridional flow (for example, Kavishe, 1983), vertical velocity is usually not a routinely measured quantity. In regions of significant terrain variations laterally, the vertical velocity at the surface can be computed from a form of a wind advection equation of the horizontal field (Haltiner and Williams, 1980). In any case, the surface vertical velocity is usually small and may be taken as zero, for practical purposes.

Before objective analyses can be performed on

meteorological data, spatially sparse fields must be interpolated onto a mesh. The pattern of the three dimensional flow field is then obtained which is essential in many disciplines. Various interpolation/extrapolation methods have been postulated. The best method - the Optimum interpolation technique (Gandin, 1965) produces an interpolated field from data points irregularly spaced in both space and time. The method however requires a time history of the data, assuming that a persistency of past characteristics carries on into the future. The method is most appropriate for interpolating synoptic-scale data, but fails for smaller scales where day to day variations may be important.

A continuous field at the surface may also be obtained over a grid mesh by the Least-Squares Polynomial approach. The method involves minimising the chi-squared goodness of fit data using n-degree polynomials. Panofsky (1949) used third-degree polynomials to fit fields of wind and pressure over a whole grid. Alternatively, Thiessen´s (1911) approach of defining polygons so that interpolations are done for areas with the influence of individual stations rather than for the whole region, has been used to ease computations (for example, Green and Sibson, 1978). Although the method provides a smooth field, it consumes much computation time and calls for simpler techniques.

Weighted Average interpolation methods have been used by various authors with varied modifications. The weighting factor has previously been based, among other methods, on the radius of influence (for example, Cressman, 1959), least squares fitting (Endlich and Mancuso,1968) and direction of flow (for example, Shepard, 1968). Goodin et al (1979) found

a fair compromise between the second degree polynomial fitting procedure and the inverse square distance (r^{-2}) weighting scheme in regard to computational costs and accuracy. Inverse distance (r^{-1}) weighting is appropriate for vertical interpolations since the measured data is hardly very accurate (Goodin et al, 1980).

Vertical wind shears follow certain specified patterns within the surface layer depending on the stability of the atmosphere. Such representations include formulae such as the power law, Deacon's profile, and logarithmic wind profiles (Sutton, 1953; Brown, 1974;Pasquill,1974; among others). The power law has been used in extrapolating the measured surface winds vertically in the layer in studies involving meso-scale flows, and lesser scales (for example, Nappo,1977; Sherman,1978; Oludhe, 1987). Nappo (1977) used in addition the logarithmic wind profile with the delicate assumption of application throughout the planetary boundary layer.

The power law exponent has been previously determined from atmospheric stability conditions (Pendergast, 1976). Where unknown, a value of 1/7 (appropriate for neutral conditions) is usually used. The atmosphere is hardly ever neutral as buoyancy is usually present even in minute quantities (see Pasquill and Smith, 1983). The exponent may be determined from a least squares fit of multiple level data (Sherman, 1978), a procedure that requires sufficient wind-measurement levels in the vertical not commonly encountered in routine observatories. Within the surface layer, buoyancy effects have been included in the logarithmic wind shear by arguments of Monin and Obukhov, an idea that has greatly improved analyses for conditions that are not necessarily under neutral stratification.

The surface boundary layer, being a zone within which the vertical stresses are nearly constant, implies that the turning of the wind with height is negligible. (Pasquill and Smith, 1983). In regions of complex topography, the turning of the winds with height is appreciable. Using measured data, Nappo (1977) determined the angular deviation of the wind direction with height for different stability conditions and found the greatest deviation in stable conditions, lesser in transition cases and least in unstable periods. The respective deviations were 79, 67 and 20 degrees for complex terrain. The turning over flat terrain was smaller for stable and transition periods but negligible for unstable conditions. Nappo's (1977) results indicate a similarity between flow over complex terrain and a flat urban area.

To facilitate changing direction in the vertical, Endlich et al (1982) devised a logarithmic interpolation procedure that treats the vertical variations of the zonal and meridional components of the wind separately, using measured surface parameters and those at the top of the mixing layer. Although the approach gives the greatest weighting in the lowest levels, the equation as used throughout the boundary layer fails to account for the interacting processes of buoyancy and mechanical forces in the surface layer where they are most pronounced. Experiments done indicate that except for solid barriers, the surface layer wind direction as measured at the anemometer level is nearly constant throughout the surface layer (Pasquill and Smith, 1983; Oke, 1987).

Outside the tropics where the Coriolis force is of comparable magnitude with the pressure gradient force, winds

at the top of the boundary layer may be estimated by applying Ekman-layer equations while assuming the applicability of the geostrophic approximation (Holton, 1979). With the geostrophic wind as the upper limit, Endlich et al (1982) have interpolated the wind field in the mixed layer using anemometer level winds as the lower level values. Measured values interpolated vertically to grid levels have been used by Goodin et al (1980). For regions in close proximity with the equator, not only is the geostrophic approximation invalid (Holton,1979), but there is a scarcity of multiple tower measurements. The vertical structure is mainly available at radiosonde stations, most of which have upto two soundings in a twenty-four hour period. In such cases, Sherman (1978) suggested a methodology where interpolation is done linearly from the the top of the surface layer, with the upper boundary´s horizontal wind speed and direction taken from a synoptic analysis.

Pasquill (1974) has classified atmospheric stability into eight categories ranging from extreme instability through neutral stability, to extreme stability. These conditions change with time throughout the day, from day to day, and seasonally depending on the amount of solar radiation input at the surface and the nature of the surface receiving the insolation. Extreme instability is characteristic of low wind speeds (less than 2.5ms^{-1}) and maximum insolation. Extreme stability on the other hand occurs for wind speeds of the order of 1m/s with no surface heating and an inverted temperature profile. Neutral conditions occur for sufficiently high wind speeds (in excess of 12m/s) and no buoyancy effects (Pasquill and Smith, 1983).

To minimise the error commonly introduced by assuming neutral conditions, various authors have divided the day and night according to times derived from the above parameters. Nappo (1977), for instance, divided the stabilities such that 1000-1600 local time (LT) represented unstable conditions, an interval that varied from day to day depending on the cloudiness. 1600-2100 LT and 2400-1000 LT represented transition and stable periods respectively. In boundary layer modelling, Abu Bakr (1988) used the sunrise and sunset times as transition periods, with the daytime and nighttime representing unstable and stable conditions respectively.

The depth of the entire planetary boundary layer consisting of different distinct zones characterised by their respective type of transfer processes has been found to fall in the night to a few kilometres in the morning (Haltiner and Williams, 1980) as dictated by changes in meteorological parameters. These variations are also noticeable seasonally throughout the year. The surface boundary layer, a region that greatly determines the depth of the entire planetary boundary layer, is usually taken as a fraction of one-tenth to one-twentieth of mechanical and unstable planetary boundary layer depths, and smaller for stable boundary layers (Harris, 1979; Okeyo,1987). Typically, the depth of the surface layer ranges from 10 to 30m, and may be as high as 100m, or more, in mountainous regions (Brown, 1974; Sherman, 1978).

The vertical extent of the mixing layer depends on the strength of stresses at the surface, but may be capped by an upper level inversion which then acts as a buffer zone to vertical fluxes (Oke, 1987; Pasquill and Smith, 1983). The depth has been found to be greater when breakdown processes

occur due to the presence of features such as synoptic disturbances (for example, frontal convergence zones), mountain ranges and convective clouds. Elevated inversions are thought to be influenced by upper level large scale subsidence such as results from the sinking arm of the Hadley circulation (Abu Bakr, 1988), or from subsidence warming of the trade wind regime.

Many prognostic models have been developed which incorporate the strength of elevated inversions (for example, Deardoff 1972; Tennekes 1973; Carson 1973; and Van Dop et al 1982). These models apply the idea of turbulence in the lower levels that results in upward transport of eddies before they are halted by elevated inversions. Other models account for the effects of cloud cover (for example, Deardoff, 1976). Diagnostic models specifically for computing stable boundary layer depths have been postulated using surface friction velocity and the coriolis parameter (Zilitinkevich, 1972; Caughey et al, 1979; Harris, 1979; Venkatram, 1980). These models make use of empirical constants that can change if the location of design is dissimilar to the area of application. For neutrally stratified atmospheres, other models exist (Harris,1979; Pasquill and Smith, 1983).

Estimations can be made for the depth of the Planetary boundary layer (PBL) testing the consistency of modelled depths. Wind maxima heights have been used by Clarke (1970) and Nappo (1977) to estimate the depth of the PBL. For nighttime conditions, the mixing height has been shown to be less than the height of the wind maxima by about 20% (Beyrich and Klose, 1988). Patnaik et al (1980) using mean maximum climatic surface temperature and vertical profiles of

temperature and wind speed in Te-Phi gram plots have estimated maximum mixing heights for use in studies on atmospheric pollution transport potentials over Africa on a monthly basis. Estimates for daytime mixing heights can also be derived from the heights of elevated temperature inversions and relative humidity profiles (Deardoff, 1972).

Spatial variations of the boundary layer thickness depends on terrain features where changes in terrain elevations and wind field over a prescribed horizontal scale are significant (Barr and Kreitzberg, 1975). Terrain effects are more significant during the day than at night. Endlich et al (1982) have suggested an equation for estimating the depth of the mixing layer at regions remote from observatories which use terrain heights. Urban centres may, however, influence the depths more than terrain elevations (Pasquill and Smith, 1983; Oke, 1987).

A climatological picture of the prevailing meteorological parameters can be obtained by the use of time averaging techniques. In studies on wind field therefore, the persistent patterns of speed and direction in time and space requires a preliminary analysis of the raw data to be applied in considerations involving flow regimes. Kavishe (1983) used arithmetic averages of wind components in the zonal and meridional directions for bulk data in studying mean wind flow patterns over Africa. Though sufficient for synoptic analyses, the procedure eliminates the effects of changes in nocturnal/diurnal patterns as well as the effects of seasonal variations. Arithmetic averages of velocity components to determine the dominant flow have been used by Nappo (1977) for mean areal directions. The procedure nevertheless gives low values of the mean wind speed when opposing wind

directions are considered, and could adversely affect model results which may either diminish or amplify due to the cumulative errors introduced. Standard deviations are a good measure of internal variations (Gupta, 1985), and coefficients of variation provide a reasonable measure of the representativeness of the calculated arithmetic means (Nappo, 1977; Gupta, 1985; Abu Bakr, 1988). Frequencies of wind speed and direction (wind roses) have been used by Ng'ang'a (1976) in studies on diffusion potentials in Nairobi.

Principal component analysis (PCA) techniques have been used on wind field studies by many authors, among them, Ludwig and Byrd (1980), and Endlich et al (1982). Oludhe (1988) has applied PCA in stochastically modelling wind power potentials in Kenya. PCA, which has also been used by Ogallo (1980) in time series analyses of rainfall in Kenya, determines unique properties of the variables thereby eliminating the lesser important properties. PCA is mostly applied when considering bulk, voluminous data, but may also be applied in studies where data sets are input at each observation time (Endlich et al, 1982). This procedure would be most appropriate for data covering long spans of time of the order of many years.

Chapter Two

2.0 Region of Study

2.1 The Physical Environment

Nairobi is a province with an area of about 750 square kilometres situated in the southern hemisphere between latitudes $1^{\circ}11'S$ and $1^{\circ}27'S$ and longitudes $36^{\circ}40'E$ and $37^{\circ}06'E$. A rapidly growing commercial, administrative and industrial centre lies approximately at the central part of the domain at about 1670m above mean sea level (AMSL) at roughly $36^{\circ}49'E$; $1^{\circ}18'S$. The city is large enough to modify the local weather pattern. East of the city, the land slopes gently but not uniformly to a height of 1480m AMSL in the north eastern sector and to 1500m AMSL at the south eastern boundary, where again it rises gently. Further east, the terrain takes the form of the "Nyika" plateau which borders the region. West of the city, the area is marked by hilly terrain rising to about 1900m AMSL on the western edge. Ngong hills on the outskirts of the region lies at an altitude of 2460m AMSL in the south western direction, 25km from the city centre. North-westwards, the terrain rises before reaching the Rift Valley situated much further west.

Whereas the eastern and southern portions are generally plain with few or no trees, the northern, western and south-western parts are dominated by dense to scattered vegetation. The most significantly vegetated areas include the Karura forest toward the northern boundary, north of the city; Kiambu forest on the northern edge; Band forest south west of the city; and Dagoretti and Embakasi forests on the western border.

Figure 2.1 is a map of the topography of the region of study while figure 2.2 shows interpolated terrain elevations of the domain obtained by using an inverse square distance weighting methodology described in section 6.3.

The climate of Nairobi is governed by synoptic systems at high levels (about 700mb and above) but greatly influenced by local features at the surface. Though a tropical region, the area has a weather pattern that differs from other regions within the same zone. Temperatures are on the average very low because of the high altitude of the province, and its environs (Ng´ng´a 1976) . The lowest temperatures are experienced in the period from June to August due to the prevailing cloudiness at the time. During the above mentioned period, the Mascarene high pressure cell is displaced close to the equator when the sun is at the Tropic of Cancer (northern hemisphere summer), cold surges of air are injected in the form of souther-westerly/ south-easterly trade winds inland. The winds carry only little moisture; mechanical lifting by orographic features causes the winds to encounter upper level westerlies resulting in cloudiness with occasional drizzles over the region (EAMD, 1962). Strong low-level inversions occur during this period due to subsidence warming from a quasi-permanent monsoon at the 700-600hPa level. The south-east/south-west monsoons last from May to the end of September, and are characterised by backing and increase of surface wind speed as the day warms up, followed by a veering and decrease of speed after sunset (Ramsey, 1966).

The highest temperatures are experienced when the sun is at the Tropic of Capricorn in the months of December to March with the maximum figures in January-February. Winds being

predominantly strong dry north-easterlies begin in October and continue until the end of April and produce cloudless conditions. They are characterised by veering in wind direction and increase in speed as the day warms up, followed by a backing and decreasing speeds after sunset (Ramsey, 1966). Long rains are experienced between March and May due to the presence of a trough (the Inter-Tropical Convergence Zone or ITCZ) created by the overhead position of the sun. Another but weaker trough (ITCZ) during the period from October to November results in the short rains season. Precipitation may result due to convergence of the mainly north-easterly flow from the Arabian anticyclone (which is displaced slightly southward to the Indian Ocean so that the northeasterlies inland have a long trajectory over the maritime conditions and carry some moisture) and the moist south-easterlies from the south-Africa subtropical latitudes (mainly the Mascarene high), accompanied by terrain induced vertical motion. The diurnal range of temperatures for the region is large but the annual range is considerably small (Ng'ang'a, 1976). The frequency of cloudiness is quite high.

Soils across the region are mainly of clay type, especially in the western portion. Being an urban area, residential sites occur throughout the domain with the highest density on the eastern part of the city and may act as surface roughness elements.

FIG. 2.1: NAIROBI TOPOGRAPHY
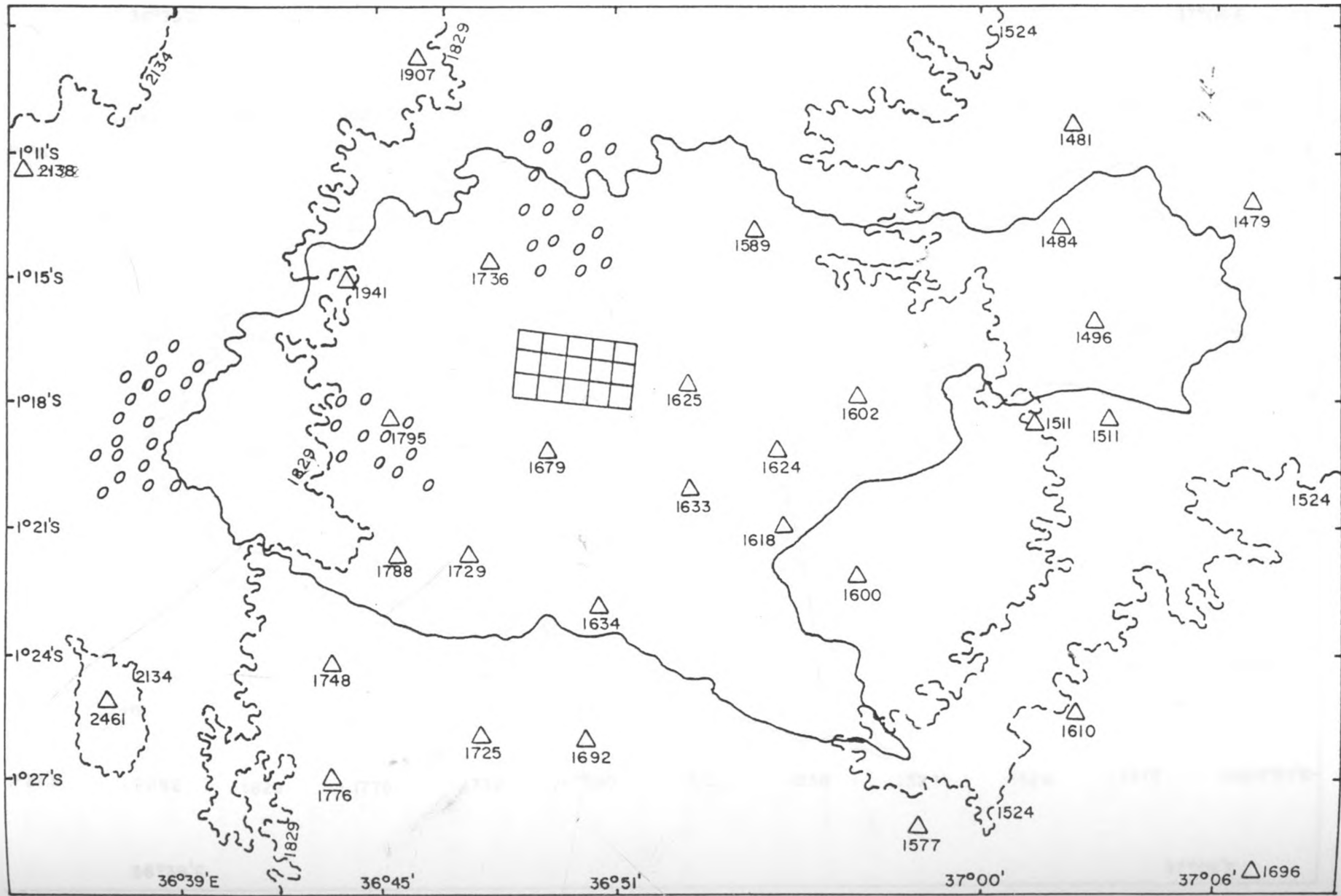
KEY

△ Terrain elevation (m) M.S.L.

City centre / Industrial area

Forest land

SCALE

5   0   5   10Km

36°39'E   37°06'E

·2134   ·1930   ·1830   ·1828   ·1743   ·1608   ·1526   ·1524   ·1515   ·1481   ·1481

1°11'S—   —1°11'S

·2097   ·1847   ·1826   ·1753   ·1736   ·1627   ·1536   ·1324   ·1501   ·1485   ·1480

                  +1941

·1995   ·1843   ·1825   ·1770   ·1684   ·1625   ·1607   ·1544   ·1524   ·1497   ·1501

·1952   ·1851   ·1821   ·1746   ·1675   ·1632   ·1624   ·1582   ·1529   ·1511   ·1519

·2079   ·1829   ·1825   ·1729   ·1652   ·1627   ·1617   ·1609   ·1543   ·1524   ·1524

·2101   ·1829   ·1748   ·1723   ·1676   ·1613   ·1526   ·1526   ·1524   ·1610   ·1553

△2461

1°27'S— ·2092   ·1829   ·1776   ·1730   ·1700   ·1612   ·1538   ·1524   ·1524   ·1578   ·1660 —1°27'S

36°39'E   37°06'E

SCALE

5   0   5   10   15Km.

FIG. 2.2 : INTERPOLATED TERRAIN ELEVATIONS (m) (A.M.S.L.)

2.2 **Data Base**

The study covers a period of one year (1986) in an attempt to include all possible seasons. The year chosen was the most recent with the most easily accessible, properly stored data.

Surface data included wind speed and direction at the anemometer height (10m); air temperature and relative humidity at screen height, and vertical profiles of soil temperature at 5cm, 10cm and 20cm depths. Global radiation measurements taken at the roof top (12m) and cloud cover information formed part of the surface data. Upper air data available at only one station (Dagoretti) from radiosonde ascents and pilot balloons consisted of day and night vertical profiles of temperature, relative humidity, speed of and direction of wind, and pressure levels (geopotential heights). Topographic data was got from maps obtained from the Survey of Kenya.

Of the seven stations considered, three (Kabete, Machakos, and Thika) are agrometeorological stations. Dagoretti and Narok are full time synoptic stations, while Wilson and Jomo Kenyatta are aeronautical stations. Wilson operates for 15 hours a day. Airport stations had data available for every hour while the other synoptic stations had three-hourly data. Agrometeorological stations have three observations a day. A summary of the stations is outlined in table 2.1 and their locations are given in figure 2.3 which also shows the grid mesh used in the study. Measurements are usually given as time averages and not necessarily at the time of observation.
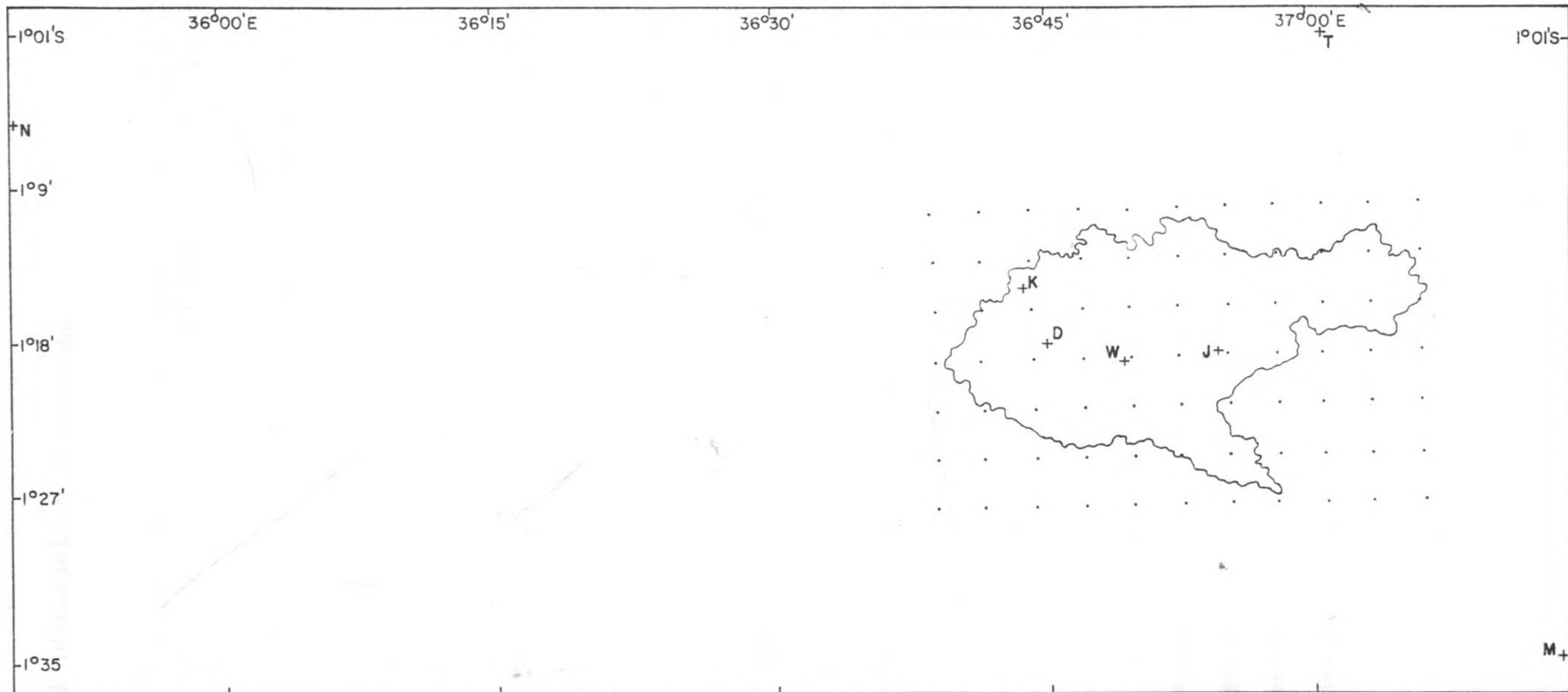
FIG. 2.3 GRID SYSTEM AND DATA STATIONS (+) : Jomo Kenyatta (J) , Wilson (W) , Dagoretti (D) , Kabete (K) , Thika (T) , Machakos (M)

and Narok (N)

Table 2.1: Description of Stations

Station	Code no. 9163-	Type	Location	Elevation (m) AMSL	Physical Features in the Vicinity
Kabete	708	Agro	01° 15′S 36° 44′E	1941	terrain fluctuates
Narok	737	Syno	01° 08′S 35° 50′E	1980	plain
Jomo-Kenyatta	740	Aero	01° 19′S 36° 55′E	1624	Scattered bushes
Dagoretti	741	Syno	01° 19′S 36° 45′E	1795	forested land
Wilson	742	Aero	01° 19′S 36° 49′E	1679	scattered trees
Machakos	745	Agro	01° 35′S 37° 14′E	1600	plain
Thika	748	Agro	01° 01′S 37° 06′E	1463	plain

NB   Urban sites have residential as well as commercial
structures.

Agro=Agrometeorological

Syno=Synoptic

Aero= Aeronautical

Chapter Three

3.0 Background Theory

Planetary boundary layers consist of three distinct zones. The lowest layer, called the laminar or viscous layer is only a few centimeters thick. The presence of a solid boundary induces frictional forces on particles that reduces their rate of flow, and hence momentum, nearest to the surface. The resulting vertical shear produces a shearing stress that increases with the frictional effects of the surface. Transfer within this layer is by molecular conduction.

Immediately above the viscous layer is the highly unstable, super-adiabatic surface boundary layer within which the shearing stresses are regarded as constant. From the level above the frictional layer up to the top of the surface layer which extends up to a few tens of metres or to over one hundred metres for areas with hilly terrain, the stresses decrease by only a small amount. This zone is therefore also referred to as the surface- or constant-stress layer. Vertical motion within this layer is caused mainly by the mechanical forcing of the surface on the horizontal flow, a process called forced convection.

An accurate description of small scale processes that determine the depth of the entire boundary layer, involves the solution of Reynold´s equations of molecular analogy within the surface stress layer. The vector form of the equations is given by

$$\frac{dV}{dt} = \frac{-1}{\rho} \nabla P + K \nabla^2 V - g\hat{k} - f(\hat{k} \times V) \tag{3.1}$$

where K is the vectorial eddy coefficient, and $f = 2\Omega \sin\varphi$ is the coriolis parameter. ρ and g are the air density and the gravitational acceleration. Expressed as a sum of short time mean and eddy fluctuations, the above equation on averaging and simplifying yields for the x-direction (see for example, Haltiner and Williams, 1980)

$$\frac{d\bar{u}}{dt} = \frac{-1}{\rho}\frac{\partial \bar{p}}{\partial x} + f\bar{v} + \frac{1}{\rho}\frac{\partial}{\partial x}\left[-\overline{\rho u'u'}\right] + \frac{1}{\rho}\frac{\partial}{\partial y}\left[-\overline{\rho u'v'}\right]$$
$$+ \frac{1}{\rho}\frac{\partial}{\partial z}\left[-\overline{\rho u'w'}\right] \tag{3.2}$$

Similar expressions exist for the y- and z-directions. The covariances are representative of the eddy fluxes of x-momentum per unit area, in that

$$-\overline{\rho u'u'} = \tau_{xx} = \rho K_x \frac{\partial u}{\partial x}$$

$$-\overline{\rho u'v'} = \tau_{xy} = \rho K_y \frac{\partial u}{\partial y} \tag{3.3}$$

$$-\overline{\rho u'w'} = \tau_{xz} = \rho K_z \frac{\partial u}{\partial z}$$

with τ as the force exerted on a surface by the air being dragged over it and may be referred to as the surface shearing stress. The frictional force exerted by the surface on the air above is of opposite sign. Neglecting the horizontal stresses ($-\overline{\rho u'u'}$) and ($-\overline{\rho u'v'}$) which are of considerably lesser magnitude than the vertical stress ($-\overline{\rho u'w'}$) and assuming that the acceleration term within the layer is small compared to

other terms, we get a balance between the the coriolis
force and the vertical stress term. Expressed
vectorially, introducing the geostrophic wind V_g and
leaving out the subscript xz on τ, we obtain

$$f\hat{k} \times (V - V_g) = -\frac{1}{\rho}\frac{\partial\tau}{\partial z} \tag{3.4}$$

where the geostrophic wind is given in relation to the
pressure gradient force by

$$-\nabla(p/\rho) = f\hat{k} \times V_g \tag{3.5}$$

An analogy for the surface boundary layer turbulent
flux densities of sensible and latent heat is given
respectively by

$$Q_H = \rho C_p \overline{w'T'} \tag{3.6a}$$
$$Q_L = \rho L_v \overline{w'q'} \tag{3.6b}$$

where T' and q' are the absolute temperature and moisture
perturbations. The specific and latent capacities of
heat are C_p and L_v.

In tropical regions the balance between the
pressure gradient and coriolis forces is not uniform and
the flow is cross-isobaric. The coriolis parameter is
small, and at the equator the geostrophic approximation
is not valid. The flow, moreover, is dictated by the
physical factors such as topography which prevail over
dynamic factors.

Wind speed profiles within the surface layer follow
a wind shear relationship of the form

$$\frac{\partial u}{\partial z} = \frac{u_*}{\varkappa z} \phi_m(z/L) \tag{3.7}$$

where ϕ_m is a momentum function that accounts for buoyancy effects with the Monin-Obukhov scale length L, being a measure of the ratio of mechanical turbulence stresses to buoyancy forces. L may be interpreted as the height at which the magnitudes of mechanically and thermally produced turbulence are equal (that is, the level where buoyant forces and mechanical or shear related forces become comparable in turbulence generation). Generally, the magnitude of L is greater during the day than at night; L decreases in unstable conditions (becomes more negative) and increases in stable stratifications. The friction velocity, U_*, is a parameter dependent on the degree of turbulence and the resulting eddy stresses. $\varkappa$ is the Von Karman constant. Integrating equation (3.7) gives the wind speed at any level z. Assuming $U = 0$ at the surface roughness length, z_0 the speed is given by an expression of the form (see for instance, Pasquill and Smith, 1983)

$$\bar{U}(z) = \frac{U_*}{\varkappa}\left(\ln\left(\frac{z}{z_0}\right) + f_m\left(\frac{z}{L}\right) - f_m\left(\frac{z}{L}o\right)\right) \tag{3.8}$$

The surface roughness parameter, z_0, is a measure of the aerodynamic roughness of the surface. Its magnitude ranges from small values of the order of millimetres over calm water, to larger values of a few metres for large forested or mountainous areas and cities, depending on a city's silhouette and lateral area.

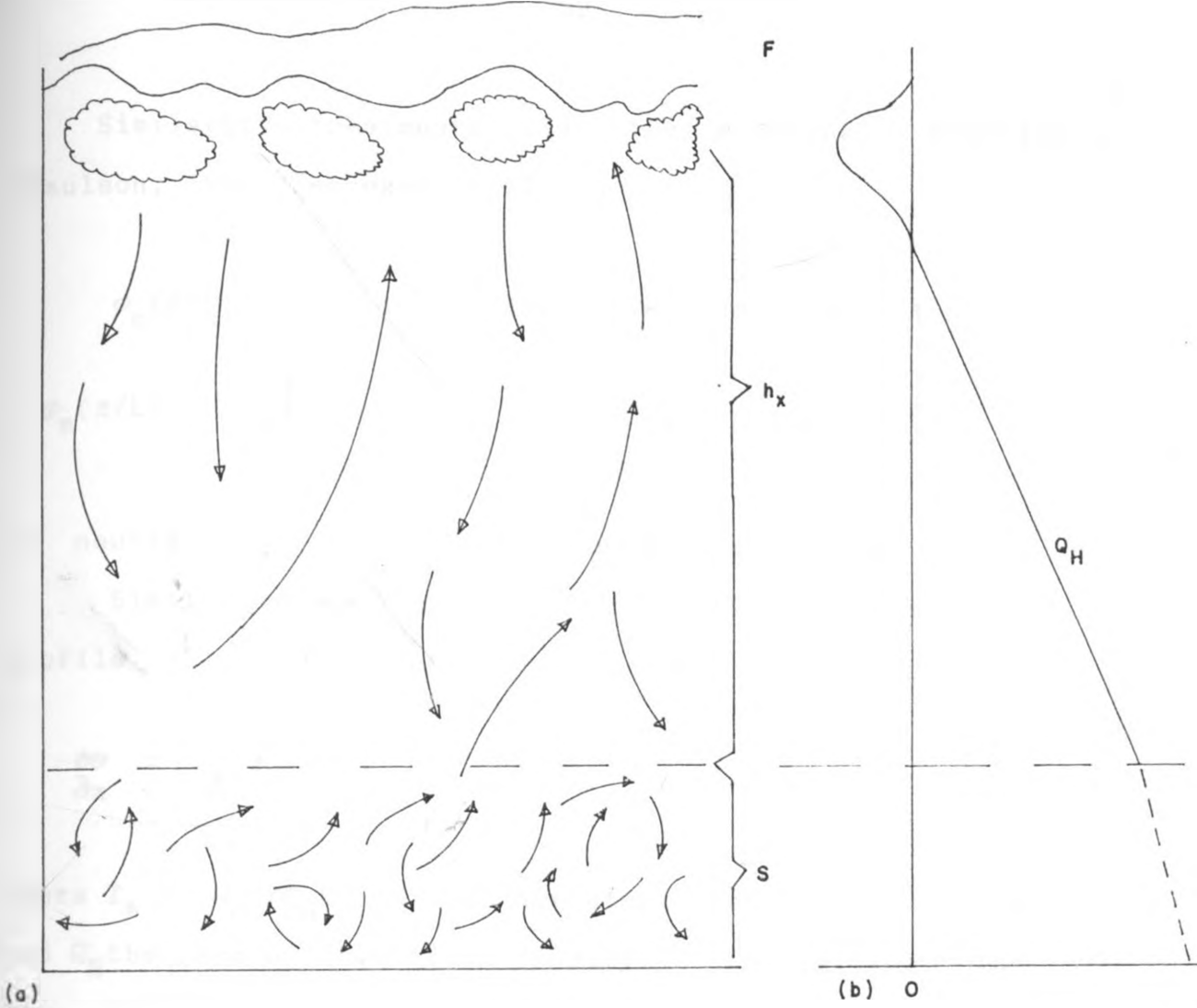# STRUCTURE OF THE PLANETARY BOUNDARY LAYER

FIG.3.1 (a) DAYTIME BOUNDARY LAYER STRUCTURE SHOWING THE SURFACE LAYER (S)
MIXED LAYER (h_x) , FREE ATMOSPHERE (F)

(b) SENSIBLE HEAT PROFILE　(oke, 1978)
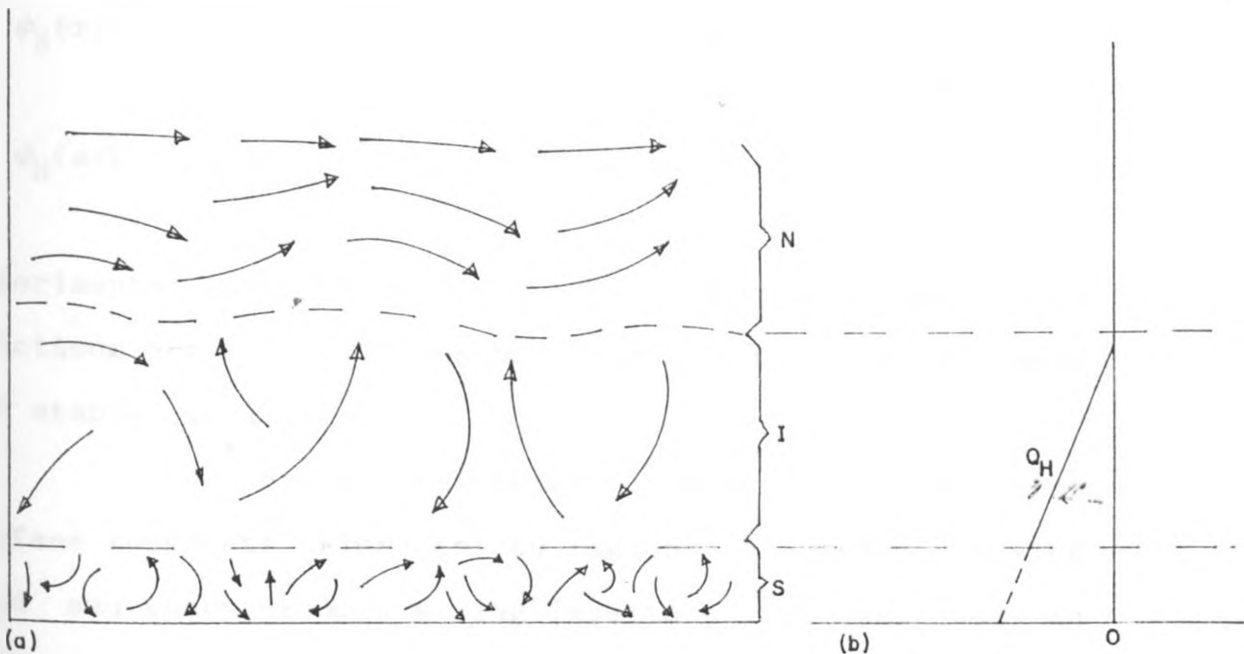
FIG. 3.2 (a) NIGHTTIME BOUNDARY LAYER SHOWING THE SURFACE LAYER (S),
INVERSION (I) AND NEUTRAL LAYER (N)

(b) SENSIBLE HEAT PROFILE　(oke, 1978)

Similarity treatments give the momentum function (Paulson, 1970; Tennekes, 1972) as

$$\phi_m(z/L) = (1 + 4.7 \ z/L) \ \text{[Stable conditions]}$$

$$\phi_m(z/L) = \left(1 - 15z/L\right)^{-1/4} \text{[Unstable conditions]}$$

(3.9)

In neutral flow, the momentum function tends to unity.

Similar expressions exist for the flux of heat whose profile is given by

$$\frac{\partial \theta}{\partial z} = \frac{T_*}{\varkappa z} \ \phi_H(z/L)$$

(3.10)

where $T_* = -Q_H/\rho C_p U_*$ is the turbulent temperature scale and Q_H the sensible heat flux density at the surface. The heat functions corresponding to stable and unstable conditions are given by the empirical equation

$$\phi_H(z/L) = (1 + 4.7 \ z/L) \ \text{[Stable conditions]}$$

$$\phi_H(z/L) = \left(1 - 16z/L\right)^{-1/2} \text{[Unstable conditions]}$$

(3.11)

Experiments have shown that $\phi_m > \phi_H$. However, both functions decrease for unstable conditions but increase for stable conditions.

An eddy at the surface forced up by the surface roughness elements to regions of faster moving wind and momentum upon mixing imparts a net decrease in velocity at the upper level. The converse is true for

downward moving eddies. Since down drafts have greater
momentum, the net effect is an increase in momentum
downwards. Vertical transfer of momentum is greater
during unstable conditions than during stable conditions
which dampen vertical propagation.

Above the surface boundary layer is a deeper mixed
layer which forms the third division of the boundary layer.
In this layer, transfer of fluxes upwards is caused
entirely by density differences in the vertical
stratification that eventuates in free convection. This
layer is also called the adiabatic mixing layer. Here,
thermals (turbulent parcels of warm air) carry momentum,
moisture and heat as they ascend, transferring the
quantities to upper levels. Surface heating induces
buoyancy forces on parcels, the strength of the force being
a function of the amount of the surface heating and the
characteristics of the surface. The heated parcels whose
size is determined by the area receiving the insolation,
rise rapidly in the lower layers but decrease in their rate
of ascent at upper levels due to the entrainment of colder
air into the parcels and the increasing drag force upon the
now grown, bigger parcels. Thermal ascent eventually stops
when the heat energy is lost, the parcels attaining the
same temperature with the rest of the surrounding upper
level air, or on meeting an inversion layer. Alternatively,
cloud formation and latent heat release may halt the
ascent.

The stability of a parcel of air in the
atmosphere is dependent on the vertical temperature
stratification. A displaced parcel would ascend if its
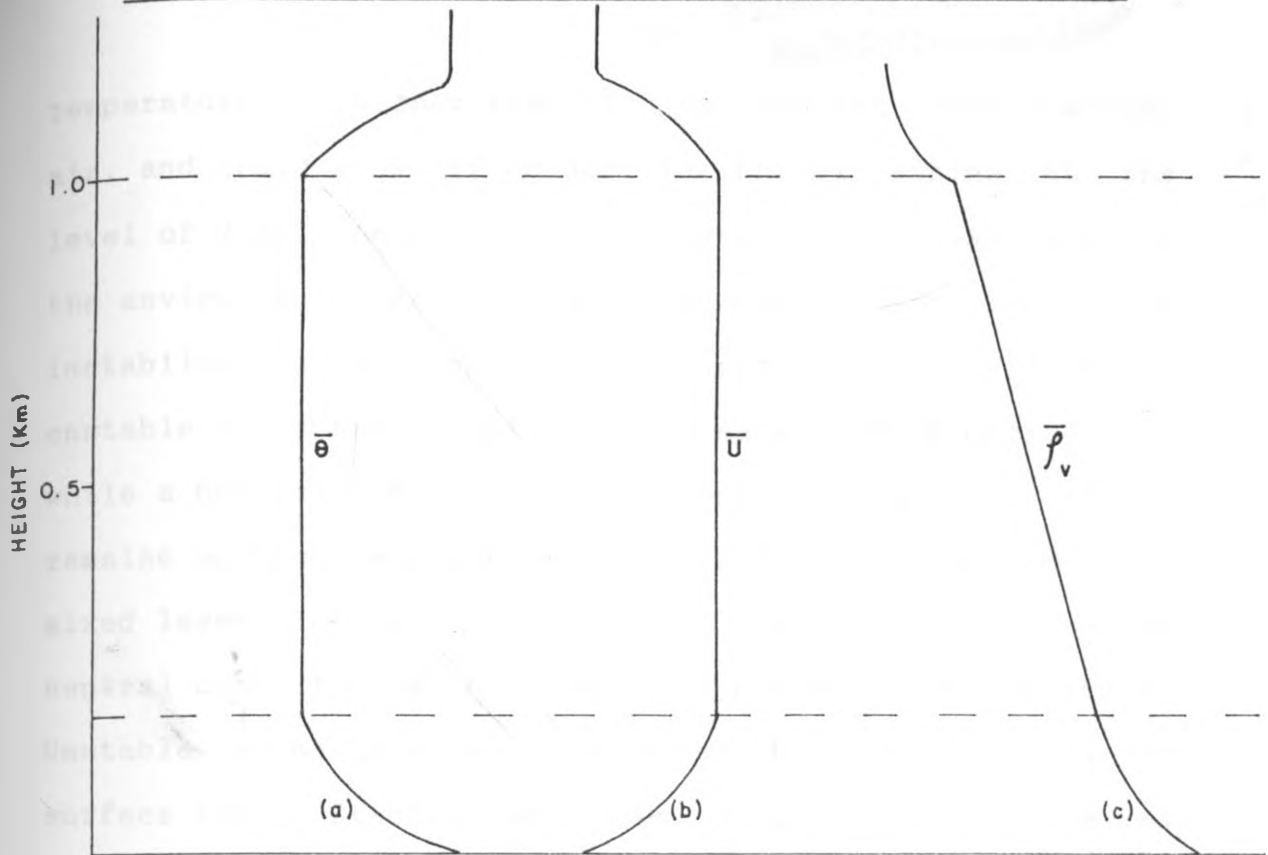
FIG. 3.3 : DAYTIME CONVECTIVE BOUNDARY LAYER
(a)POTENTIAL TEMPERATURE $-\bar{\theta}$, (b)WIND SPEED$-\bar{U}$, VAPOUR DENSITY$-\bar{\rho}_v$

(oke, 1987)
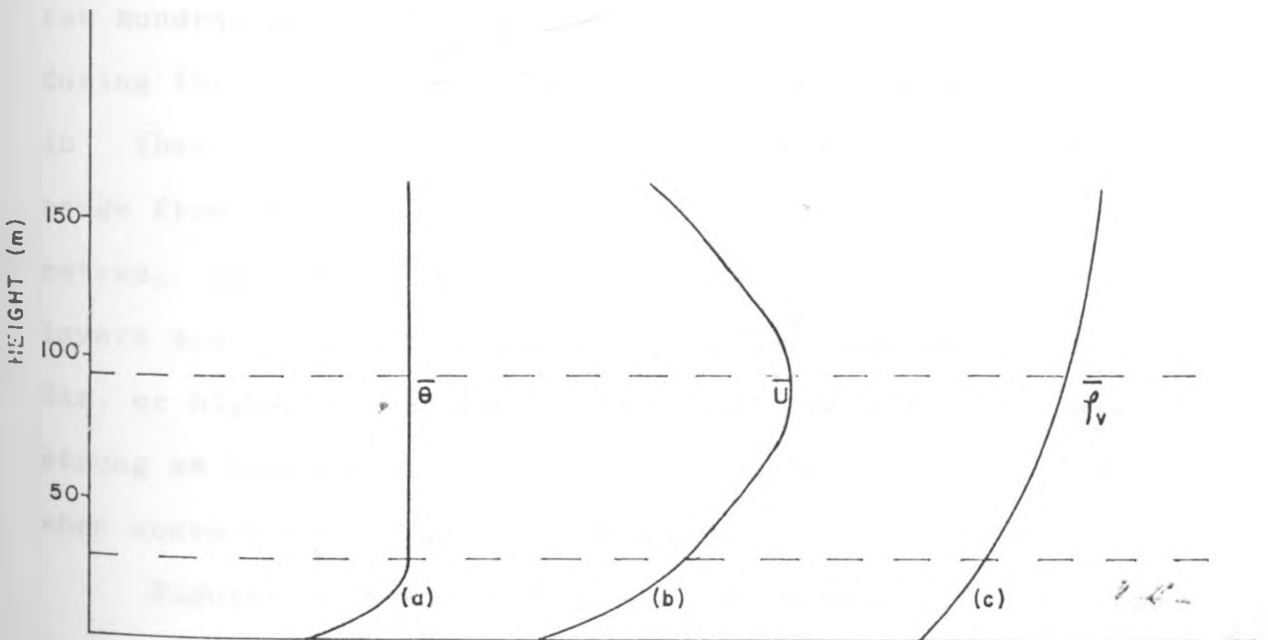
FIG.3.4 : NIGHTTIME STABLE BOUNDARY LAYER
(a) , (b) AND (c) AS ABOVE (FIG. 3.3)

(oke, 1987)

temperature is higher than the surrounding environmental air, and would sink if colder. The parcel remains at the level of displacement if its temperature equals that of the environment. A Parcel's ascent implies its instability with respect to the surrounding air or an unstable atmosphere. Sinking implies a stable environment while a neutral atmosphere is where the displaced parcel remains at the new position. Vertical mixing within the mixed layer during the day creates approximately neutral conditions with constant potential temperature. Unstable conditions are then found at low levels in the surface layer. Stable atmospheres occur above the mixed layer during the day and in the surface layer during the night. Inversions are brought about by either radiative cooling from below, adiabatic warming from above, or by the advection of warmer air or cooler air.

The entire planetary boundary layer extends up to a few hundred metres during the night and a few kilometres during the day, depending on the mechanism used in their formation. Stable (nocturnal) boundary layers range from a depth of a few tens to a few hundred metres, say 400m, whereas unstable (diurnal) boundary layers are generally of the order of 1km, and may reach 3km, or higher either when vertical velocities are strong as happens in disturbed boundary layers, or when convective clouds are present.

Figures 3.1a and 3.2a show the divisions in the daytime and nighttime planetary boundary layer respectively. The ideal wind pattern is also shown.
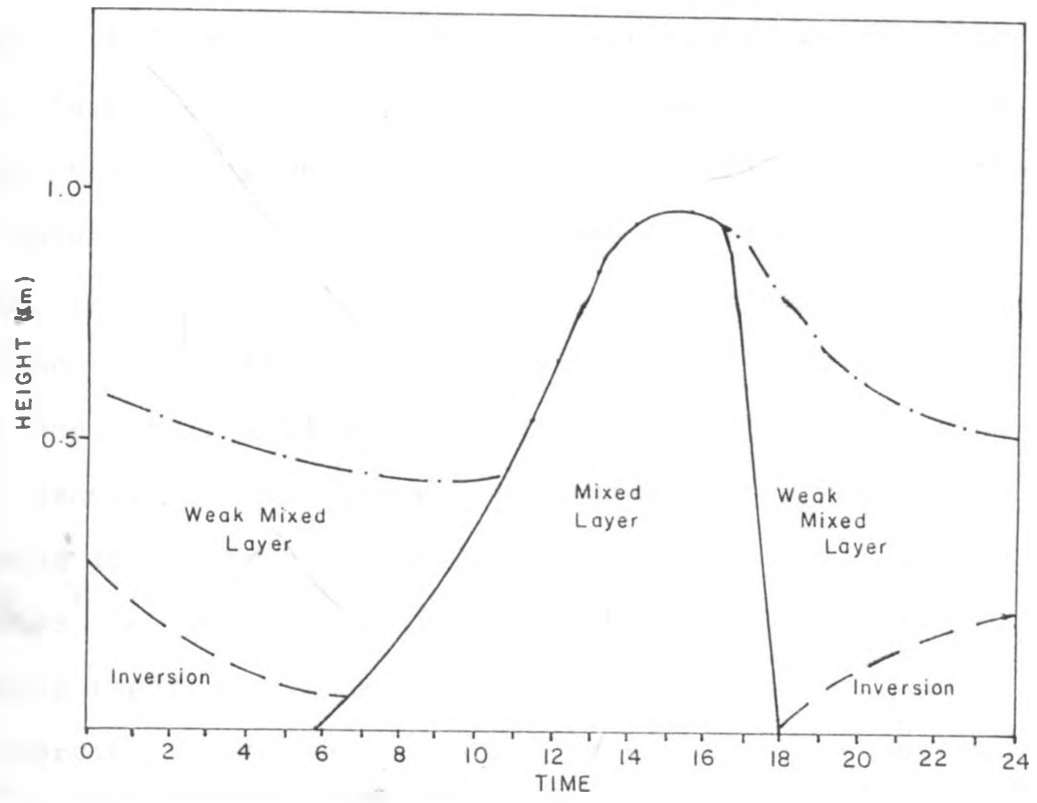
FIG.3.5 : DAILY VARIATION OF THE PLANETARY BOUNDARY LAYER -
THE CLASSICAL STRUCTURE (Oke, 1978)
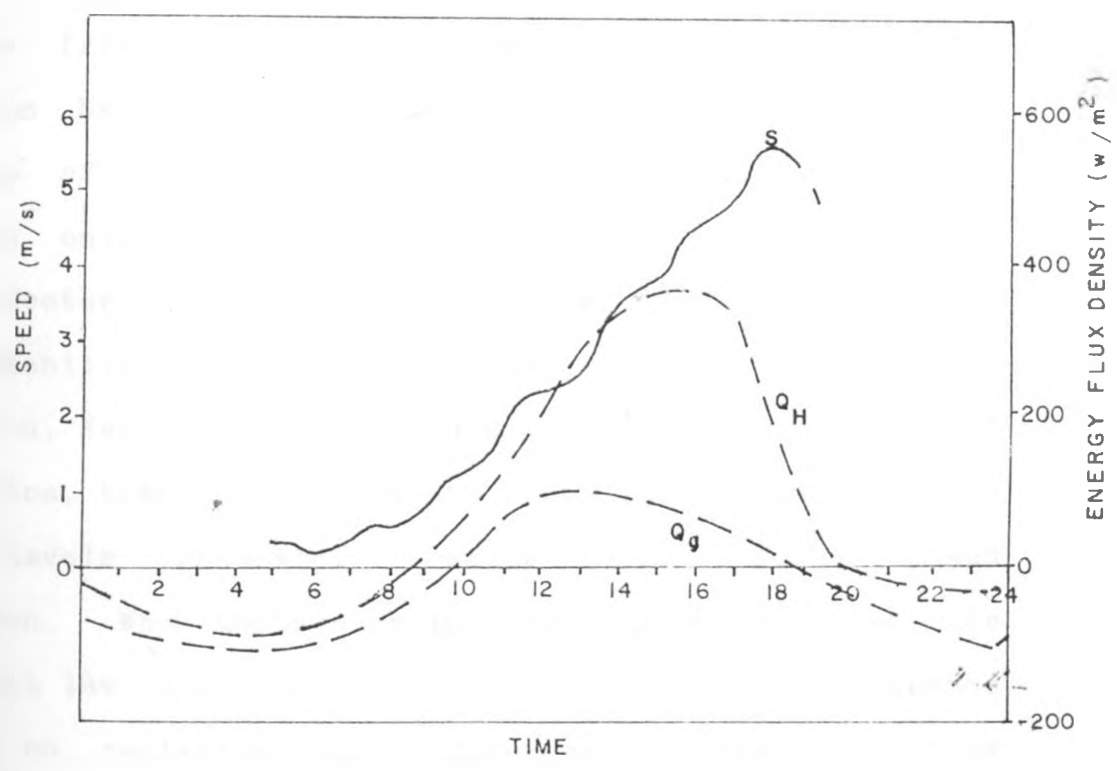
FIG. 3.6 : DAILY WIND SPEED (S) AND HEAT FLUXES OF SENSIBLE
HEAT (Q_H) AND GROUND HEAT (Q_g) - A CLASSICAL PICTURE
(oke, 1987)

Unstable boundary layers are characterised by a lapse profile of potential temperature within the surface layer, constant in the mixed layer because of vertical overturning, and an inversion profile above the mixed layer (figure 3.3a). The mean profile of wind is such that it is logarithmic in the surface layer and nearly constant in the mixed layer as a result of mixing and the vertical transfer of momentum. The wind speed generally decreases thereafter before again increasing in the free atmosphere (figure 3.3b). Figure 3.3c shows the idealized profile of vapour density — decreasing rapidly within the surface layer and above the inversion, but maintaining a nearly constant gradient that decreases with height within the mixed layer. Sensible heat flux, and implicitly the vertical kinematic flux of sensible heat, decreases linearly from the surface becoming negative below the inversion base and reaches a minimum (negative) value at the top of the mixed layer. The decrease in the surface layer is only slight (figure 3.1b).

Nocturnal boundary layers are influenced by low level stability that results from terrestrial radiation. Mechanical turbulence is the main cause of convection, transferring heat from the lowest layers to levels immediately above the surface-based inversion. When turbulence is very weak as is often the case with low wind speeds, the inversion then depends mainly on radiative flux divergence. The resulting potential temperature gradient is such that it depicts an increasing profile (inversion) in the now shallow surface

layer, but constant above (figure 3.4a). The wind speed profile generally increases up to the top of the inversion layer which is occasionally marked by a low level nocturnal wind maxima or "jet" (figure 3.4b). Vapour density increases with height in the low levels (figure 3.4c), while sensible heat decreases up to the inversion top, above which it is zero as shown in figure 3.2b.

Neutral boundary layers are possible when high wind speeds, in excess of 12m/s and overcast skies are prevalent. Implicitly, buoyancy forces are neglected and mechanical forces are used to define growth processes within the layer. Turbulent kinetic energy used is obtained from strong instabilities within the surface layer and the wind direction shear in the Ekman-spiral layer. Purely neutral boundary layers rarely occur as buoyancy forces are commonly manifested even in small quantities. Near-neutral conditions are usually present at sunrise and sunset. A classical pattern of the daily variation of the depth of the planetary boundary layer is shown in figure 3.5 for subtropical regions.

A typical cycle of daily variations of wind speed and the fluxes of sensible and ground heat is given in figure 3.6.

Using a stability parameter, boundary layers have been classified according to their formation mechanisms into three categories: stable, mechanical, or convective boundary layers. The parameter is given by the ratio of the product of friction velocity, U_*, and the Von Karman constant, $\varkappa$; to the product of the Monin-Obukhov scale

length, L, and the coriolis parameter f, or symbolically (Harris, 1979),

$$\mu = \frac{\varkappa}{Lf} \underline{u}_*$$
(3.11)

Stable boundary layers occur for the parameter greater than 1, while convective boundary layers exist for the parameter less than -20; mechanical boundary layers are identified for the parameter between 1 and -20.

Many approaches are employed in attempting to simulate the depth of the planetary boundary layer and the method used depends on the accuracy desired in the area of application. Prevailing synoptic weather systems are also of concern when studying boundary layer depths. Most precise procedures involve the treatment of turbulent fluxes specified in the depth close to the earth's surface given for sufficient vertical levels, and the inclusion of convection thereby satisfactorily incorporating heat, momentum and moisture. Though such a procedure would adequately resolve the boundary layer depth, the approach of parameterisation is more commonly used due to lack of sufficient upper air data and lesser computing time. This method involves using just a minimum number of levels, say one or two close to the surface, to describe the turbulent fluxes in the whole of the planetary boundary layer. The third and simplest approach is by applying schemes derived from empirical equations that use as few parameters as possible. Though such a procedure would be adequate for applications that do not demand high precision, and within the area where the model is developed, it is not necessarily site

independent.

Principles governing boundary layer thicknesses as influenced by terrain undulations horizontally have been given (see for instance, Barr and Kreitzberg, 1975). Generally, regions of low mountains or low hills have a boundary layer structure whose depth is flat at night, but tends to slope less steeply than the terrain during the day when convection is absent. Regions of high mountains have a nighttime boundary layer whose slope tends to slope slightly less than the terrain. The tendency for the daytime boundary layer is that it slopes less steeply than the terrain, except when strong convective activities are present over the peaks, especially during summer conditions. Islands' and coasts' boundary layer thickness remains relatively constant for both day and night but that over the adjacent land is relatively high during the day and low at night; the slope is opposite to that of the terrain at night. Relatively flat terrain's mixing depths have a flat top (Endlich et al,1982).

Chapter Four

4.0 Surface Wind Field Regime

4.1 Regime   Algorithm

In essence, time averages of any meteorological   parameter give its time history. The prevailing patterns show a bulk climatological   representation which could be   more   useful for practical considerations even though day to analyses can   on   individual basis be more   important   in   assessing diurnal effects in   many   applications.   The   magnitude   of deviations from time means,   given   commonly   by   standard deviations, on the other hand show the representativity   of the mean.

The   traditional   approach   of   averaging   using bulk   data over   periods   of many   years,   months   or   days smooths   out characteristics   within the parameter   under consideration that   would   be   present in   analyses   where shorter   time intervals   are   utilised.   Available   data necessitated   the prevailing   patterns   to   be   calculated over   intervals   of three   hours   using simple   statistical methods.   The   time interval   was   chosen   for   consistency for stations that did not provide data over   shorter   time intervals,   though   hourly   data   was   available   for   some stations. For any set of values of   a   parameter X_i the. time average, $\bar{X}$,   and   the   standard   deviation, σ,   were obtained using the ordinary arithmetic   mean   and   standard deviation formulations such that,

$$\bar{X} = \frac{1}{N} \sum_{i=1}^{N} X_i \qquad (4.1)$$

$$\sigma = \left[\frac{1}{N-1} \sum_{i=1}^{N} (X_i - \bar{X})^2 \right]^{1/2} \qquad (4.2)$$

where the total number of i observations, N, denotes the number of values averaged in a given month for any particular synoptic hour. For each month, the average diurnal variations were then given by the above procedure. Coefficients of variation were obtained using the usual relation (Gupta, 1985):

$$CV = \frac{\sigma_x}{\bar{x}} \qquad (4.3)$$

The vectorial resolution of the wind field into the zonal, u, and meridional, v, components from the wind vector was done using the convention of positive eastward, positive northward. Accordingly;

$$u = -| V | \sin\theta \qquad (4.4a)$$
$$v = -| V | \cos\theta \qquad (4.4b)$$

where V and θ are respectively the wind vector and direction. The transposed form of (4.4) used in time averaging is

$$\bar{\theta} = \tan^{-1} \left(\frac{\bar{u}}{\bar{v}} \right) \qquad (4.5a)$$

$$\bar{V} = \left(\bar{u}^2 + \bar{v}^2 \right)^{1/2} \qquad (4.5b)$$

with the signs of u and v giving the quadrant

of Θ and hence the average direction. Equations (4.5) give the mean magnitude of the wind vector and the average direction of wind, which are important in flow modelling. For haphazard wind directions though, as is common during the early morning periods, the equation gives particularly low values of the wind vector especially when the direction of the wind over the period changes considerably for the hour. The contrasting directions give a reduced strength of the mean flow. Analyses that depend on the speed of the wind only and are not affected by the temporal fluctuations in direction as is the case in studies on the depth of the boundary layer would be more accurate if a slightly different formulation were adopted. Where the upper extreme would be of greater importance, the methodology employed involved the computation of the mean wind speed using equation 4.1 directly.

Spatial analysis of the sparsely distributed original data was interpolated/ extrapolated to grid points using an inverse square distance scheme. Details of the procedure are given in section 6.3.

4.2 Results and Discussion on the Surface Wind Regime

Wind field patterns at the surface are mainly controlled by surface insolation. In Nairobi, the period between May and September is generally cold due to prevailing cloudiness. April and October are hot and wet; the rest are predominantly hot and dry.

Using only the three-hourly (synoptic) data, time averaged wind speeds are least in the morning, just before sunrise, for all the months. This minimum coincides with the mean minimum screen-height temperature and alternates between 0600 and 0700 local time, depending on the time of sunrise. This is tantamount to the loss of heat through long wave radiation during the night, leaving the lowest amount in the morning. During the period between May and September inclusive, radiative cooling evidently occurs rapidly so that long before midnight the speeds fall significantly. In fact, calm conditions are experienced frequently from as early as 2100 local time at Dagoretti during June and July, an observation that can be attributed to the influence of the surface roughness features on the now weak flow. High wind speeds after sunset are maintained until as late as midnight during the warmer months from October to April because of a greater amount of heat input during the day as contrasted to the colder period when a comparatively smaller input is realised. Vertical mixing due to momentum exchange between upper and lower levels is favoured with surface heating. During the day, the net transfer of momentum is downwards so that wind speeds in the lower atmosphere are raised as the day progresses. Decreasing vertical mixing during the night leads to low wind speeds at the surface, more so in the

morning. The same argument holds for the warmer period and the colder months when there is greater and lesser momentum exchange, respectively.

For all the three stations: Dagoretti, Wilson and Jomo Kenyatta, the increase in wind speed upto 0900 EAST, only two hours after the minimum speeds are experienced, is quite significant for the warmer months. The leap is appreciably smaller as the colder period is approached for the same local time. Wind speeds then increase steadily as the day progresses with the maximum values in the late afternoon to the evening depending on the season and the location of a station. The seasonal cycle of the wind speed is similar but not identical to the diurnal pattern. Speeds fall as we move from February so that minimum speeds are encountered in the period June/July before they increase to a maximum in October, clearly due to changes caused by the seasonal movement of the sun to the heat distribution. Table 4.1 gives a summary of the wind speed averages, while typical diurnal and seasonal patterns are shown in figures 4.1a for February (warm and dry), June (cold and moist) and November (short rains); and 4.3a and b (0600 and 1200EAST).

The greatest internal variations of the wind speed as deduced from coefficients of variation occurred in the early morning period for all the months (table 4.2) while the most steady speeds, on the other hand, were identified as from the late afternoon to the evening hours. The variations were higher during the night than daytime, and during the colder season than the warmer period. Spatially, wind speeds eastward of the region of study were more steady than for the westward located station of Dagoretti, and exhibited the

least variability before sunset.

Examination of the spatial variations revealed that the highest wind speeds occurred at Wilson, followed by Jomo Kenyatta, and least at Dagoretti during daytime. The highest values before sunrise were identified at Jomo Kenyatta. Whereas there was a distinct difference between the speeds of wind at Dagoretti and both Wilson and Jomo Kenyatta, the difference between values at Wilson and at Jomo Kenyatta was not significant. Figures 4.3a and 4.3b give some aspects of spatial variations of wind speeds.

Surface directions of flow vary as expected with the diurnal movement of the overhead sun. The nocturnal pattern was caused by both the differences in space in the amount of heat energy stored from daytime activities and the influence of the surface features on the synoptic flow. Veering of the winds with time as the day progressed was a distinct, smooth process. The most significant change in the wind direction on a diurnal basis was between late morning (0900 EAST) and late afternoon (1500 EAST), depicting the influence of surface heating. During the northern winter represented by the period from December to February, wind directions steadily changed from north-easterly to easterly from 0900 to 1500 local times with a tendency of becoming weak south easterlies to weak southerlies after sunset at Dagoretti. In contrast the flow directions after sunset at Jomo Kenyatta was a reverse of the daytime cycle. The flow during April and October was predominantly easterly but assumed weak southerly flow at night at Dagoretti in contrast to that at Jomo Kenyatta which became more and more northerly. The period of the northern hemisphere summer between May and June depicted a flow pattern changing from southerly in the late morning to south-

easterly, a reversal of what was observed for the northern winter. The flow became more easterly after sunset at Jomo Kenyatta but once again southerly at Dagoretti. Weak westerlies to northerlies were identified at Jomo Kenyatta in the late night hours (from midnight) during July and August. Table 4.3 gives a summary of wind directions after time averaging while figures 4.2 and 4.3c and 4.3d give the typical variations in direction, diurnally for February (warm and dry), April (wet) and July (cold and moist); and seasonally (0900 and 1500 EAST) respectively.

Comparing the flow patterns at grid points (figures 6.1-6.4) with the general flow of Kenya it is clear that the microclimate of Nairobi appreciably alters the general flow at the surface. Details on this patterns have been considered in section 6.4.

Table 4.1: Mean Surface Wind Speeds (m/s) for 1986

Hour/Month	Jan	Feb	Mar	Apr	May	Jun	Jul	Aug	Sep	Oct	Nov	Dec
0000												
Dagoretti	1.2	2.3	1.2	2.1	1.1	0.3	0.0	0.8	1.0	1.7	1.4	1.8
JKIA	3.1	3.4	2.8	2.1	1.1	1.5	1.9	1.8	1.7	3.2	2.5	2.2
Wilson	–	–	–	–	–	–	–	–	–	–	–	–
0300												
Dagoretti	1.0	1.0	0.7	1.9	0.8	0.3	0.0	0.2	0.4	1.0	1.6	0.8
JKIA	1.7	2.6	2.3	2.1	1.1	1.5	1.9	1.8	1.7	3.2	2.5	2.2
Wilson	–	–	–	–	–	–	–	–	–	–	–	–
0600												
Dagoretti	0.4	0.4	0.7	1.0	0.4	0.0	0.2	0.1	0.3	0.6	1.3	0.4
JKIA	1.6	1.6	2.1	1.6	1.6	1.3	1.7	1.6	1.3	1.5	2.5	1.6
Wilson	1.6	2.0	1.7	1.7	1.2	1.2	1.4	1.2	0.8	2.0	2.5	1.9
0900												
Dagoretti	3.4	3.2	3.0	2.5	1.7	1.0	0.5	0.8	1.3	2.3	2.5	2.5
JKIA	3.5	4.0	3.1	3.0	2.2	2.4	2.6	1.8	2.6	3.8	4.3	3.5
Wilson	4.3	4.3	3.3	3.4	2.6	1.9	1.7	2.4	2.8	3.7	4.5	3.4
1200												
Dagoretti	3.5	4.4	5.0	4.1	2.4	1.9	1.5	2.6	2.4	3.9	4.0	3.8
JKIA	5.0	6.6	5.9	4.2	2.7	2.6	2.5	3.4	3.4	5.6	5.6	5.6
Wilson	5.8	7.4	6.7	5.3	3.4	2.8	3.2	3.0	4.3	6.0	6.0	5.6
1500												
Dagoretti	3.9	5.5	5.5	4.5	3.0	2.2	2.4	3.2	3.3	4.7	3.8	4.0
JKIA	5.5	7.0	7.5	6.3	3.7	2.7	3.5	4.0	4.0	6.9	6.2	6.1
Wilson	5.6	7.5	8.0	5.9	5.0	3.5	3.9	5.1	5.2	7.2	6.1	6.3
1800												
Dagoretti	4.0	5.0	5.4	3.5	2.4	1.2	2.7	3.5	3.2	3.9	3.1	3.7
JKIA	7.0	8.3	5.0	5.0	4.2	3.6	4.5	5.9	6.2	7.3	5.7	6.9
Wilson	7.1	8.0	8.1	5.8	4.5	3.3	4.5	6.3	7.0	7.5	5.8	6.8
2100												
Dagoretti	2.3	3.0	2.8	2.4	1.6	0.4	0.5	1.7	1.3	2.9	1.8	2.4
JKIA	3.9	4.9	4.5	3.8	2.4	2.2	2.2	3.2	3.3	4.9	3.8	4.0
Wilson	–	–	–	–	–	–	–	–	–	–	–	–

NB. JKIA = Jomo Kenyatta International Airport
   Hour = EAST

Table 4.2: <u>Coefficients of Variation for Surface Wind Speed</u>
<u>(1986)</u>

Hr./Mth	JAN	FEB	MAR	APR	MAY	JUN	JUL	AUG	SEP	OCT	NOV	DEC
0000												
Dagoretti	1.3	0.9	1.3	0.8	1.5	3.2	***	1.4	1.4	1.1	1.3	1.0
JKIA	0.6	0.5	0.6	0.7	0.7	0.9	0.9	0.6	0.7	0.4	0.6	0.7
Wilson	-	-	-	-	-	-	-	-	-	-	-	-
0300												
Dagoretti	1.4	1.4	1.7	0.9	1.6	3.1	***	2.7	2.1	1.3	1.0	1.4
JKIA	0.8	0.6	0.5	0.8	1.2	1.0	0.6	0.8	0.9	0.5	0.7	0.8
Wilson	-	-	-	-	-	-	-	-	-	-	-	-
0600												
Dagoretti	2.4	2.4	1.7	1.5	2.6	***	8.5	5.4	2.5	1.8	1.2	2.5
JKIA	1.5	1.0	0.9	1.1	0.9	1.2	0.8	0.8	1.0	1.0	0.7	1.1
Wilson	1.1	1.0	1.2	1.2	1.4	1.5	1.1	1.4	1.7	1.0	0.9	1.2
0900												
Dagoretti	0.5	0.5	0.5	0.9	0.8	1.2	2.6	1.6	1.2	0.6	0.6	0.9
JKIA	0.5	0.4	0.6	0.8	0.7	0.8	0.6	0.9	0.6	0.6	0.6	0.4
Wilson	0.4	0.4	0.6	0.8	0.7	1.0	1.0	0.8	0.7	0.6	0.5	0.6
1200												
Dagoretti	0.4	0.3	0.3	0.5	0.7	0.8	1.1	0.5	0.7	0.4	0.3	0.5
JKIA	0.4	0.3	0.4	0.5	0.6	0.6	0.7	0.5	0.6	0.1	0.4	0.4
Wilson	0.3	0.3	0.4	0.5	0.6	0.7	0.7	0.8	0.4	0.4	0.3	0.4
1500												
Dagoretti	0.5	0.3	0.2	0.4	0.5	0.6	0.7	0.4	0.5	0.3	0.4	0.4
JKIA	0.4	0.3	0.3	0.4	0.5	0.5	0.4	0.4	0.6	0.4	1.0	0.3
Wilson	0.4	0.3	0.3	0.4	0.3	0.5	0.4	0.4	0.4	0.3	0.4	0.3
1800												
Dagoretti	0.4	0.3	0.3	0.6	0.8	1.2	0.5	0.3	0.5	0.4	0.5	0.5
JKIA	0.3	0.2	0.5	0.6	0.4	0.5	0.3	0.3	0.3	0.3	0.4	0.3
Wilson	0.4	0.2	0.3	0.5	0.5	0.6	0.3	0.3	0.3	0.3	0.4	0.3
2100												
Dagoretti	0.9	0.4	0.6	0.7	1.0	2.0	2.0	1.0	1.2	0.6	0.8	0.6
JKIA	0.3	0.3	0.4	0.4	0.8	0.7	0.7	0.6	0.5	0.3	0.4	0.4
Wilson	-	-	-	-	-	-	-	-	-	-	-	-

NB. JKIA = Jomo Kenyatta International Airport
    *** = calm conditions
    Hr. = EAST; Mth = Month

Table 4.3: <u>Mean Surface Wind Directions (360°)</u>

Hour/Month	Jan	Feb	Mar	Apr	May	Jun	Jul	Aug	Sep	Oct	Nov	Dec
0000												
Dagoretti	130	140	160	170	170	180	***	180	170	160	150	150
JKIA	50	40	40	30	70	170	230	350	10	40	40	50
Wilson	-	-	-	-	-	-	-	-	-	-	-	-
0300												
Dagoretti	70	70	60	100	130	180	***	60	120	70	90	50
JKIA	30	20	20	90	110	220	260	360	360	60	50	40
Wilson	-	-	-	-	-	-	-	-	-	-	-	-
0600												
Dagoretti	70	70	80	100	170	***	160	80	120	100	80	60
JKIA	360	10	50	70	160	220	220	310	230	50	70	40
Wilson	360	360	30	60	210	240	230	20	190	60	70	50
0900												
Dagoretti	70	70	70	90	120	170	180	130	140	80	80	60
JKIA	40	40	50	80	180	190	190	160	120	50	60	40
Wilson	50	50	60	80	140	180	170	130	120	60	70	50
1200												
Dagoretti	80	80	80	80	140	170	160	110	110	90	80	80
JKIA	50	40	60	80	120	190	170	130	100	70	50	50
Wilson	70	60	70	80	140	180	170	130	90	60	60	70
1500												
Dagoretti	100	90	90	100	130	160	150	130	100	90	80	90
JKIA	60	70	70	80	110	160	140	120	110	80	70	60
Wilson	80	80	70	90	120	160	130	110	100	70	70	70
1800												
Dagoretti	80	80	90	90	120	120	100	100	100	90	90	80
JKIA	80	70	70	70	110	90	90	90	90	80	70	60
Wilson	70	70	80	80	120	90	90	90	90	80	70	70
2100												
Dagoretti	80	110	140	160	170	170	170	170	170	150	130	120
JKIA	70	60	70	60	110	60	70	80	90	70	60	60
Wilson	-	-	-	-	-	-	-	-	-	-	-	-

NB *** indicates calm conditions.
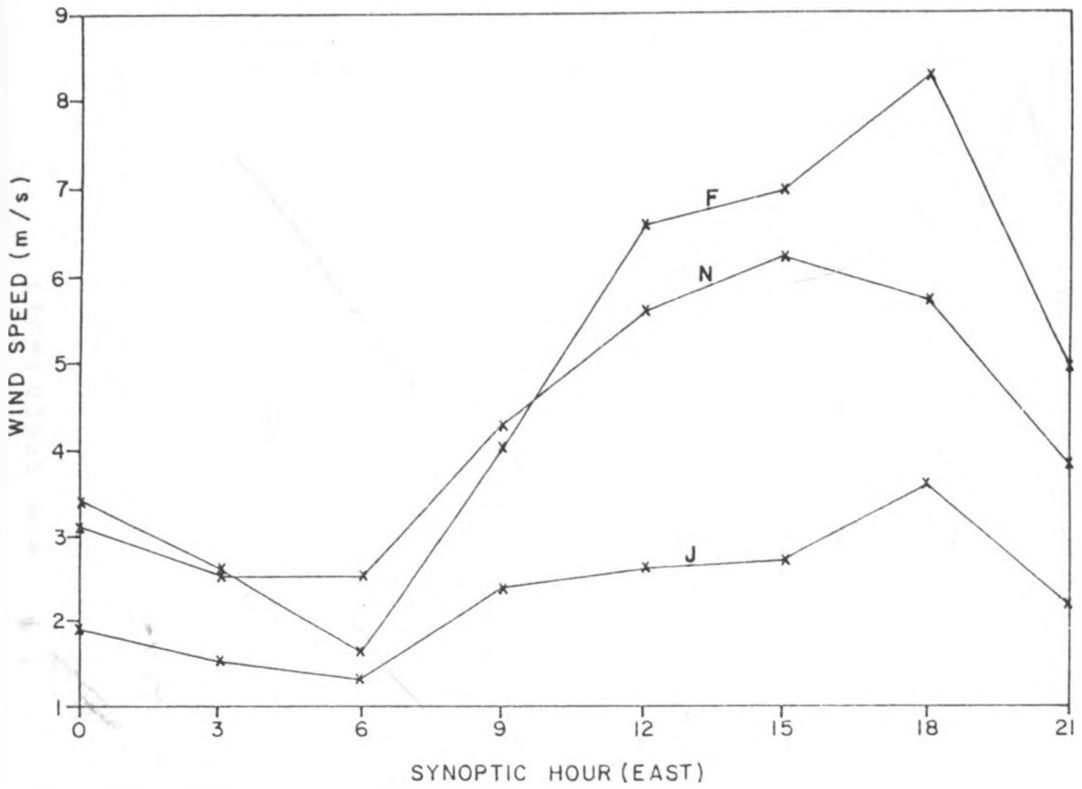   JKIA = Jomo Kenyatta International Airport
   Hr. = EAST

FIG. 4.1 : DAILY VARIATION OF WIND SPEED (m/s) AT JOMO KENYATTA FOR FEBRUARY (F), JUNE (J) AND NOVEMBER (N)
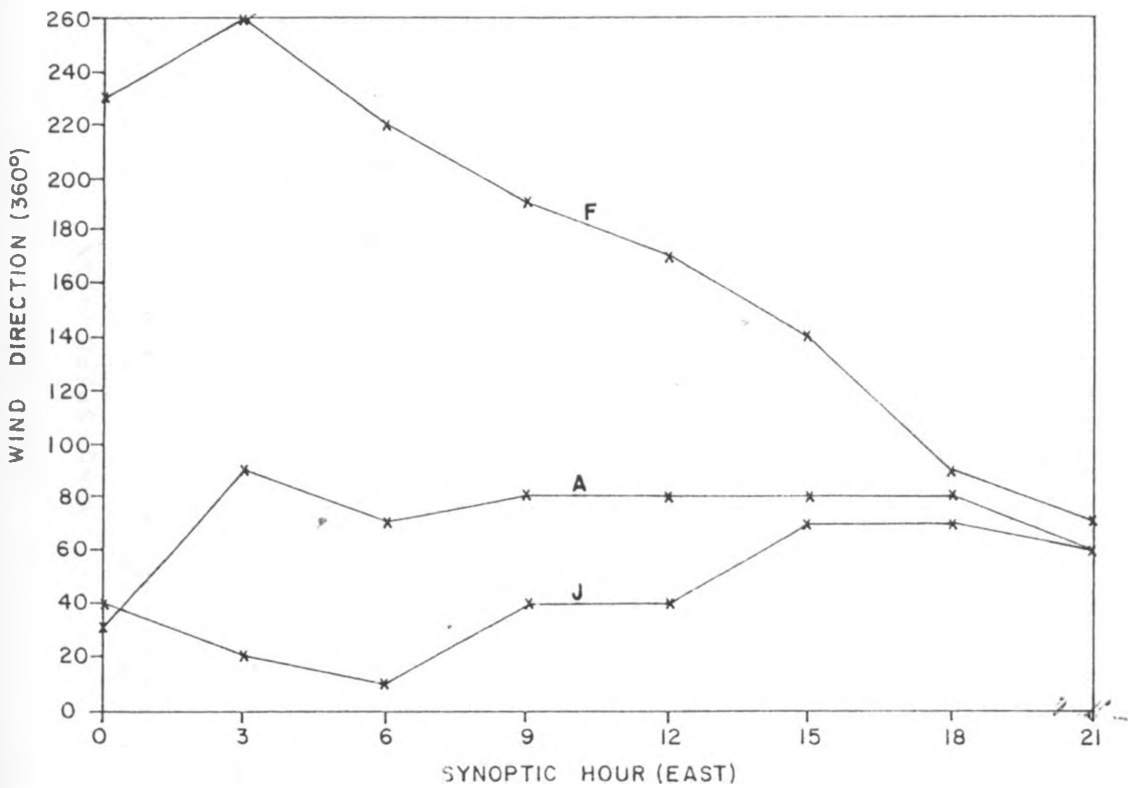

FIG. 4.2 : DAILY VARIATION OF WIND DIRECTION (360°) AT JOMO KENYATTA FOR FEBRUARY(F), APRIL(A) AND JULY (J)
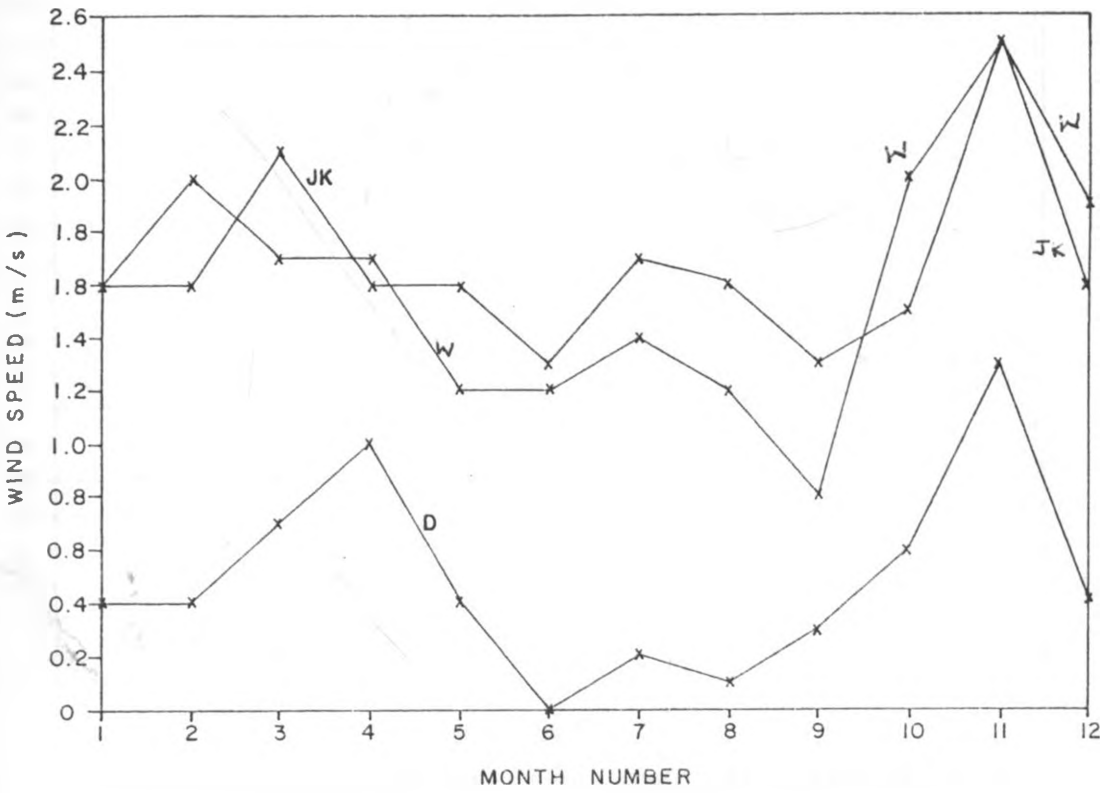
FIG. 4.3a : SEASONAL WIND SPEEDS (m/s) AT 0600 EAST FOR
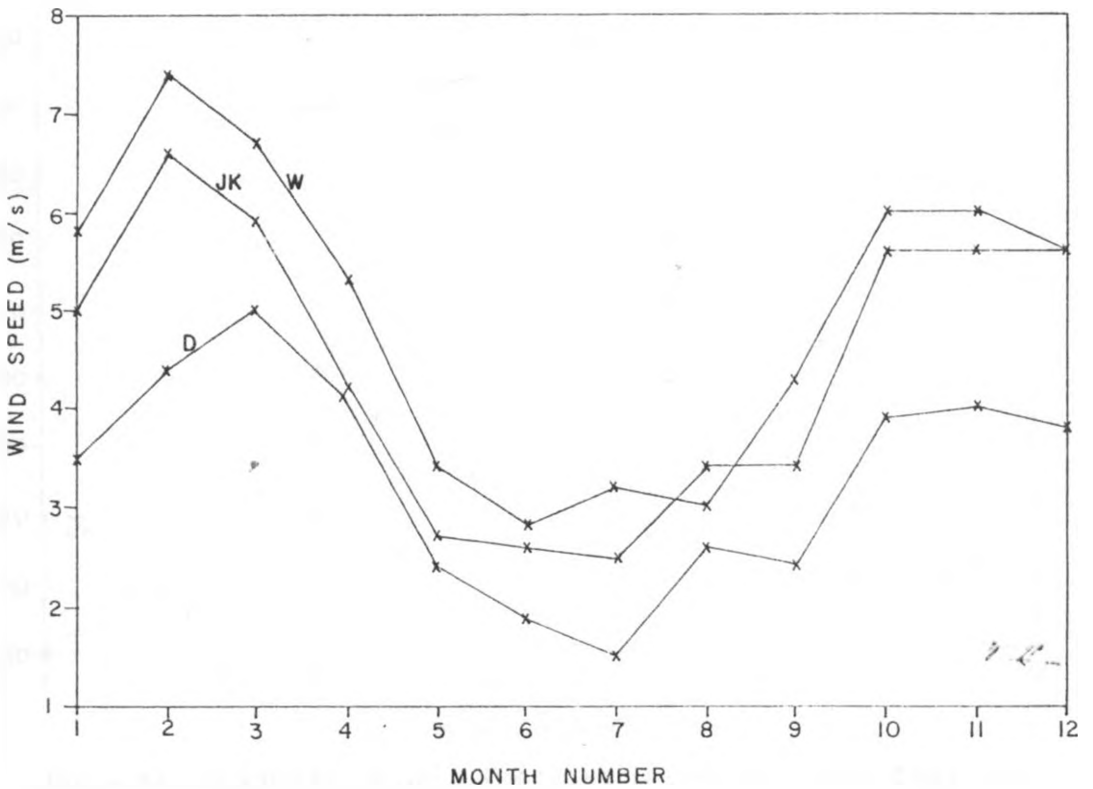JOMO KENYATTA (JK), DAGORETTI (D) AND WILSON (W)

FIG. 4.3b : SEASONAL WIND SPEEDS (m/s) AT 1200 EAST FOR
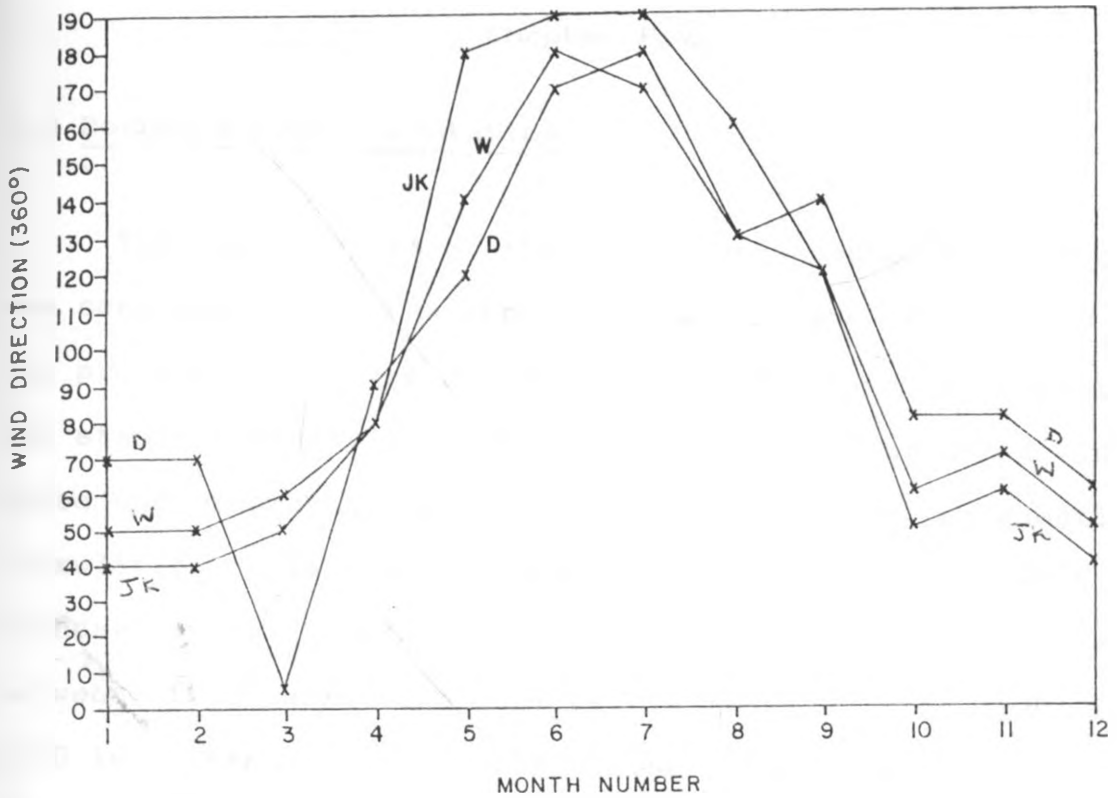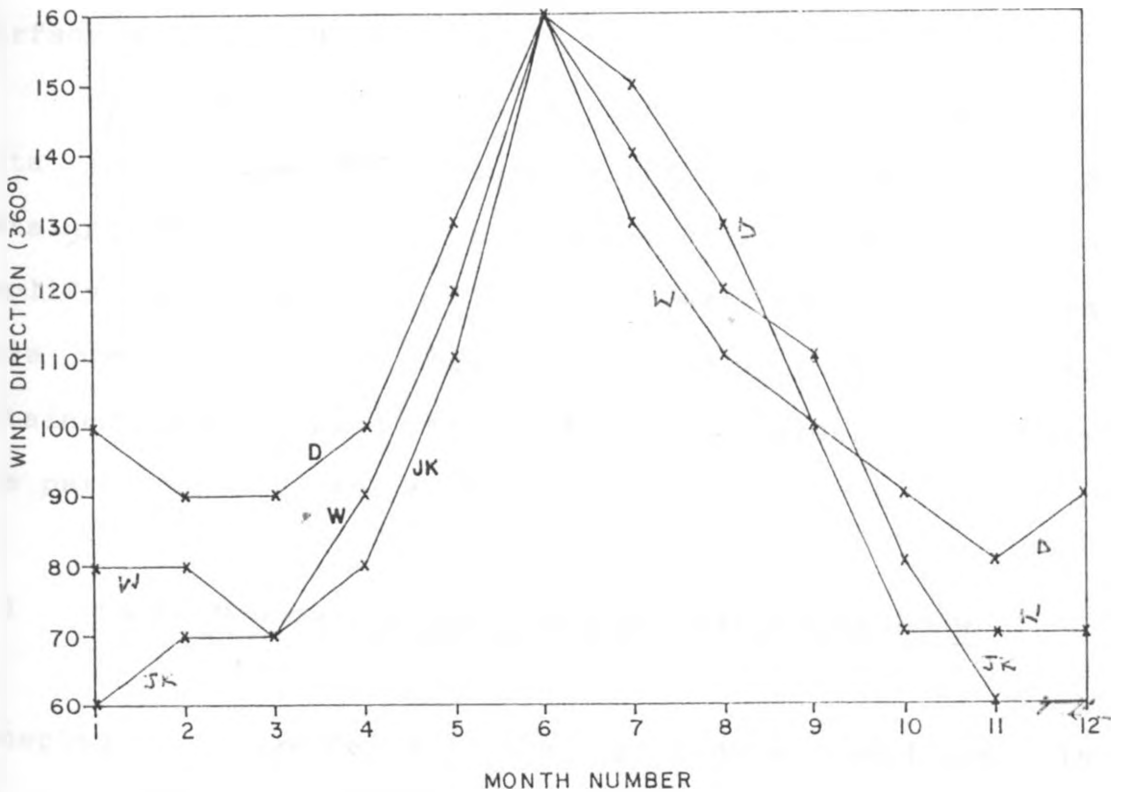JOMO KENYATTA (JK), DAGORETTI (D) AND WILSON (W)

FIG. 4.3c : SEASONAL WIND DIRECTIONS (360°) AT 0900 EAST FOR
JOMO KENYATTA (JK), DAGORETTI (D) AND WILSON (W)

FIG. 4.3d : SEASONAL WIND DIRECTIONS (360°) AT 1500 EAST FOR
JOMO KENYATTA (JK), DAGORETTI (D) AND WILSON (W)

Chapter Five

5.0 Boundary Layer Simulation

The daily cycle of the planetary boundary layer was computed using the approach taken by Abu Bakr (1988). The procedure involves a diagnostic formulation to compute the stable boundary layer at every synoptic hour using wind speed and temperature observed at the hour. A prognostic formulation is employed in simulating the daytime unstable boundary layer. Stable conditions were assumed to exist between after sunset and just before sunrise, from 2100 to 0600 local time (LT.). Unstable conditions range from 0700 to 1800 LT., and one-hour intervals in the transition periods at sunrise and sunset were taken to represent near-neutral conditions. The sun rises in Nairobi between 0600 and 0700 LT. so that truly unstable conditions at the surface occur an hour later.

One advantage of using observed data over predicted data in numerical experiments is that the actual state is obtained. Many estimation errors are eliminated that would amplify with time if wholly or partially generated values were used. These can then be compared with the results obtained from the prediction analyses in order to verify the performance of the model employed.

5.1 Stable Boundary Layer Computational Formulation

Accepted universally, the procedure employed in computing the thickness of a thermally stratified stable boundary layer, H_N, (see Caughey et al, 1979)

incorporates the friction wind U_*, the Monin-Obukhov scale length, L, and the coriolis parameter, f. The depth in metres is given by

$$H_N = c \left[\frac{U_* L}{f} \right]^{1/2} \tag{5.1.1}$$

with the parameters in SI units. where c is a constant of proportionality whose magnitude has been given variously between 0.2 and 0.7 (Pasquill and Smith, 1983).

Now the equation cannot be applied at the equator, where the coriolis parameter vanishes. Very close to the equator, the beta-plane approximation could be applied in order to include the effects of the earth's rotation. Far away from the equator, the suppression on the depth due to the rotation of the earth increases. Equation 5.1.1 was used in this form at $1.3°S$, the average latitude along which the data stations are located. A low value of f implies that the adjustment on the depth of the layer resulting from the earth's rotation is minimal. The result obtained strongly depends on the choice of the constant c. The constant was taken to be c=0.2, which is the lower limit of the empirically derived range. This choice was made so that the computed values conform to the expected diurnal cycle when the calculated mixing heights for stable conditions are exceptionally high, so as to agree with the daytime estimates. This is the case when the wind speeds after sunset are exceedingly high. A constant value was used throughout the analyses. Equation 5.1.1 becomes,

$$H_N \cong 110 \ (U_* L)^{1/2} \qquad\qquad (5.1.2)$$

The Monin-Obukhov parameter, L, for stable conditions is given for any temperature T_a at screen height and friction wind U_* at the anemometer height by

$$L = \frac{T_a \ U_*^{\ 2}}{g \varkappa T_*} \qquad\qquad (5.1.3)$$

with $g=9.81ms^{-2}$ and $\varkappa=0.41$ denoting respectively the acceleration due to gravity and the Von Karman constant.

The friction temperature, T_*, is given by

$$T_* = \frac{-Q_H}{\rho_a C_p U_*} \qquad\qquad (5.1.4)$$

where $\rho_a = 1.21kg/m^3$ is the density of air and $C_p = 1004$ J/kg/K is the specific heat capacity of air at constant pressure. Q_H stands for the sensible heat flux at the surface. In the absence of sensible heat flux, the friction temperature has previously been estimated for a prairie grass region to have a value of 0.08K using vertical profiles of temperature and wind velocity (Venkatram, 1979). This figure is based on the fact that for nighttime conditions, Q_H and U_* are directly correlated, and the downward heat flux decreases with time during the night in almost direct proportion to the decrease in the friction wind.

While using a constant value of T_*, one assumes that its variation during the night is within a small range. Definitely, the prevailing weather may appreciably change

the correlation between Q_H and U_*. Precipitation, for instance, may alter the turbulent temperature scale through intricate processes such as latent heat release or absorption during condensation or evaporation. Cloud cover generally increases the heat flux at the surface by preventing the possible loss of terrestrial radiation. Abu Bakr (1988) found that T_* over the Sahara varies between 0.07 ± 0.05. Sudan is predominantly semi-arid with a low frequency of cloudiness.

The friction velocity in the stably stratified layer for wind speed U_a measured at the anemometer height z_a is given by the relationship (Venkatram, 1979)

$$U_* = U_a \varkappa \left[\ln \frac{Z_a}{Z_o} + 4.7 \frac{Z_a}{L} \right]^{-1} \qquad (5.1.5)$$

where $\varkappa = 0.41$ is the Von Karman constant. Z_0 is the roughness parameter. Substituting for L from equation 5.1.3, we obtain a quadratic equation for the friction wind velocity given by,

$$U_* = \frac{1}{2\xi_1} \left[\xi_2 \overset{+}{-} (\xi_2^2 - 4\xi_1\xi_3)^{1/2} \right] \qquad (5.1.6)$$

where $\xi_1 = \ln\left[\frac{z_a}{z_o}\right]$

$\xi_2 = U_a \varkappa$

$\xi_3 = 4.7\varkappa g Z_a T_*/T_a$

Equation 5.1.6 is only applicable if the term under the radical sign is non-negative. Depending on the values chosen for T_* and Z_0 and the observed screen height air

temperature T_a, the wind speed should be about or greater than 2m/s. In Nairobi, the wind speeds are quite low in the morning transition hours just before sunrise. The lowest values are found in the western sector of the domain due to the topography. The values, on averaging, are hardly above 2m/s in the early morning. But for a narrow, highly viscous band close to the surface, the surface boundary layer hardly ever has a neutral stratification. Purely neutral conditions require very high winds and no buoyancy effects. From Prandtl's theory (Sutton, 1953), the friction velocity is given for neutral conditions by

$$U_* = U_a \varkappa \left[\ln \frac{Z_a}{Z_o} \right]^{-1} \qquad (5.1.7)$$

which, apart from the term under the radical sign, is similar to but twice equation 5.1.6.

Equation 5.1.6 has two roots. The positive square root was used in this study as it gave results that were consistent with the generally expected cycle of the nocturnal boundary layer. Near-neutral conditions occur in the morning transition hours.

When equation (5.1.3), with T_* substituted, is solved simultaneously with equation (5.1.5), both the friction wind, U_*, and the Monin-Obukhov scale length, L, are obtained iteratively. This is achieved by assigning a starting value to L (say L=5) and proceeding with the iteration until a desired accuracy is obtained for U_*. This procedure was applied in computing the friction wind for the transition period and the result compared with the value obtained by the alternative method of equation 5.1.6.

The approach could not be used throughout the night for lack of soil temperature data which is necessary for computing the sensible heat flux, Q_H.

The roughness parameter Z_0 has been estimated over a wide range by various authors for regions with similar roughness elements (compare Brown, 1974; Lumley and Panofsky, 1930; Fleagle and Businger, 1918). A region with sparse vegetation has the value given from 0.1 to 0.4m, while urban, mountainous or densely forested areas have been estimated to have the parameter from 0.4 to over 10m. These wide ranges require that actual values be obtained over a region of study, a procedure that requires expensive, highly sensitive instrumentation. In fact, Z_0 depends strongly on the slope of terrain and the direction of flow: whether into or away from the features concerned.

The friction velocity was computed using different values of the roughness parameter and turbulent temperature scale, as the two are both empirically derived, their accuracy being strongly affected by the locality. The values used for Z_0 range from 0.2 for the stations located east of the domain, to 0.4 and above, for westward stations, depending on the surface features. T_* was used in different experiments between 0.02 and 0.12.

5.2 Unstable Planetary Boundary Layer Modelling

Buoyancy during daytime is favoured by the unstable thermal stratification. Thermals produced by surface heating ascend until halted by some mechanism which may be

a synoptic system or changing intrinsic or extrinsic properties of the warmer air parcel. The model used here is based upon the concept of the expected dynamics in an unstable boundary layer capped by an upper level inversion in which vertical eddy fluxes are halted by the stability of the air aloft according to Tenneke's (1973) argument.

The strength of the elevated inversion influences the stoppage of the ascending eddy in that strong inversions rapidly halt the vertical motion. A weak inversion weakly affects the ascent of the vertical fluxes of heat, moisture and momentum.

Heat exchange occurs at the interface between the mixed layer and the stable layer above. Consequently in the mixed layer, turbulent heat flux shows a linear variation between the surface layer and the inversion: the two source levels (Abu Bakr, 1988).

The model is adopted from Van Dop et al's (1982) version designed for computing the depth of the boundary layer for a convectively mixed layer characterised by a linearly decreasing vapour density profile, constant potential temperature and wind velocity in the vertical as depicted in figure 3.3. The flux of sensible heat is assumed to decrease linearly up to the base of the potential temperature inversion. The heat flux becomes negative in the top most 10% of the mixed layer (below the inversion base) as shown in figure 3.1b. Additional changes in the vertical heat structure that could result from radiative heat release or absorption, latent heat release or absorption, and other heating processes, are neglected. It is to be expected that the presence of dense

convective cloud cover and the presence of radiative elements can significantly complicate the Thermal structure. This property should be included in "event" modelling (day to day basis), but may not adversely affect time averaged climatological analyses. The model's development is described in detail by Abu Bakr (1988). and the reader is referred to this source for more detail.

Further assumptions in the model include uniformity of the parameters in space over the region having the dimensions of a rectangular box. The air should be incompressible across the slab. The model was developed for cloudless skies. Cloud cover may lower the boundary-layer depth by reducing the in-coming short wave radiation and subsequently the surface sensible heat flux. Deep cumulus convection allows the fluxes to penetrate to much higher levels. The model may predict higher or lower values for seasons when the above conditions prevail. The prognostic equation is given by

$$H_D(t + \Delta t) = H_D(t) + \frac{\partial H_D}{\partial t} \Delta t \qquad (5.2.1)$$

where the daytime mixing height, H_D, is computed at time steps, Δt, for any future time. Subsequent predictions based on previous heights are computed sequentially.

The equation requires a starting value of H_D in the morning hours and progressively estimates the diurnal growth by incorporating the variations of heat and momentum fluxes. The starting value of the mixing height was taken to be the value obtained in the morning transition period using the equation for the stable

boundary layer (5.1.2). This period was assumed to occur between 0600 and 0700 LT. throughout the study. Obviously, the transition changes from month to month. These alterations are however small for an equatorial region. The time step was taken to be three hours (10800s). To account for the small changes in the morning period before the meteorological parameters adjust themselves to a steady state, it was essential to include two more hours between 0600 and 0900; at 0700 and 0800 EAST, so that the time step is one-hour for this intervening period. This was necessary as a leap from 0600 to 0900 EAST produced large numerical errors.

The partial rate of change (or growth rate) of the unstable boundary layer depth is given by

$$\frac{\partial H_D}{\partial t} = \frac{(\overline{\theta \omega})_o [1 + 2c_1(1+\chi^2)]}{H_D \phi (1-\chi)} \qquad (5.2.2)$$

where $\chi = \dfrac{c_2 \varkappa L}{c_1 H_D}$,

and c_1 and c_2 are empirical constants such that $c_1 = 0.2$ and $c_2 = 5.0$; $\varkappa = 0.41$ is the Von Karman constant, and L is the Monin-Obukhov scale length. The inversion strength, or the gradient of potential temperature above the inversion is obtained using equation 5.2.3

$$\phi \equiv \frac{\partial \theta}{\partial Z} = \left(\frac{P_0}{P}\right)^{R_d/C_p} (\Gamma_d - \gamma) \qquad (5.2.3)$$

where $R_d = 0.286$ is the dry gas constant and $C_p = 1004$ J/kgK is the specific heat capacity of air

at constant pressure. P_0= 1000hPa is the standard pressure, and P is the pressure at the inversion base. Γ_d= 9.8×10^{-3}K/m is the dry adiabatic lapse rate. The gradient of air temperature above the inversion base, $\gamma = -\dfrac{\partial T}{\partial Z}$ is obtained from radiosonde data. To determine the inversion strength, daily profiles of moisture and temperature from Te-Phi gram plots were analysed to determine the inversion base. The gradient of potential temperature above the lowest upper level inversion was then computed using (5.2.3). On those occasions when no distinct temperature inversion was observed, the lowest positive change (increase) in the gradient of the temperature profile (which in some cases coincided with a negative change, or decrease, of the relative humidity profile) was used to define the potential temperature inversion base and for computing the inversion strength. This procedure was used for both day and night conditions for a period of one year, and thereafter averaged per month. The procedure was repeated for a neighbouring year, 1977, in order to estimate missing data for the months of January, February and March. Estimation was done by the method of the ratio of means.

Across the whole domain of study, radiosonde data is only available at one station (Dagoretti) which is on the western side of the region at an elevation of 1795m above mean sea level (AMSL). The other stations considered are Wilson at 1679m AMSL, 9km east of south east of Dagoretti, and Jomo Kenyatta at 1624m AMSL, 18km east of Dagoretti. It

was assumed that the inversion strength was the same for all the three stations, and the value computed at the radiosonde station was representative for the whole domain. It is possible, though that close to the urban centre the temperature structure in the vertical can be altered.

Again the inversion strength can be expected to vary as a function of time in accordance with the changing weather parameters: mainly the surface insolation and the advection field. Though the depth of the inversion diminishes in the lower layers as the day advances, the potential temperature gradient in the upper levels does not vary much for stationary and quasi-stationary climates (Abu Bakr, 1988) The climate of Nairobi is not stationary. Diurnal as well as seasonal changes occur in both local and synoptic fields.

An attempt to account for daily variations of the inversion strength is hampered when only two recordings are made during he day's 24-hour period. Inclusion of diurnal effects was made on the delicate assumption of a linear variation between the 0200 local time (LT.) ascent, through the 1400LT. sounding, up to the evening transition period. This is the only non-subjective method that could be applied to incorporate the changes over the daytime cycle, and may be closer to the actual state than by assuming a constant value. In any case, the difference between the day and night observed values of the inversion strength ϕ was very slight for months with no rainfall.

The kinematic heat flux at the surface ($\overline{\theta w}$)$_0$ was obtained from the turbulent flux density of

sensible heat at the surface, Q_H, given by applying the formula

$$(\overline{\theta w})_o = \frac{Q_H}{\rho_a C_p} \qquad (5.2.4)$$

where the air density and specific heat capacity at constant pressure have the values given in the previous section (5.2). Q_H was got from the energy balance equation in its approximate form,

$$Q_H \cong R_N - Q_g \qquad (5.2.5)$$

with the moisture heat flux Q_E ignored. R_N and Q_g respectively stand for the net radiation and the ground heat flux. The net radiation is the difference between the net incoming short wave radiation S_N, and the net outgoing long wave radiation, L_N. S_N was obtained from the measured global radiation S_g using the relationship

$$S_N = (1 - A) S_g \qquad (5.2.6)$$

where A is the surface albedo. S_g was obtained from Moll-Gorczynski solarimeter measurements. A, the surface albedo, was taken for different experiments between 0.3 and 0.1. The diurnal variation of albedo (Mwingira, 1980) was also incorporated for scientific consistency The value of A is a minimum at about midday (figure 5.1).

The net outgoing long wave radiation was obtained from an empirical equation for cloudless conditions such that,

$$L_N = \varepsilon_s \sigma T_a^{\,4} \, [1 - (a + b\sqrt{e})] \tag{5.2.7}$$

The Stefan-Boltzmann constant σ was taken to be 5.74×10^{-8} $W/m^2 K^4$. The emissivity of the surface has the value $\varepsilon_s = 0.98 \cong 1$; $a = 0.61$, $b = 0.05$ are empirical constants. The vapour pressure, e, was determined from relative humidity, R.H, using

$$e = e_s(T_a) \times R.H \tag{5.2.8}$$

where the saturation vapour pressure, $e_s(T_a)$, was obtained from Smithsonian Meteorological tables. The expression (5.2.7) may predict lower values for cloudy skies, but it accounts for the moisture content in the atmosphere. The ground heat flux, Q_g, was obtained from the equation of thermal conduction in the soil

$$Q_g = -K_{HS} C_s \, \frac{\partial \bar{T}}{\partial z} g \tag{5.2.9}$$

where K_{HS} is the thermal diffusivity of a soil, and C_s is the soil's volumetric thermal capacity. The product of K_{HS} and C_s is λ, the soil's thermal conduction, and the negative sign refers to the decrease in thermal capacity when heat loss occurs from the soil during the night. For a clay soil with 40% pore space, C_s varies between 1.42 and 3.1 $MJ/m^3 K$ respectively for dry and saturated soils; and K_{HS} ranges from 0.18×10^{-6} to 0.51×10^{-6} m^2/s respectively for dry and saturated conditions (Oke, 1987). Soils in Nairobi which are mainly of clay type are usually dry except during the two rainy seasons when

they are persistently wet.

Soil temperatures are measured at three depths: 5cm, 10cm and 20cm for 1200 and 1600 local time (LT.), except at 0800LT. when measurements are taken for lower depths. The gradients used in equation (5.2.9) were calculated from values below the ground surface to allow for sufficiently stable conduction since values at the surface disallow this condition. Values at intervening levels were got using graphical methods, up to the surface level. Basing on the expected diurnal patterns (Oke, 1987 and figure 3.6), the average soil temperatures, $\bar{T}_g$ were interpolated and extrapolated for various depths by constructing curves using the values for the three hours, to give approximate gradients for the hours with no observations, before applying the finite difference form of equation (5.2.9). Though cumulative errors are likely to arise from the interpolation/extrapolation procedure which is likely to be subjective, the values were taken to be representative, considering the small magnitudes of the gradients obtained.

Equation 5.2.5 of the energy balance would also include the flux of latent heat, radiative terms and error terms for completeness. The most significant of these, the latent heat flux, intricately depends on the wind speed, the amount of moisture in the atmosphere, net radiation and diffusivity. The latent heat flux has been estimated for open water surfaces using hydrological considerations which may overestimate or underestimate the heat flux adversely for land areas (Priestley, 1959). Now a loss of heat at the surface through latent heat effects is usually accompanied by
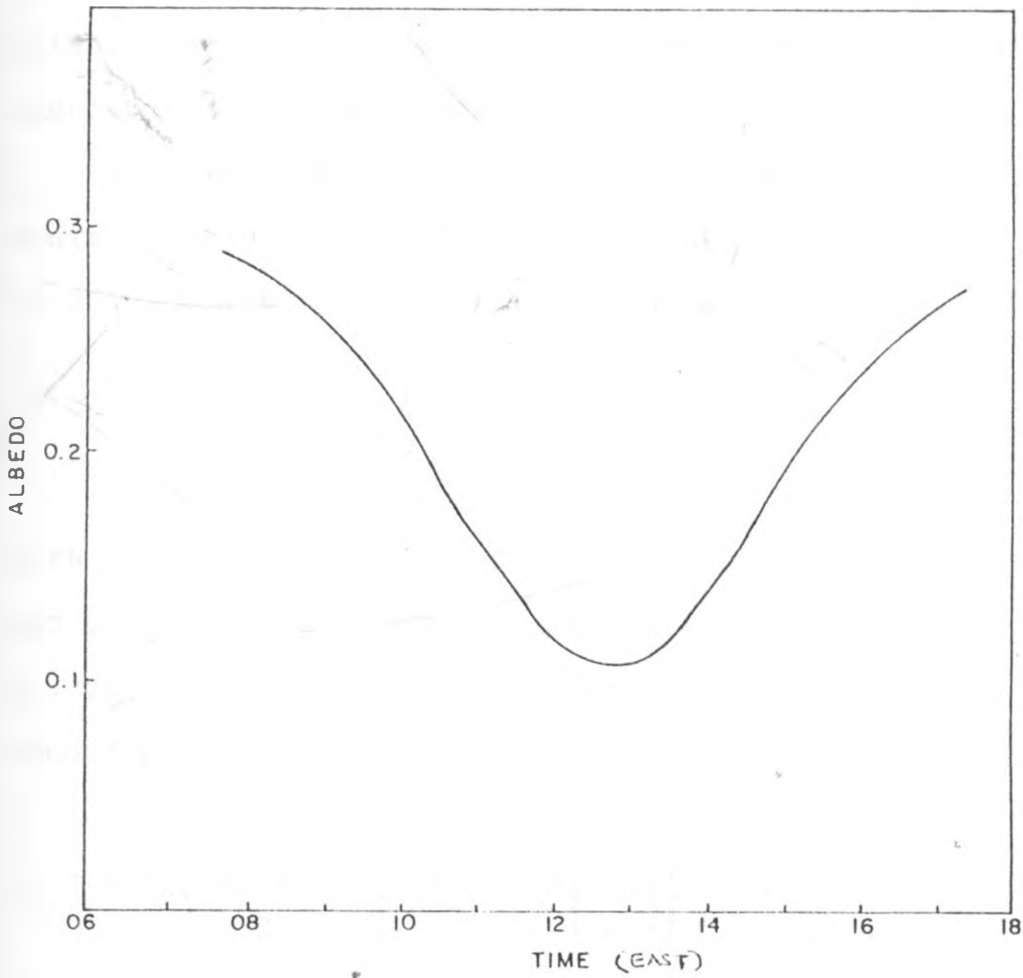
FIG. 5.1: DIURNAL CYCLE OF SURFACE ALBEDO (After Mwingira,1980)
for 1978

latent heat release through condensation processes at higher levels. The requirement for the model of a constant gradient of the kinematic heat flux throughout the mixing layer partially annuls latent heat effects. Even so, moisture effects are partly included in the computations of the net long wave radiation (5.2.7) and the ground heat flux (5.2.9). Intuitively, the inclusion of latent heat in planetary boundary layer models is bound to improve their accuracy. In the present model, latent heat effects at the surface would decrease the magnitude of computed results.

The remaining parameter in equation (5.2.2), the Monin-Obukhov scale length, L, was got from equation (5.2.10) below (see Priestly, 1959, for instance)

$$L = \frac{-\rho C_p U_*^3}{\varkappa\, Q_H\, g/T_a} \qquad\qquad (5.2.10)$$

with the symbols as defined earlier in section 5.1, and g/T_a being a buoyancy parameter. The friction wind, U_*, is given for the anemometer level, Z_a for unstable conditions (Panofsky, 1963) by a

$$U_* = \varkappa\, U_a \left\{ \ln \frac{Z_a}{Z_o} - \psi\left(\frac{Z_a}{L}\right) + \psi\left(\frac{Z_o}{L}\right) \right\}^{-1} \qquad\qquad (5.2.11)$$

with Z_o denoting the surface roughness aerodynamic measure. The last term in the brackets is usually small, but may be quite significant for regions marked by high surface features (Haltiner and Williams, 1980). Paulson (1970) gives the integration result by

$$\psi(Z/L) = 2 \ln \left(\frac{1 + x}{2}\right) + \ln \left(\frac{1 + x^2}{2}\right) - 2\tan^{-1}x + \pi/2$$

(5.2.12)

in which (Businger, 1971) $x = (1 - \gamma\frac{Z}{L})^{1/4}$, $\gamma = 15$. x has a non-complex solution if either L is negative or exceeds 150 (for $Z_a=10m$).

Equations (5.2.10) and (5.2.11) were solved simultaneously for L and U_*. Using measurements at 16m, values of z/L have been computed previously for idealised sites and conditions and lie between -0.005 and -5.0 (Pasquill and Smith, 1983). This is equivalent to the interval $-3200 \leq L \leq -3.2$. A value of L=-5.0 was chosen as the starting figure in the iterative process after Abu Bakr (1988). The iteration was stopped when the relative error in L was less than or equal to 1.26%. The diurnal variation of L is dictated by the magnitude of wind speed (U_*) and sensible heat flux (Q_H). The minimum values occur in the afternoon when surface insolation is maximum, but the highest values are expected to occur in the evening and morning transition hours.

5.3 Spatial Variations in the Boundary Layer Depth

A major assumption in calculating the depth of the planetary boundary layer is that the variables are uniform in space. However, this is most appropriate if the region under consideration is homogeneously flat. Whereas the mixing heights also depend on vegetation and the setting of urban structures, an equation to account for slopping terrain effects developed by Endlich et al (1982) to estimate the depth at remote regions was implemented to investigate terrain effects on horizontal flow. A modified basic equation gives the mixing height H at any height above mean sea level (AMSL) h by

$$H = H_a + k(h - h_a) \qquad (5.3.1)$$

where H_a is the temporal depth computed at a height h_a AMSL. The slope factor, k, varies in time between 0 and 1, depending on whether the boundary layer is flat or parallel to terrain, typical for night and day values respectively. Values in between give intermediate slopes. Values greater than one give slopes steeper than the terrain slope, and negative values give slopes opposite to terrain slopes. An analysis was performed using k=0.2 for nighttime and k=0.5 for daytime to predict the spatial characteristics resulting from terrain effects using values obtained in the previous sections' analyses.

Table 5.1: Monthly Mean Inversion Strengths (K/km) at 0200

and 1400 (EAST) at Dagoretti for 1986

Month/Hour	0200EAST	1400EAST for 1986
January	10.9	14.7
February	-	13.8
March	-	11.4
April	11.0	5.0
May	11.1	10.2
June	14.1	15.3
July	15.5	19.6
August	14.9	18.9
September	14.8	13.4
October	8.9	6.8
November	10.2	9.7
December	12.5	10.6

Table 5.2: Mean Diurnal Surface Albedo (After Mwingira, 1980)

for 1978

Local Time	Albedo
0900	0.28
1000	0.22
1100	0.15
1200	0.12
1300	0.10
1400	0.14
1500	0.18
1600	0.23
1700	0.26

5.4 **Planetary Boundary Layer Model Results**

Since the model used for simulating the daytime cycle of the
planetary boundary layer depth involves a 'jump' technique,
the early morning estimates greatly influence the results
obtained for the rest of the day. Low initial estimates imply
a greater 'leap' than when higher values are used. The leap
also depends on the other input parameters, mainly the
surface insolation and wind speed. The progressive growth by
convection currents of the mixing heights after the initial
jump as obtained from the modelling analyses had a rapid rate
from the late morning hours (0900EAST) before stabilising in
the late afternoon. This was a consequence of the diurnal
cycles of sensible heat and of wind speed given in table 4.1.

The highest growth rates could be noticed in April and
October, the two months that depicted outstandingly high
afternoon mixing heights as contrasted with the intervening
period from May to September, clearly because of the low
inversion strengths in the former. The mixing heights for
July and the adjacent months were particularly low as given
by the model, primarily because of the high inversion
strengths during this period. The rate of increase of the
model mixing heights, being definitely a result of the
daytime heating and the inherent wind speed pattern, was low
in the colder months but higher for the warmer period. The
influence of some input parameters is exemplified in figures
5.2a and 5.2b.

Model results for both the nocturnal/diurnal and
seasonal changes of the planetary boundary layer depths are
given for Jomo Kenyatta and Wilson in tables 5.3 and 5.4.
Some aspects are graphically portrayed in figures 5.3 and 5.4

for the nocturnal/diurnal and seasonal structures respectively. Except for April and October when convective clouds present destroy the elevated capping inversion, the results suggest a stoppage on the vertical flux that results from interactions between surface heating and the frictional drag force on the flow field by the elevated inversions. The kinematic heat flux increase as the day progresses favours buoyancy over mechanical stresses resulting in upward propagation.

Surface albedo only affects daytime computations. The formulation adopted here uses variable albedo after Mwingira (1980) where values as given in table 5.2 decrease to a minimum at midday before once again increasing upto sunset. Nevertheless, separate experiments performed assuming constant surface albedo showed a very slight change on the results. The use of 0.1 instead of 0.3 increased the maximum mixing heights at sunset by only about 1/12 of the heights for the warmer months and by just 1/8 for the colder period.

Calculated values of the soil heat fluxes from the measured temperature gradients were particularly low. Late afternoon values of the soil heat flux (when there is maximum net radiation) were just 7% of the incoming global radiation during the warmer period, as compared to 10% for the morning hours. Even lower values were evident for the colder months with the soil heat flux being only 1% and 0.5% of the global radiation respectively for the late afternoon and morning hours.

Daytime values for the inversion strengths as calculated from afternoon ascent data revealed an increase from 5.0K/km in April to 20.0K/km in July, before decreasing to a value of
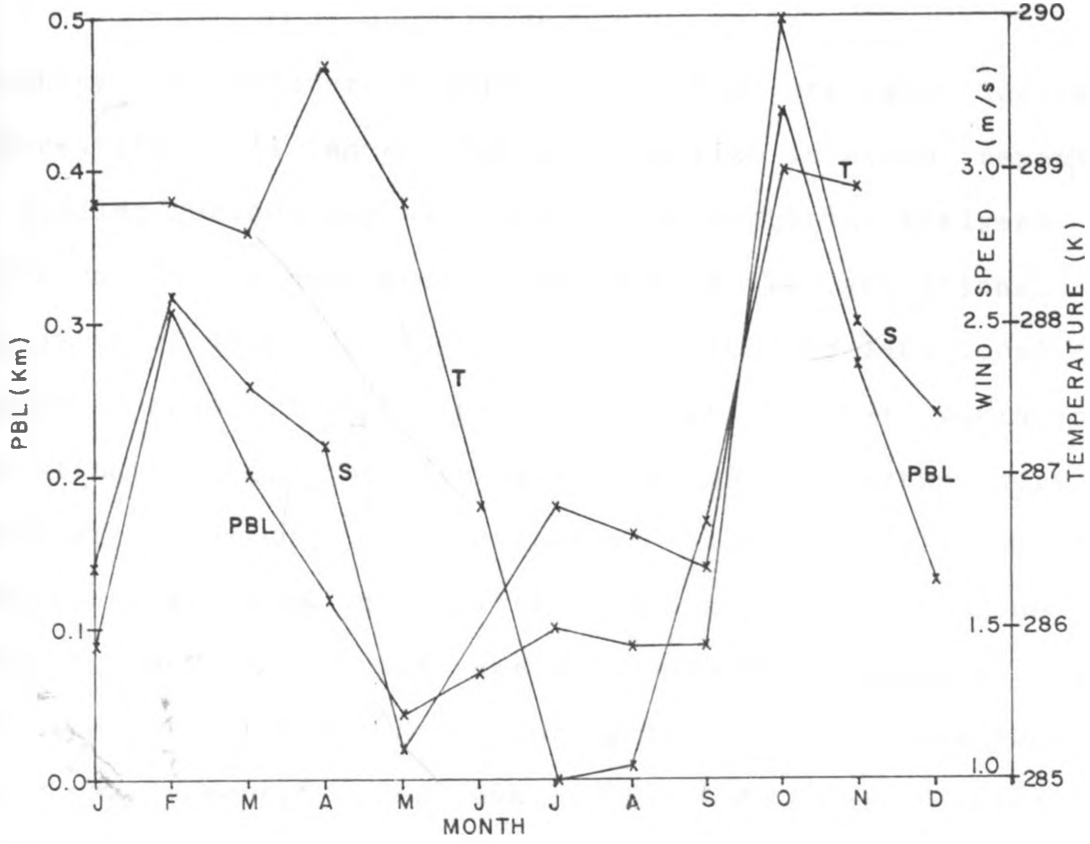
FIG. 5.2a: MONTHLY DEPENDENCE OF NIGHTTIME MODEL PBL DEPTH (Km) ON
SURFACE WIND SPEED(S) AND TEMPERATURE (T) AT JOMO KENYATTA
(0300LT) FOR 1986.
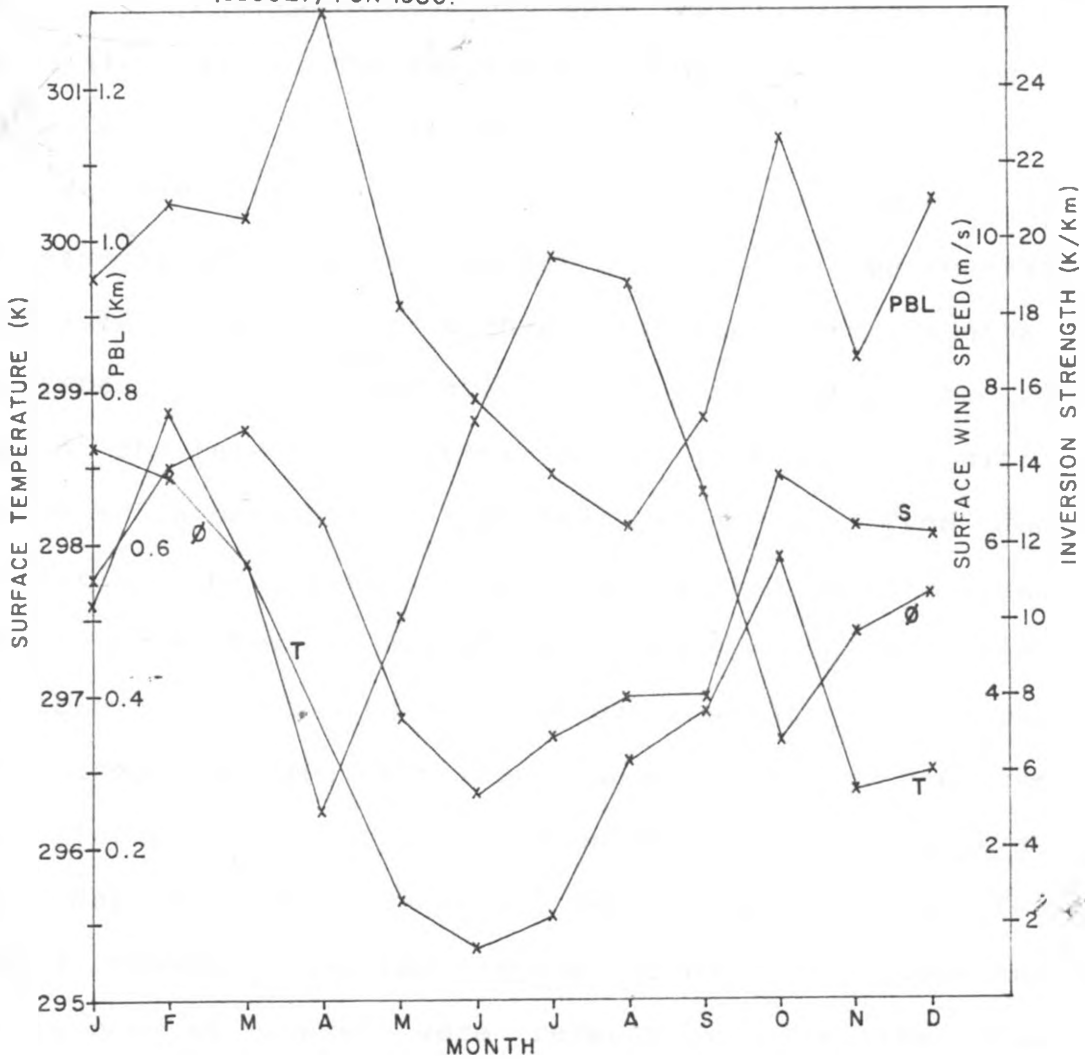
FIG. 5.2b: MONTHLY DEPENDENCE OF DAYTIME MODEL PBL DEPTH(Km) ON
SURFACE WIND SPEED(S) AND TEMPERATURE (T) AND POTENTIAL
TEMPERATURE INVERSION (∅) AT JOMO KENYATTA (1500LT) FOR 1986.

6.8K/km in October (table 5.1). The strength increased thereafter until January before a decline is again repeated. A similar periodicity was noticed for nighttime analyses but with a lesser magnitude of month to month variations. The handicap of lack of data between the 0200 and 1400 local time ascents made it impossible to deduce diurnal variations. Notwithstanding, the daytime inversion strengths were of greater magnitude than nighttime values in July, with a decrease in magnitude in the adjacent months of June and August, before the nighttime values became evidently higher for the rest of the months. During this period (June-August), a quasi-permanent upper level (700-600hPa) monsoon over the region produces strong inversions due to subsidence warming. Month to month variations are more amplified than those of the Hadley cell of the general circulation given by Abu Bakr (1988) within $15.5 \pm 1.7K/km$.

Whereas stable (nocturnal) boundary layer depths decrease steadily between sunset and sunrise, the decrease is remarkably rapid after midnight for the warmer months but persistently low throughout the night during the colder season. The rate of fall after sunset is consistent with the decrease in sensible heat stored, being higher from January to April, and from October to December, than during the period from May to August. At sunset, the now negative sensible heat flux within the inherent growth of the surface based inversion implies a reduction in buoyancy. Momentum and heat storage in the colder season was apparently weak during the day and was consequently depleted faster than for the warmer season after the evening transition. Quasi-neutral conditions at sunset were responsible for the evening retardation of the model boundary-layer growth rate as could

be deduced from the computed Monin-Obukhov scale lengths whose magnitude reflected neutrally stratified atmospheres. Near-neutral conditions were also noticed at sunrise. Results for this period (0600 - 0700EAST) gave low model results (table 5.3). Low wind speeds and low sensible heat left only a vestigial mixed layer and consequently a shallow boundary layer.

The choice of the turbulent scale of temperature, T_*, mainly affected nighttime computations and indirectly influenced daytime results through altering the estimates used as initial inputs. Basing on results obtained from the use of the standard value of 0.08, computations that utilised the upper limit of 0.12 - where an error of 0.05 is assumed (Abu Bakr, 1988) - deflated the nighttime model mixing heights by about 10%. Cases where the wind speed was too low and the radical part in the quadratic expression (5.1.6) was neglected were not affected by this alteration. This left the daytime model results virtually untampered with. Conversely, the use of the lower limit of 0.02 inflated the stable model boundary layer depths by between 10% at sunset and 50% at sunrise. The lower limit implies that the ratio of mechanical to buoyancy forces is higher than when the value of 0.08 is employed, a phenomenon that would be more appropriate at sunset. Intuitively, the upper limit is suitable as sunrise is approached.

The Von Karman constant in this work was taken to be 0.41. This was because the empirical constants were computed using this value. Nevertheless the use of the lower postulated value of 0.35 (Haltiner and Williams, 1980; Pasquill and Smith, 1983) barely affected the results.
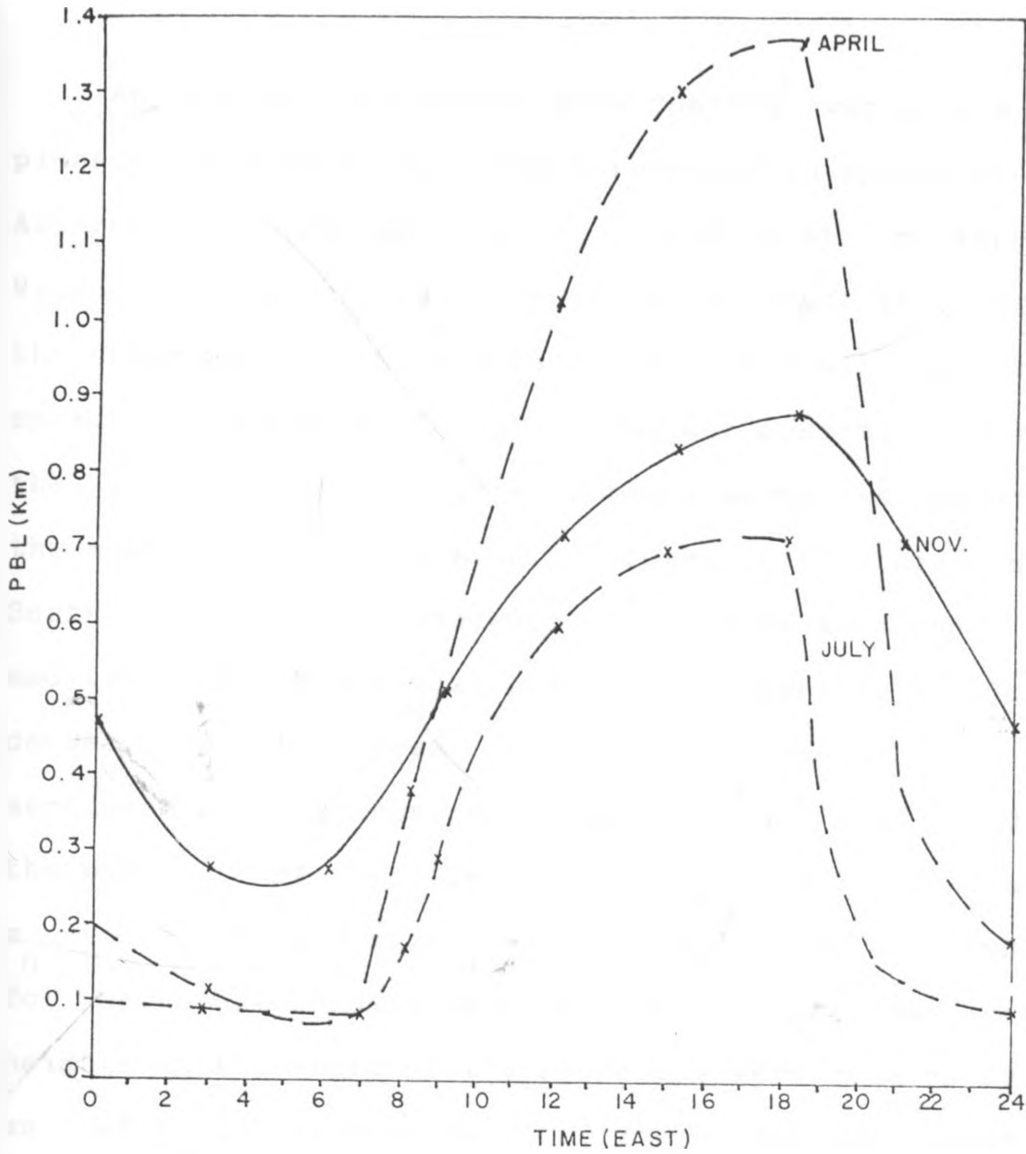
FIG. 5.3 : DAILY VARIATION OF MODEL PLANETARY BOUNDARY LAYER (P.B.L.) JULY, NOVEMBER AND APRIL.
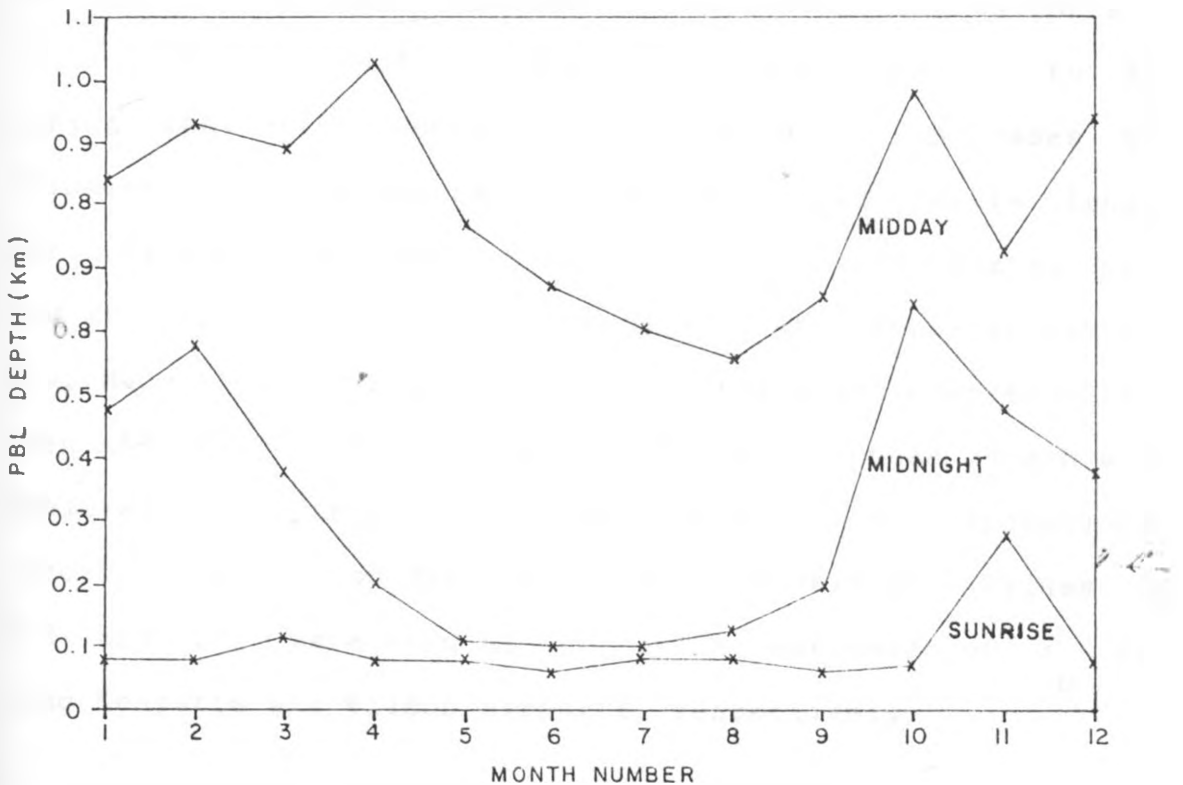
FIG. 5.4 : SEASONAL MODEL PLANETARY BOUNDARY LAYER (PBL) DEPTHS (Km) ABOVE THE SURFACE AT SUNRISE (0600EAST), MIDNIGHT

An attempt to investigate spatial variations of the planetary boundary layer depth revealed no specific pattern. Alternately high values were identified at Jomo Kenyatta and Wilson, but exceedingly low values at Dagoretti. Since all the other parameters were nearly the same with only the wind speed varying appreciably, it was not possible to establish the influence of terrain elevations alone, as deduced from the mean heights above mean sea level of the three stations. Surface roughness features played a more important role in modifying the model mixing heights. Dagoretti is close to a densely forested area. Different values of the surface aerodynamic roughness parameter, z_0, were used to determine the magnitude of the effect of surface features. A change of z_0 from 0.1 to 1.0 approximately tripled the computed depths for nocturnal conditions. Concurrently, the daytime mixing heights at the start of the prognosis were reduced by as much as 25% to 20% respectively for the colder and warmer months because of the morning "leap". Progressive computations, however, yielded higher values of the mixing heights for a Z_0 of 1.0 than of 0.1 by 10% for the colder season, to 50% during the warmer months. Greater friction increases the friction velocity and raises the Monin-Obukhov scale length for the same heat input. The high frequency of calm to very low wind speed at Dagoretti, especially when temperatures are low, made the unstable conditions in the model over-sensitive even when higher values than 1.0 of the roughness length were employed. For this reason and because of computational errors, results for Dagoretti have been omitted. Values of 0.2 and 0.25 were used as appropriate estimates of z_0 for Jomo Kenyatta and Wilson airports, respectively.

Table 5.3: Model Mixing Heights Above the Surface (m) at Jomo
           Kenyatta (1986)

Mth/Time	0000	0300	0600	0700	0800	0900	1200	1500	1800	2100
Jan.	476	87	79	94	421	548	842	955	988	748
Feb.	575	309	79	79	584	684	931	1053	1103	1116
Mar.	377	197	119	79	459	591	893	1032	1047	962
Apr.	199	119	79	94	380	522	1028	1308	1365	711
May.	111	45	79	65	305	420	765	914	948	241
Jun.	102	72	58	45	362	429	671	786	810	128
Jul.	102	102	86	94	179	294	600	693	719	128
Aug.	127	94	78	64	149	273	554	621	669	508
Sep.	196	86	58	86	241	340	650	761	819	542
Oct.	641	506	71	79	609	669	979	1125	1207	1112
Nov.	474	275	275	408	446	505	721	837	884	710
Dec.	377	128	79	58	660	727	938	1045	1077	779

Table 5.4: Model Mixing Heights (m) at Wilson (1986)

Month/Time	0600	0700	0800	0900	1200	1500	1800
January	86	94	555	646	881	986	1023
February	121	94	567	665	911	1035	1090
March	95	95	430	561	868	1019	1087
April	95	103	450	567	987	1276	1356
May	56	56	456	539	790	913	945
June	56	42	162	301	607	716	743
July	70	78	176	300	565	665	684
August	56	70	203	293	565	630	689
September	42	63	370	434	659	757	841
October	120	236	330	465	910	1077	1184
November	314	456	505	564	763	874	925
December	112	86	435	528	804	927	990

5.5 Diagnostic Consistency Checking Procedure

In meteorology, results from modelling exercises have to be compared with the actual, observed situation in order to test the accuracy of the computations. From the available upper air data at 0200 and 1400EAST, the stable and unstable planetary boundary layer depths so estimated should, by induction, roughly give the model´s consistency for the rest of the hours when no observations are available. Estimation schemes were not employed in sensitivity testing in cases of missing data as this could nullify the intended objective. To test the sensitivity of the nocturnal boundary layer computations, the early morning (0200EAST) radiosonde ascent data was used. The depth is the zone within which the surface sensible heat flux is significant (figure 3.2) usually resulting in low level wind maxima at the top of the inversion layer in wavy oscillations (Oke, 1987). Clarke (1970) suggested that the height of the wind maxima could be used to estimate the mixing height. More recent studies indicate the height to be about four-fifths of the level of the wind maxima (Beyrich and Klose, 1988). Using daily data, the average level of the wind maxima was estimated per month.

The level at which humidity assumes a decreasing lapse rate profile is the level of the potential temperature inversion and may be taken to represent the height of the diurnal boundary layer. Deardoff (1972) estimated the average mixing height to be in the middle of the transition layer of the humidity and potential temperature profiles: between the base and top of the inversion. The average heights of the lowest elevated inversion of the potential temperature and lapse profile of humidity, were calculated per month to give

an estimate of the mixing height.

5.6 Sensitivity Testing Results and Discussions

Estimated mean heights of the base of potential temperature inversion (or inversion base) and the level of change of gradient of relative humidity (or relative humidity maxima) were higher than the projected results from the model. For unstable conditions, the biggest difference was in the months of July and August (figure 5.5a). The inversion base was higher than the level of relative humidity maxima by between 100m and 500m, while the latter was in turn at a higher elevation than the low-level negative change of the profile of wind speed (figure 3.3b) by between 12% and 36% except for April, September and December when the relative humidity maxima was lower by respectively 210m, 160m, and 70m. Model results agreed with the estimated height from the wind profile for April and May (table 5.6) but differed by between 60m and 100m for June, October, November and December. The most significant differences between simulated heights and heights from the profile of wind speed occurred in the period from July to September when differences greater than 200m were identified (figure 5.5a). Whereas seasonal variations could be noticed in the values obtained from the three profiles, the heights of the inversion base of potential temperature and relative humidity maxima tended to deviate from the expected pattern as given by the model in the month of August. Even so, the seasonal pattern of the heights obtained from the wind speed profile resembled that given by the model to a reasonable degree.

Low model estimates of the unstable planetary boundary

layer depth for July, August and September as compared to the estimates from the observed profiles are definitely because of the large magnitudes of the inversion strengths and low kinematic heat flux during these months. This is due to the assumption in the model that the inversions are purely determined by processes at the surface. In these months the inversions are due to strong upper level subsidence warming. Months with lower inversion strengths gave model heights that agreed approximately with the observed.

The seasonal cycle of the estimated heights is an indication of coupling between the surface parameters and the rest of the boundary layer. This is shown by the heights estimated in the colder period when low wind speeds and temperature are recorded at the surface. It is evident that the vertical transfer of fluxes of momentum, moisture and heat occur at different rates and by different mechanisms. Much as coupling forces are the major processes involved in modifying the vertical wind structure, moisture transport could in addition be influenced by thermal changes due to latent heat release or absorption within the ascending parcels. This is deduced from the estimates for August (cold and moist) and October (warm and moist) both of which are high. The anomalously low altitude at which relative humidity maxima occurs for April makes it difficult to establish the impact of cumulus convection which is expected to dominate the wet month. As it is an episodic phenomenon, the effect of rainfall in the developing mixing heights cannot be fully accounted for.

It is possible that the coarse, epitomised nature of profile data affected the estimated mean mixing heights. The lofty heights of the potential temperature inversions could
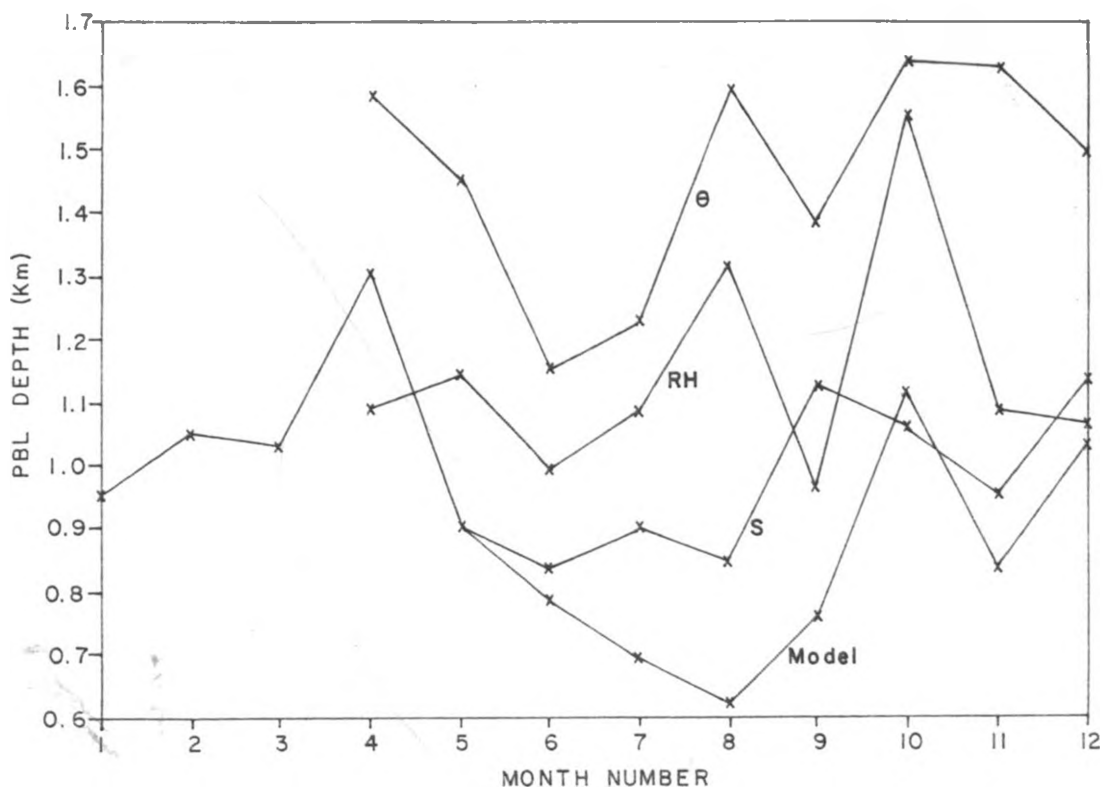
FIG. 5.5a : MEAN MONTHLY DAYTIME HEIGHTS (Km) OF ELEVATED POTENTIAL
TEMPERATURE INVERSION (θ), RELATIVE HUMIDITY MAXIMA (RH),
AND SIGNIFICANT WIND SPEED DECREASE (S) AT 1400 LT
(MODEL AT 1500LT) AT JOMO KENYATTA FOR 1986
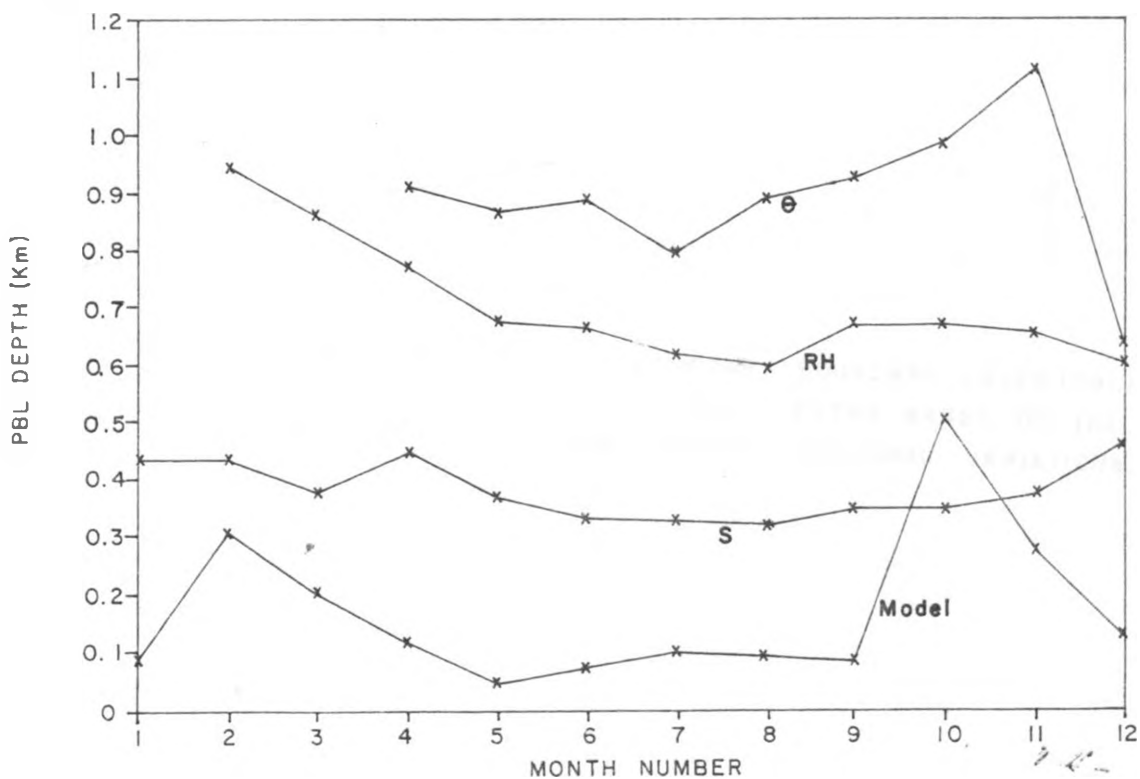
FIG. 5.5 b : MEAN MONTHLY NIGHT TIME HEIGHTS (Km) OF ELEVATED
POTENTIAL TEMPERATURE INVERSION (θ), RELATIVE
HUMIDITY MAXIMA (RH) AND WIND SPEED MAXIMA (S)
AT 0200LT (MODEL AT 0300LT) AT JOMO KENYATTA
FOR 1986
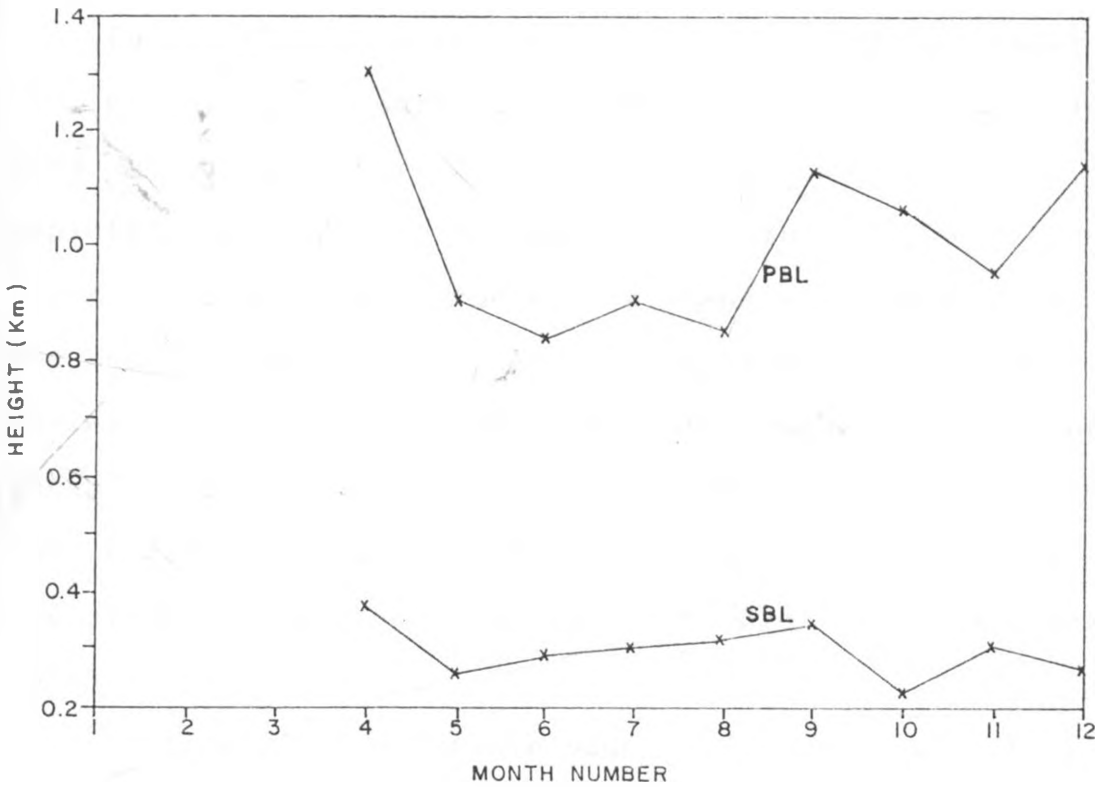
FIG. 5.6 : RELATIONSHIP BETWEEN THE PLANETARY BOUNDARY LAYER (PBL)
AND SURFACE BOUNDARY LAYER (SBL) DEPTHS BASED ON THE
OBSERVED PROFILES OF WIND SPEED : SEASONAL VARIATIONS.

also have been a consequence of changes in the heat structure resulting from latent heat release and absorption thereby modifying the daytime profile as noticed from the similarity with the heights of relative humidity maxima. The upper level inversions are likely to have been influenced by the upper level synoptic wind. The effect of the city centre's urban heat island seems insignificant as judged from the heights of the inversions which are very high.

The relationship between the surface boundary layer and the planetary boundary layer depth based on the profile of wind given in figure 3.3b was as shown in table 5.7, and depicted in figure 5.6. Accordingly, the surface boundary layer was about 30% of the entire planetary boundary layer at the hour considered, 1400EAST. It is expected that this ratio varies diurnally. The nighttime relationship could not be established due to the absence of detailed observations of the vertical profiles of wind speed at low levels. The postulated mean ratio in the sub-tropics is 10% (Harris, 1979).

Results for the stable boundary layer showed that the seasonal variability of the significant heights from the profile estimates was less explicit than for the daytime case (figure 5.5b), though their order of decreasing level of occurrence was similar to that of the unstable conditions. The potential temperature inversion base occurred at a much higher elevation in November than for the rest of the period; the lowest was in December. The height of the base of potential temperature inversion exceeded the level of maximum relative humidity by between 200m and 500m (table 5.6). The latter in turn occurred at a height that was about twice to one-and-a-quarter of the height of the low level wind maxima.

Except for February and November when the simulated values were less than the heights of the the low level wind maxima by 100m, and for October whose predicted value exceeded the wind maxima level by 160m, the model results turned out to be much less with differences in excess of 200m to 300m, implying that the model values were just one-seventh to one-third of the level of the wind maxima.

Choice of constants in the stable boundary layer model is of prime importance in improving the accuracy of the predicted values. Trivially, using a larger value of the proportionality constant of between 0.3 and 1.6 instead of 0.2 could make the projected mixing heights closer to the heights of low level wind maxima. This however should be done with extreme caution since other factors could be playing a more important role in determining the depth of the layer. In effect, the depth of the boundary layer at night has been estimated to be four-fifths (4/5) of the height of the low level wind maxima. For consistency with daytime estimates, using a proportionality constant of 0.25 seemed appropriate for the warmer months.

A constant value in time of the aerodynamic roughness parameter was reasonable for stations located in "open" areas. Stations close to vegetated zones, high rise buildings and mountainous areas need different values of the parameter so as to account for the changes in the direction of flow.

Table 5.5: Monthly Nighttime Sensitivity Testing Results   for

Jomo Kenyatta (1986)

| Month | Model 0300EAST | Profile Estimated Heights (m) at 0200EAST | | |
		Wind Maxima	R.H maxima	Inversion Base
January	87	-	-	979
February	309	433	946	-
March	197	375	860	-
April	119	448	771	914
May	45	368	673	869
June	72	331	665	891
July	102	323	619	798
August	94	319	595	896
September	86	350	668	926
October	506	347	672	988
November	275	378	658	1117
December	128	464	600	643

Table 5.6: Monthly Daytime Sensitivity Testing Results for

Jomo Kenyatta (1986)

| Month | Model at 1500EAST | Profile Estimate Heights (m) at 1400EAST | | |
		Wind Max.	R.H Max.	Inversion Base
January	955	-	-	-
February	1053	-	-	-
March	1032	-	-	-
April	1308	1305	1094	1584
May	914	903	1146	1462
June	786	839	997	1155
July	693	904	1092	1232
August	621	851	1321	1595
September	761	1130	966	1386
October	1125	1062	1558	1639
November	837	953	1089	1628
December	1045	1141	1067	1496

Table 5.7: Daytime Monthly Planetary Boundary Layer (PBL) and

the Surface Boundary Layer (SBL) Depth Based on

Profiles of Wind Speed for Jomo Kenyatta (1986)

Month	PBL	SBL	SBL/PBL Ratio
January	–	–	–
February	–	–	–
March	–	–	–
April	1308	373	0.29
May	903	255	0.28
June	839	289	0.34
July	904	301	0.33
August	851	320	0.38
September	1130	345	0.31
October	1062	224	0.21
November	953	306	0.32
December	1141	264	0.23

Table 5.8: Monthly Mean Maximum Mixing Heights (MMH) (Km)

after Patnaik et al (1980) for Africa (1957-1961)

Month	MMH(km)
January	1.4
February	1.7
March	1.7
April	1.0
May	0.9
June	0.8
July	0.9
August	1.1
September	1.3
October	1.2
November	1.0
December	0.9

5.7 Conclusions on Planetary Boundary Layer Modelling

The problem in establishing the appropriateness of the modelling procedure lies partly in the use of "non-event" data. Surface parameters being highly variable even within an hour's interval as contrasted to the more steady upper air systems may induce cumulative errors in the final results of the simulations. The difficulty is further complicated by the different levels at which the significant heights from the profiles of potential temperature, relative humidity and wind speed occur. In view of the horizontal distance from the radiosonde station to the rest of the observatories, errors due to differing altitudes may influence the ultimate result.

Although conclusive deductions cannot be made for hours other than those with upper air data, the mean mixing heights in a day's course fairly agree with those obtained from calculations by Abu Bakr (1988) in the Sudan, Patnaik et al (1980) for the whole of Africa, and nomogram results (see Harris, 1979; Pasquill and Smith, 1983) for Europe. Estimated mixing heights during the night are likely to have been influenced more by the synoptic flow as contrasted to the daytime values that are evidently more dependent on the surface parameters. Seemingly, the elevated inversions were not entirely the determining factor for the depth of the mixing layer as could be deduced from the high altitudes at which the inversions occurred. Clearly, the inversions did not act as buffer zones to the fluxes of momentum and moisture, whose significant levels from profile estimates were much lower. Differences between the observed and model estimates were primarily caused by the assumptions made in

the modelling procedure on which the results were critically dependent. Choice of model constants in addition had effects on the final results. The daytime methodology was appropriate in computing the depth of the planetary boundary layer for the warmer months; it could be modified for the colder period. Inclusion of moisture and convection explicitly would considerably improve model results. Cloudiness may distort the mixing heights so that vertical transport proceeds to higher levels than is expected (Pasquill and Smith, 1983).

Chapter Six

6.0 Discussion

To account for spatial changes in the wind speed and direction, data from the limited few observatories at seven stations was interpolated/extrapolated horizontally and vertically to provide a three dimensional outlook. The spatially sparse surface measurements were extrapolated within the surface layer using the logarithmic wind profile that incorporates the similarity theory arguments of Monin and Obukhov, thereby accounting for buoyancy and surface roughness effects. The surface layer depth was assumed to be one-twentieth of the planetary boundary layer depth (Okeyo, 1987). A logarithmic expression similar to the one used by Endlich et al (1982) was adopted in estimating the wind field in the mixed layer above the surface layer where the surface roughness effects are neglected. At every vertical level, the horizontal structure was obtained from a weighted interpolation scheme after Goodin (1979). The scheme estimates the flow direction and speed at grid points, thereby providing an instantaneous picture for the domain. The flow between the surface and the top of the boundary layer is then simulated, reflecting surface features.

6.1 Surface Boundary Layer Winds

Stable conditions assumed to be present during the nighttime periods have a vertical profile that is given by the expression

$$U(z) = \frac{U_*}{\varkappa} \left[\ln \frac{z}{z_0} + 4.7\frac{z}{L} \right] \qquad (6.1)$$

which is a transposed form of equation (5.1.5), with U_* and L computed at the anemometer level using the procedure described under section 5.1. Profiles for purely neutral conditions within the surface layer are given at any height z by the equation

$$U(z) = \frac{U_*}{\varkappa} \ln \frac{z}{z_0} \qquad (6.2)$$

where U_* is obtained using the measured wind U_a at the anemometer level z_a. Near-neutral conditions occur at sunrise and sunset. Unstable conditions are most frequent during the day. The wind profile is estimated from the relationship

$$U(z) = \frac{U_*}{\varkappa} \left\{ \ln \frac{z}{z_0} - \psi\left(\frac{z}{L}\right) + \psi\left(\frac{z_0}{L}\right) \right\} \qquad (6.3)$$

Friction wind velocity, U_*, and the Monin-Obukhov parameter, L, are obtained from equations (5.2.10) and (5.2.11) at the anemometer level.

Atmospheric stability or instability is expected to vary through the day and night cycle depending on the variations of the input parameters: wind speed and sensible heat. Only three observations within the unstable condition's period (0900, 1200 and 1500 local time) were considered. This was intended to include observations made at agro-meteorological stations which are not full time synoptic stations. Within the surface boundary layer,

fluxes are approximately constant so that the wind
direction does not change much vertically. The wind speed
is obtained by rotation of co-ordinates (with no loss of
generality) into one, for example the x-, direction. The
wind components were computed from the predicted profile
value of the wind speed using the surface wind direction
for values within the layer at any level.

6.2 Mixed Layer Profiles

In a thoroughly mixed layer, wind speed is
expected to be constant, although its direction may
spiral. The speed assumes a decreasing profile above
the inversion base, becoming near geostrophic. The coriolis
force has a smaller magnitude than the pressure
gradient force in the tropical region, and so the
Ekman-spiral layer equations are not applicable.
The wind field was estimated using the equations:

$$u(z) = u_s + (u_H - u_s) \frac{\log z - \log z_s}{\log H - \log z_s} \qquad (6.4a)$$

$$v(z) = v_s + (v_H - v_s) \frac{\log z - \log z_s}{\log H - \log z_s} \qquad (6.4b)$$

with the zonal (u) and meridional (v) components obtained
from the speed and direction using equations (4.4).
The letters H and s denote the tops of the mixing
layer and surface layer respectively, and z is the height
above the surface level. The equations give the components
at the computation height by interpolating between

the value at the top of the boundary layer and that at the top of the surface layer. Surface layer values are those obtained in the preceding section (6.1), and mixing height values are got from applying equations (4.5) to the mean synoptic values calculated from recorded radiosonde ascents. The system puts the greatest weight in the lower levels and accounts for changes in direction.

6.3 Horizontal Representation

An interpolation/extrapolation scheme used to investigate the field of flow laterally is the inverse square distance weighting approach in which values at grid points are given by the formula

$$X_{ij} = \frac{\sum_{k=1}^{N} X_k W_k(r)}{\sum_{k=1}^{N} W_k(r)} \qquad (6.5)$$

where N is the number of stations near the grid point ij, and X_k is the value obtained at station k using the methodology under sections 6.1 and 6.2. The weighting factor $W(r)$, dependent on the distance r between any given station and the grid point under consideration, is the reciprocal of the square of the distance between the station and the grid point.

$$W(r) = r^{-2}$$

Effectually, stations closest to the grid point are given the greatest weight and the contribution of stations far

away is only minimal. The obvious shortcoming of the scheme is that it does not give values outside the range between the smallest and biggest observed value. However, the procedure does not consume as much computer time as other conventional schemes and is assumed to be representative in view of the size of the region.

Direction of flow was computed by using resolved component values of wind speed and direction in equation (6.5) for stations surrounding, or nearest to, any given grid point. The corresponding equations for the direction and velocity at grid point ijk are

$$\theta_{ijk} = \tan^{-1}\left(\frac{u_{ijk}}{v_{ijk}}\right) \tag{6.6a}$$

$$V_{ijk} = \left[u_{ijk}^2 + v_{ijk}^2\right]^{1/2} \tag{6.6b}$$

The horizontal grid spacing was five kilometres. The vertical interval was taken to be the depth of the surface boundary layer.

A similar approach was adopted in determining the terrain elevations at grid points. Though the difference in terrain heights between the lowest and highest elevations was about half of a kilometre, the large horizontal distance between the two points eliminated any significant terrain effects on the horizontal flow. Terrain heights were however retained for use in spatial variations of the planetary boundary layer (section 5.3). It was apparent that the most influential surface features on the horizontal flow resulted from the effects of vegetation and urbanisation.

Since vertical velocity measurements are not available, vertical velocities were computed from the continuity equation assuming a non-divergent field with the surface value initially zero. In fact, surface vertical velocities are given for slopping terrain (Haltiner and Williams, 1980), by

$$w_s = V \, . \, \nabla h \tag{6.7}$$

where h is the terrain height and V the horizontal wind velocity vector. h is negligibly small for nearly constant terrain heights so that the surface vertical velocity is practically zero. Ideally for any height z above the surface, the vertical velocity should be,

$$w_z = w_s - \int_{z=0}^{z} \nabla \, . \, V \, dz \tag{6.8}$$

6.4 Results on the Flow-Field Model

Wind directions within the surface boundary layer were predominantly north-easterly becoming more easterly towards the north-western sector of the region for the period from November to March at 0900EAST. As the day progressed, the formerly slight veer in the morning hours became more pronounced, at the same time drifting eastward toward the middle of the region on the northern boundary. In the afternoon, the flow over the whole region assumed the easterly direction. No significant change in direction could be noticed in space in the predominantly easterly flow during April. The same was true for quasi-easterly flows of February, September and October in the afternoon. In contrast to that of May, the flow in June and July at 0900EAST maintained the southerly regime at 1200EAST but became more south-easterly as the day progressed. There was a distinct westward change in direction in the north-western sector which diminished as the flow became more south-easterly in the late afternoon (1500EAST). The veer during August was evidently farther eastward than for the other months. Graphical representations of the spatial regime are given in figures 6.1 to 6.4 for the three hours.

Surface boundary layer wind speed analyses depicted the highest values at Wilson airport during the three hours, followed by Jomo Kenyatta situated eastward. The decrease in speed west of Wilson was quite rapid at Dagoretti and decreased further north-westward at Kabete;the 0900EAST wind speeds were mainly the same for the period from June to September. At this time, the flow is from Dagoretti, north-westward to Kabete. The trend was seen to change as the day

progressed with increased surface heating and a change in
direction of the flow took place, when the winds in the
north-western sector at Kabete differed from those at
Dagoretti which had higher values. Though the winds at Wilson
and Jomo Kenyatta were nearly the same for all the months at
0900EAST, the speeds at Wilson were slightly higher for
January and August. In April, with mostly easterly flow, a
decrease in wind speed was only slight, westward of Wilson,
but decreased rapidly northward. This was true for easterly
flow in the afternoon in February and could be attributed to
the decrease in the frictional drag on the wind based on the
direction of flow in relation to the location of the
roughness elements. The lowest speeds could be noticed when
the flow direction before reaching a station was through the
forested areas. Interpolated wind speeds at the surface are
given in figures 6.5 to 6.8, while some aspects of wind speed
variation in space are given in figure 6.9 for cases of May,
July and December.

The projected change in direction at 1500EAST in the
vertical within the mixed layer was most significant in the
period from October to December when the surface easterlies
became westerlies in the layer. As contrasted to surface
southerlies in June and July assuming easterly flow in the
mixed layer, the August upper air winds tended to assume
southerly flow from surface easterlies. There was no
significant change for April, May and September, vertically.

Vertical velocities were too low, of the order of
$10^{-3} ms^{-1}$, due to the even terrain structure. Computed values
west of the domain exceeded those east of the region.
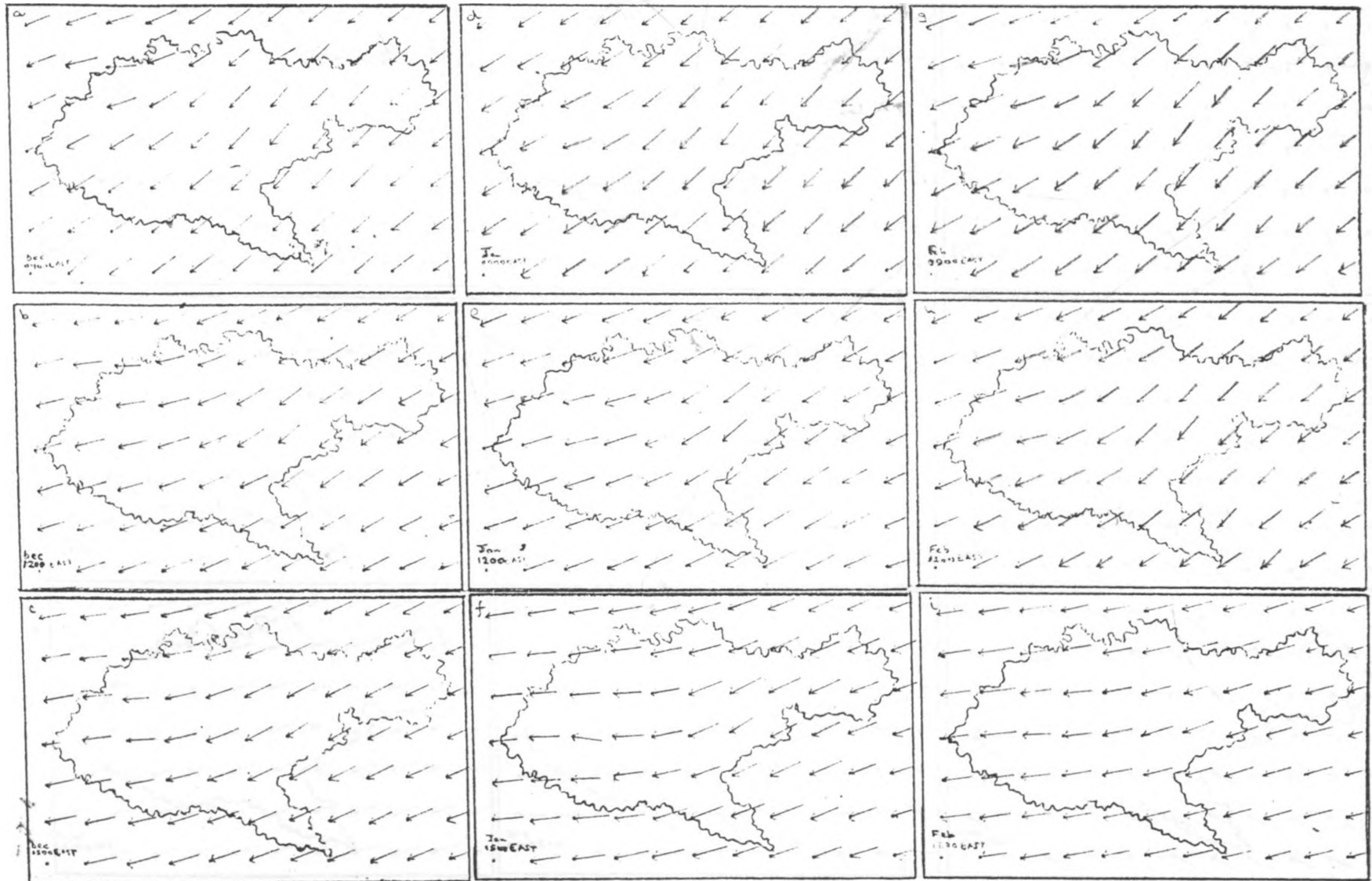
6.1: Surface Wind Directions for December, January, and February
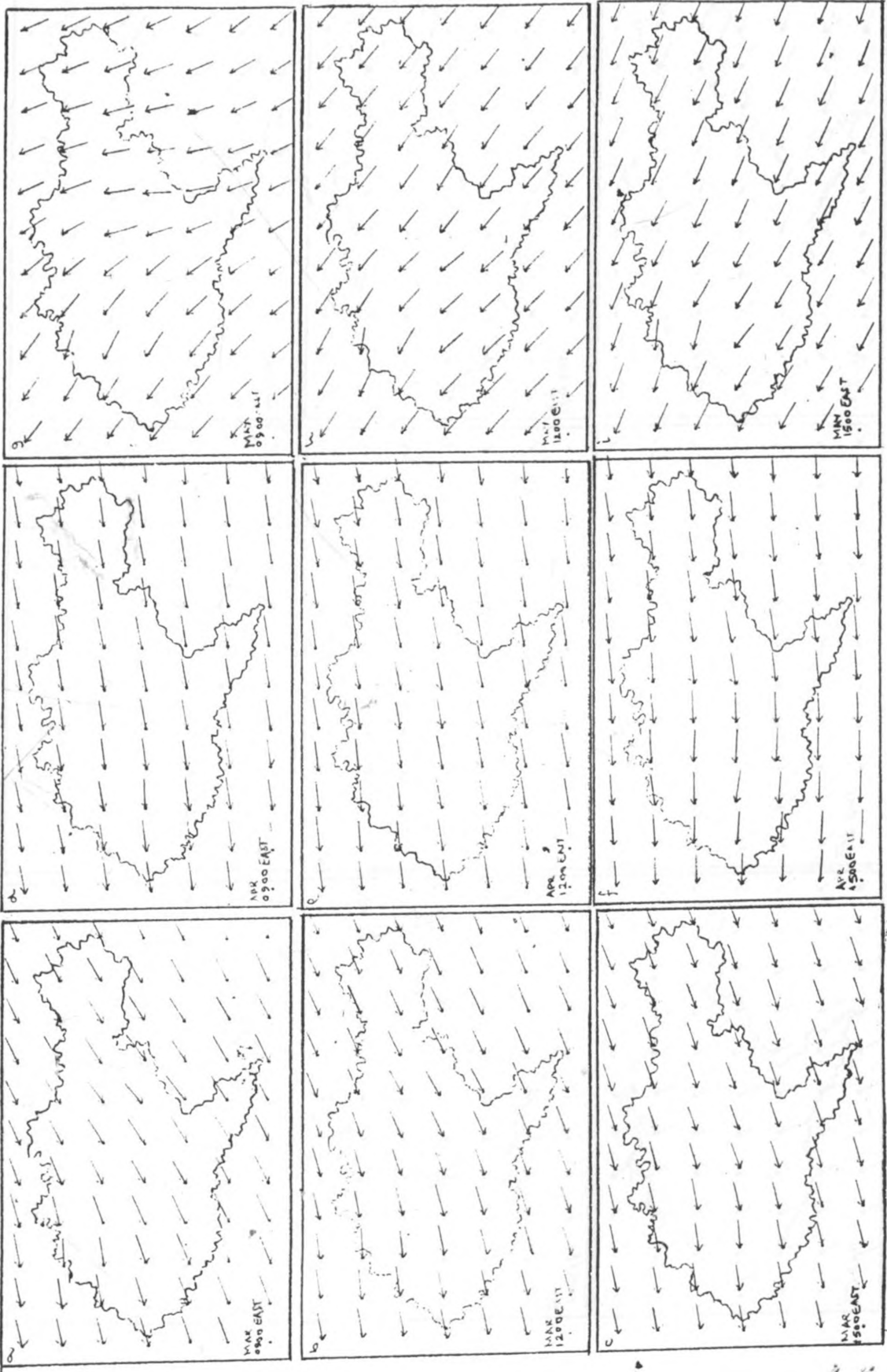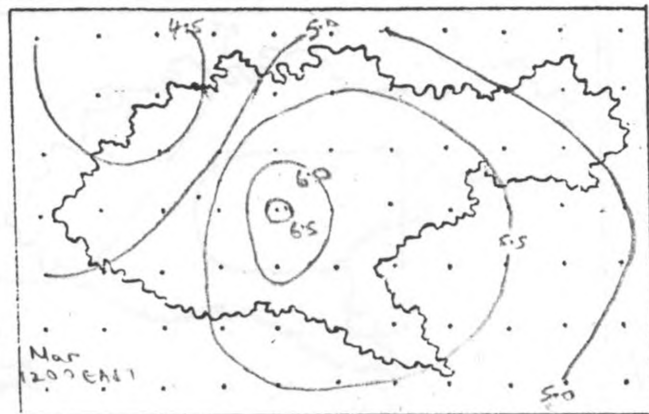
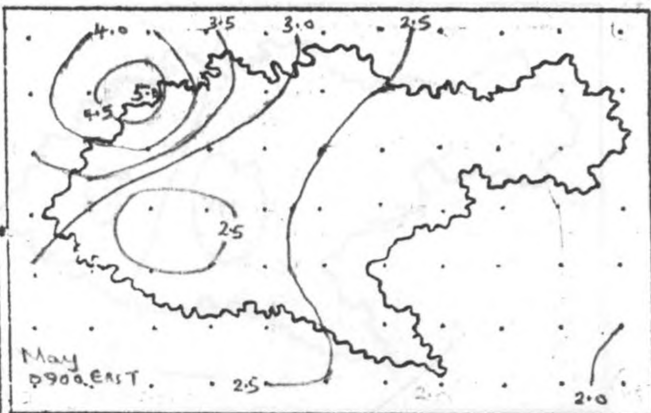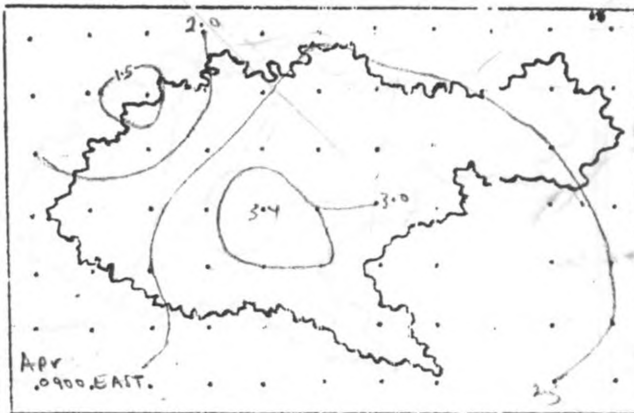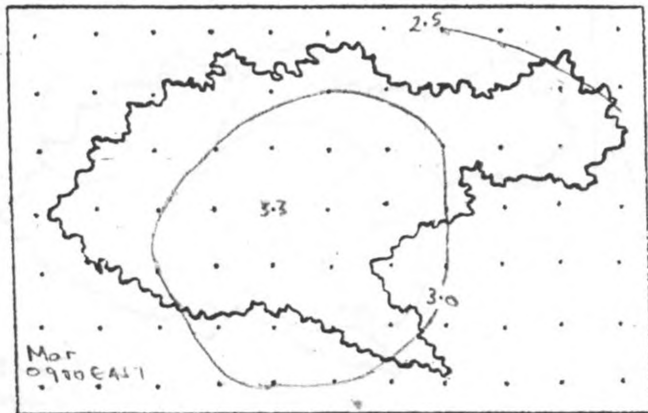6.2: Surface Wind Directions For March, April and May
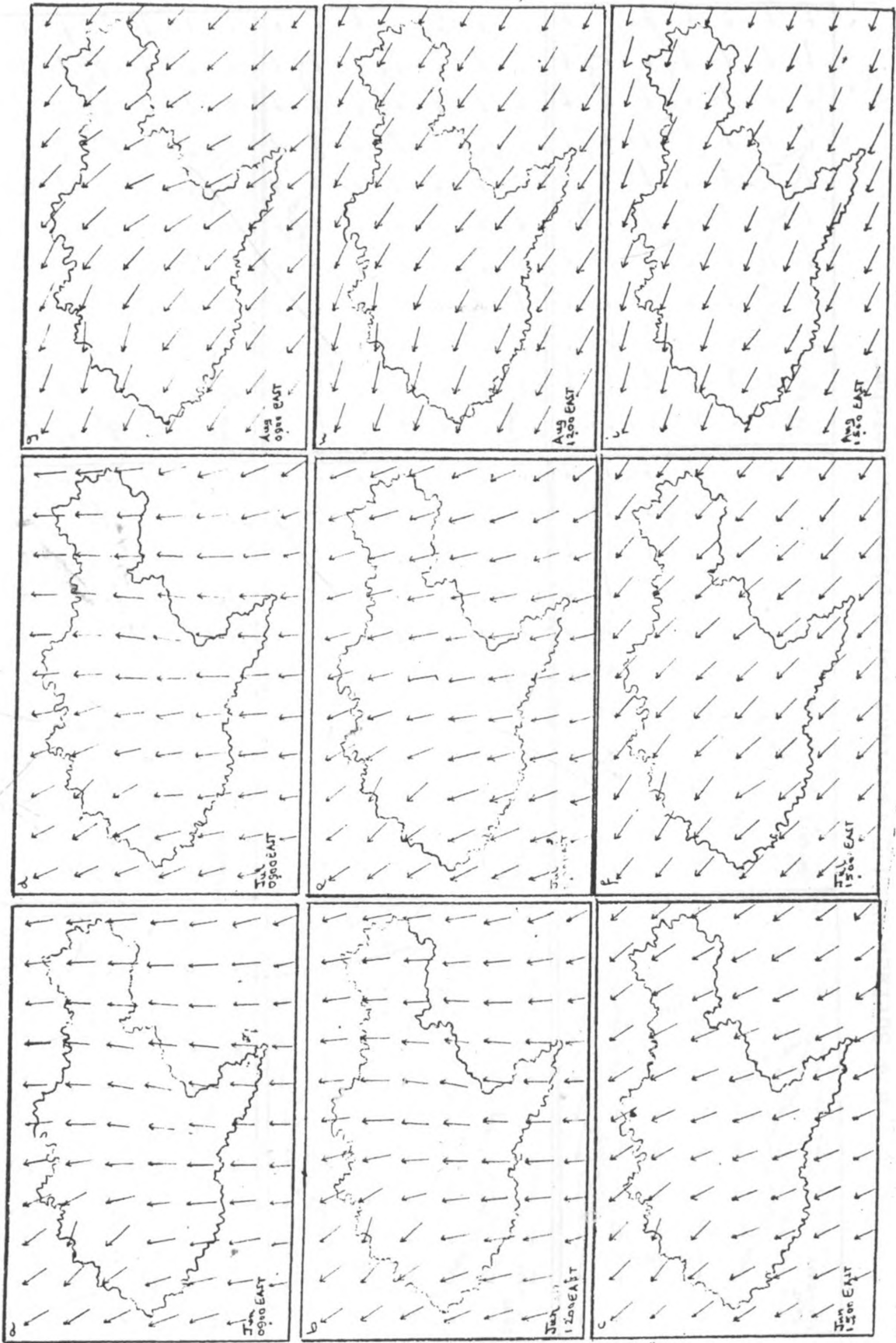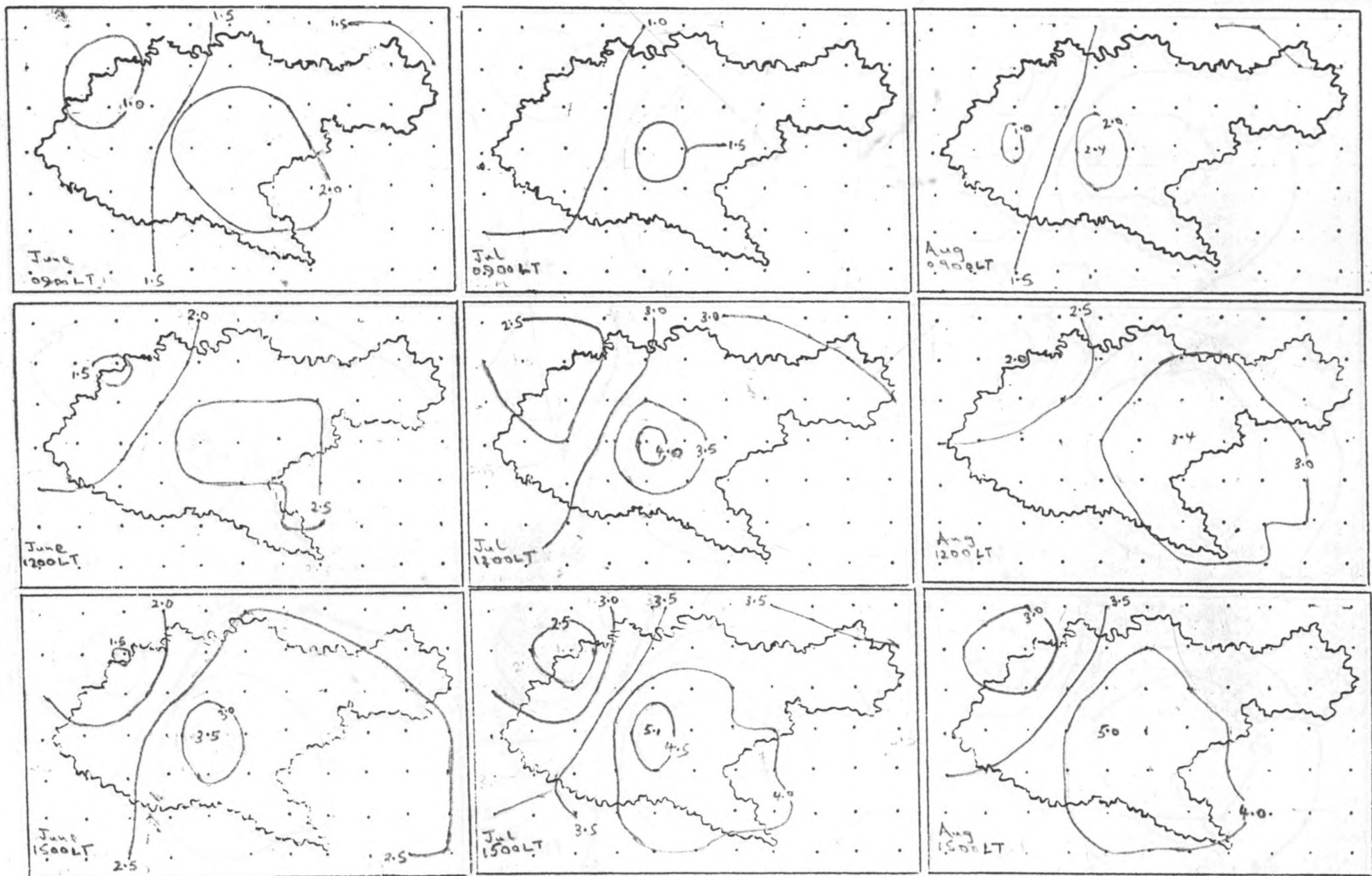
6.3: Surface wind Directions for June, July and August
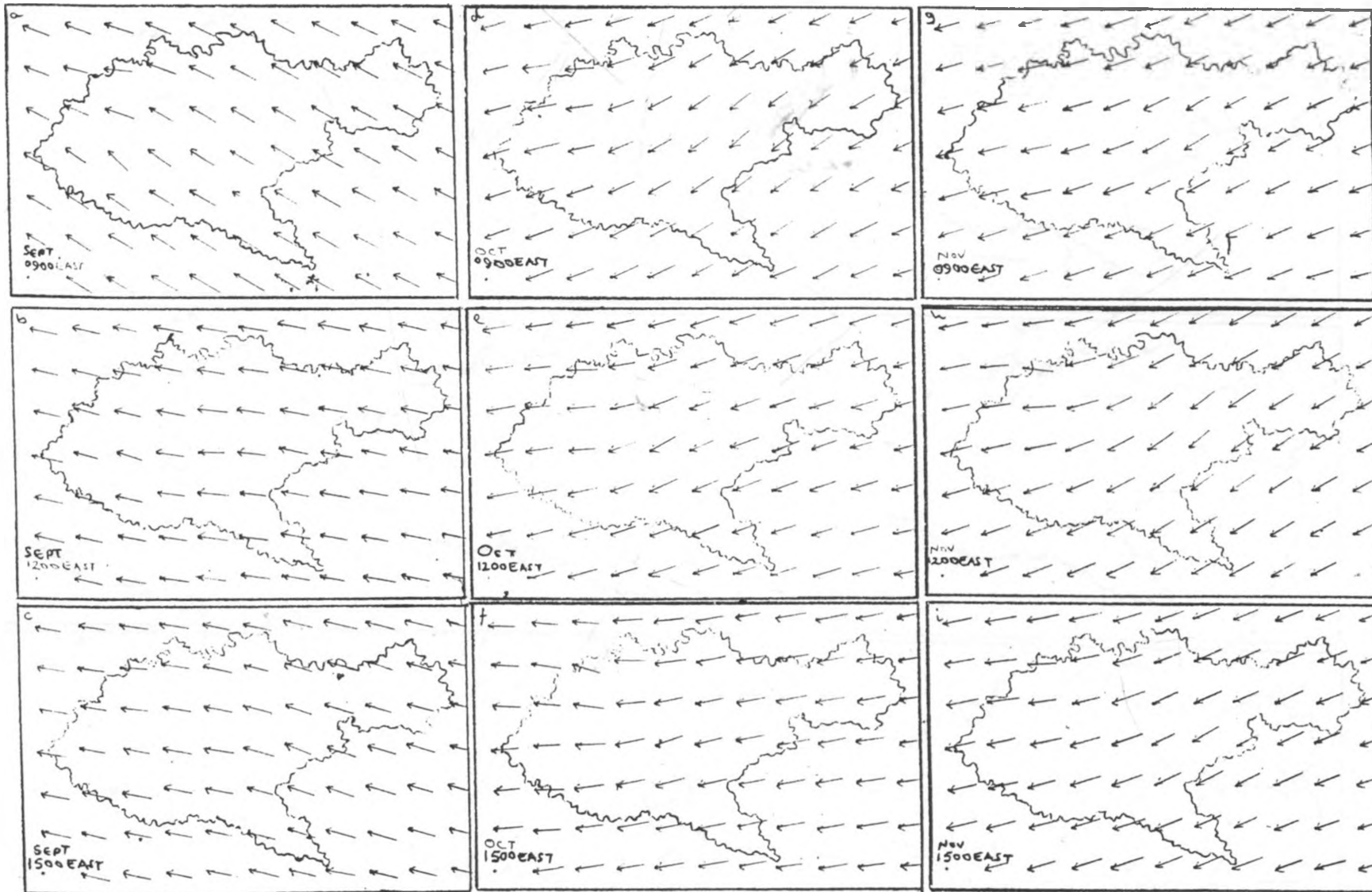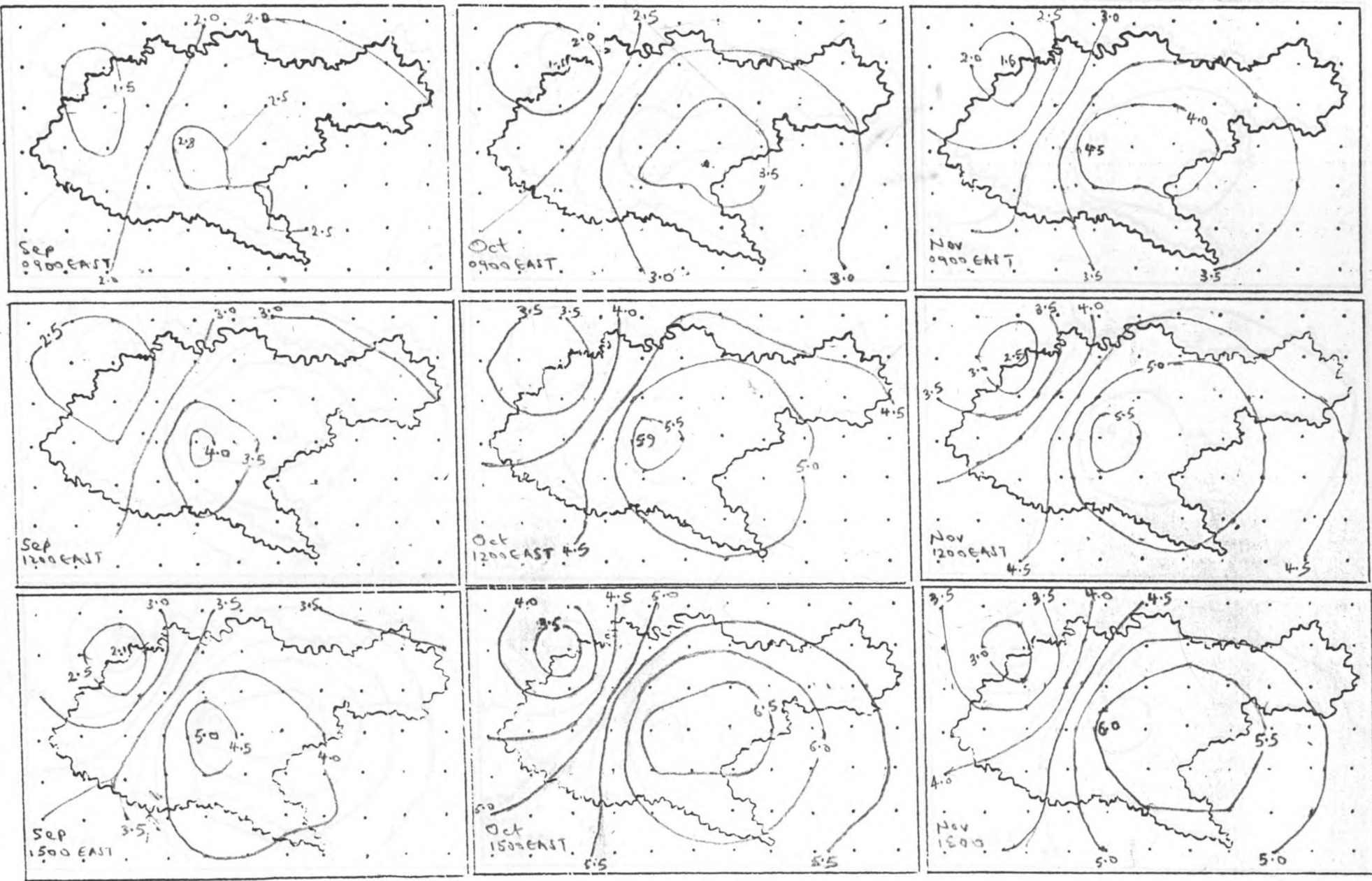
6.4 Surface Wind Directions for September, October

and November
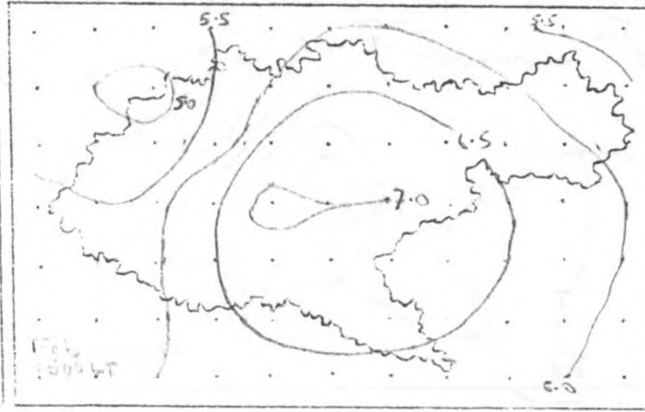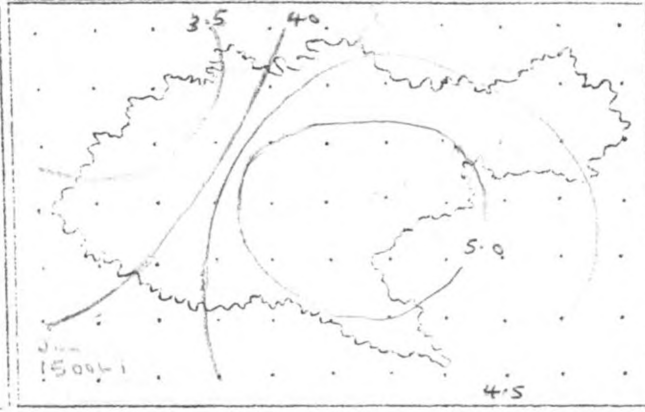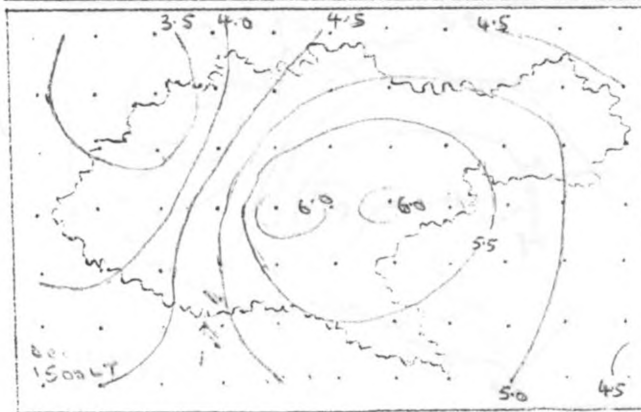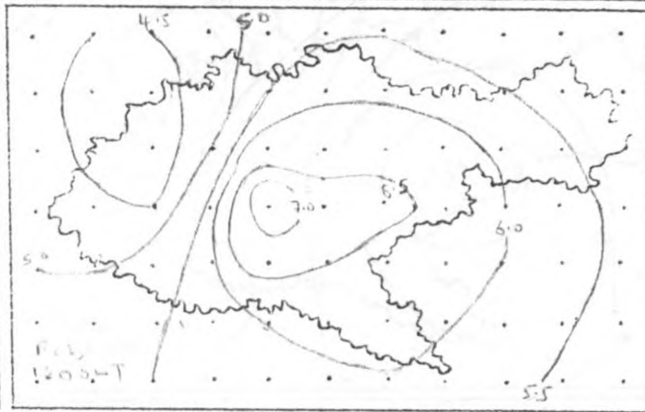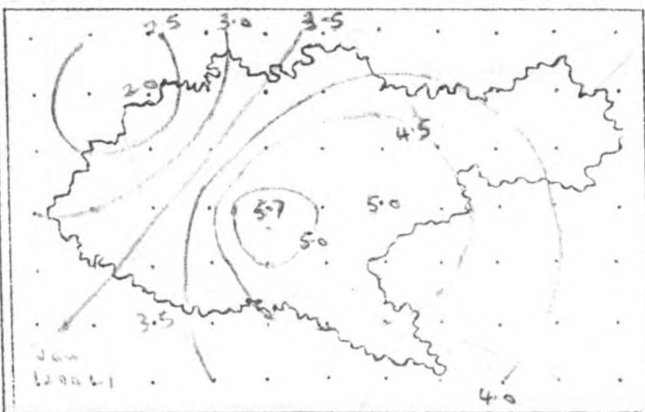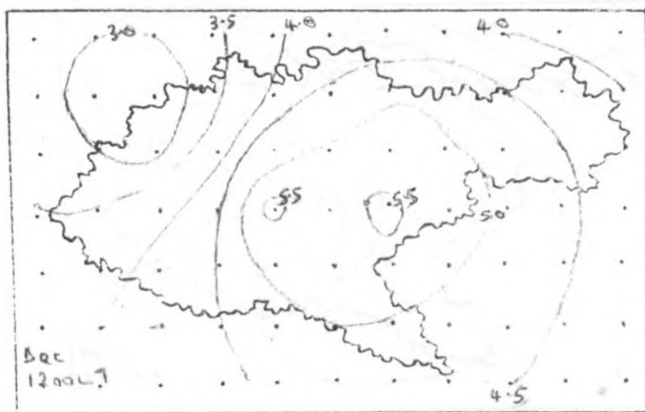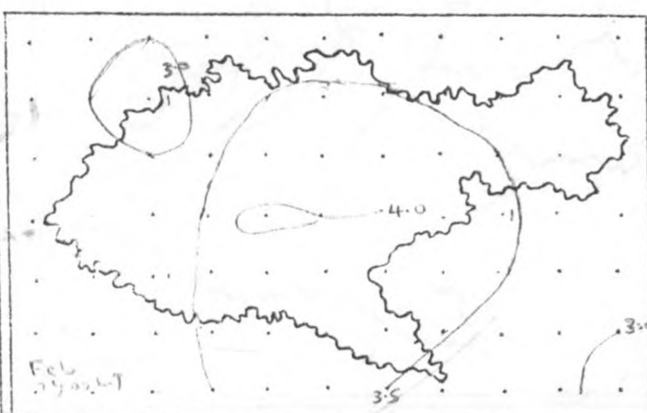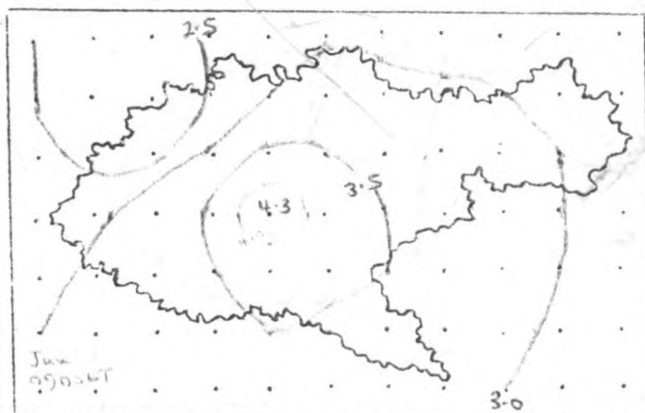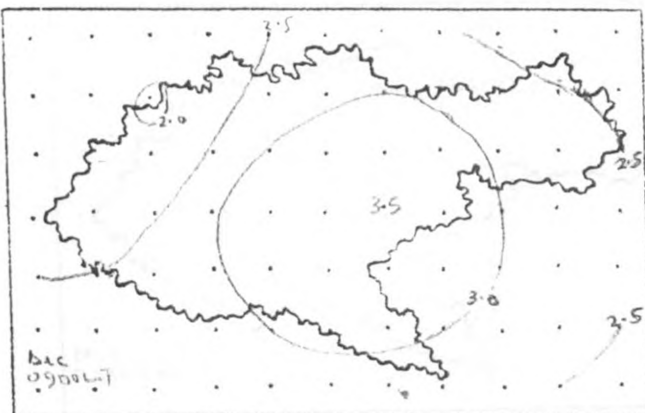
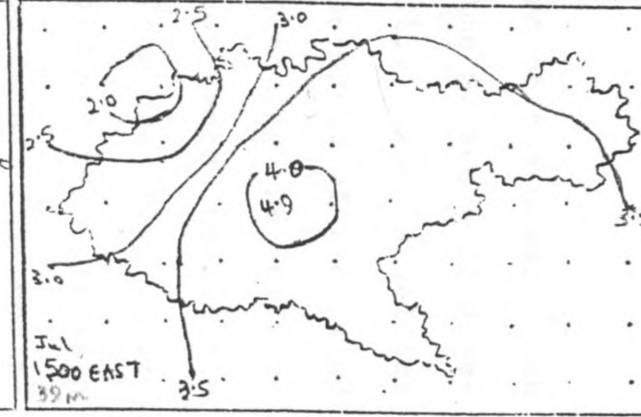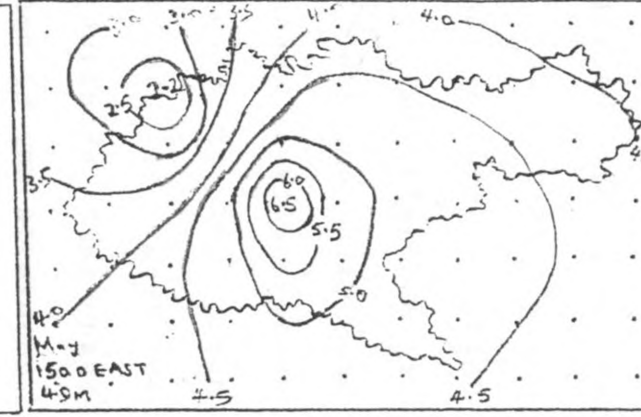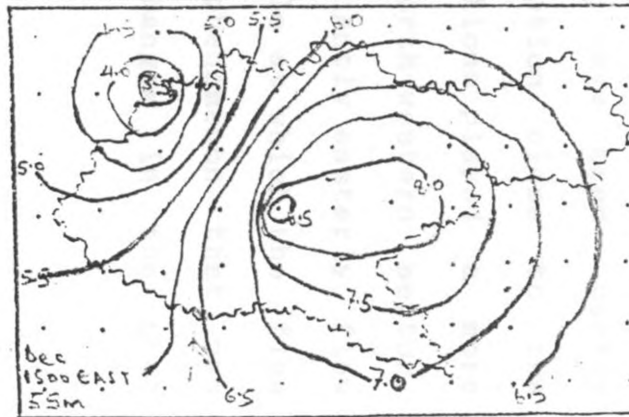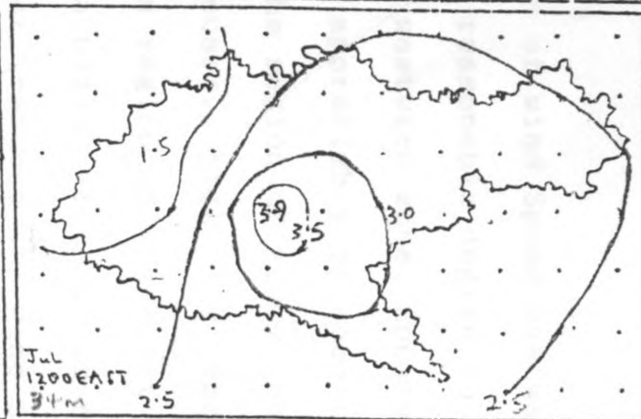6.5: Surface Wind Speeds (December, January, February) (m/s)
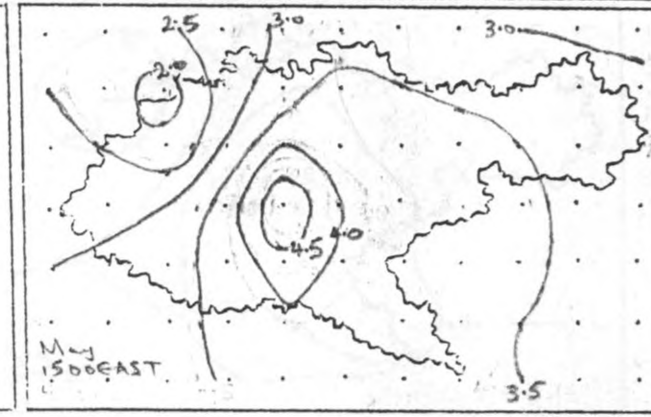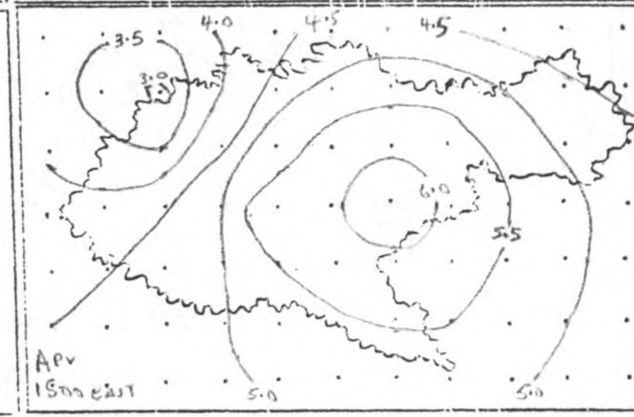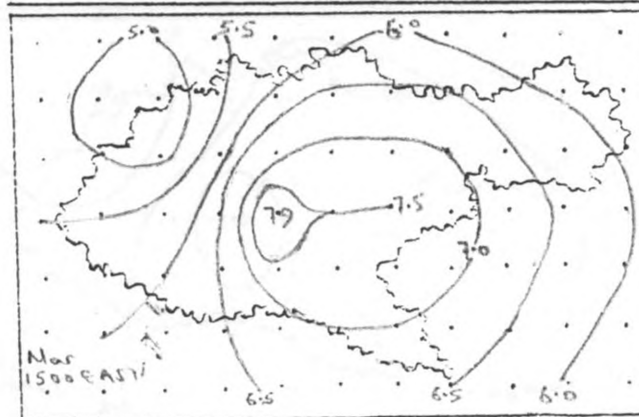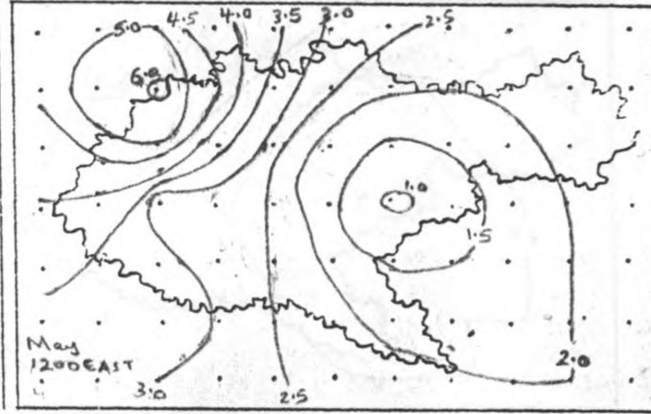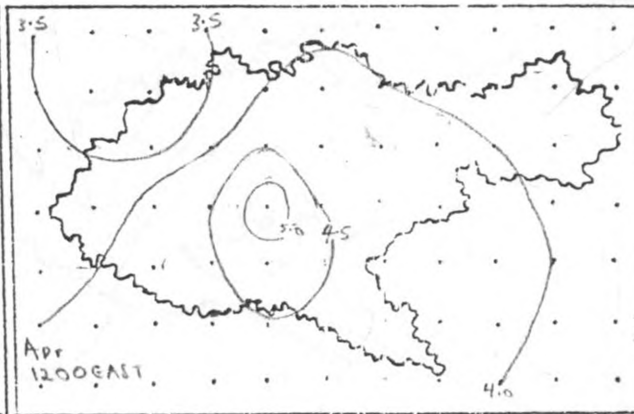
6.6: Surface Wind Speeds (March, April, May) (m/s)

6.7: Surface Wind Speeds (June, July, August) (m/s)

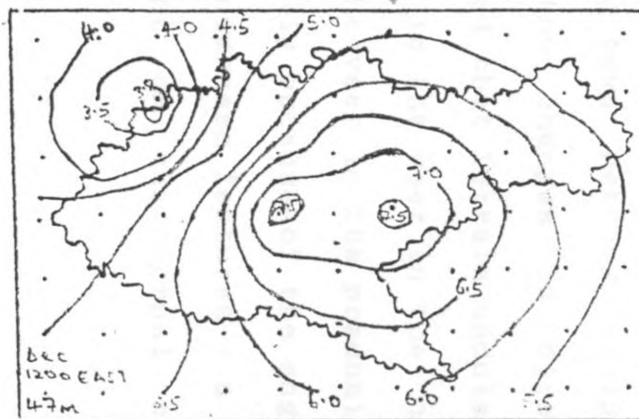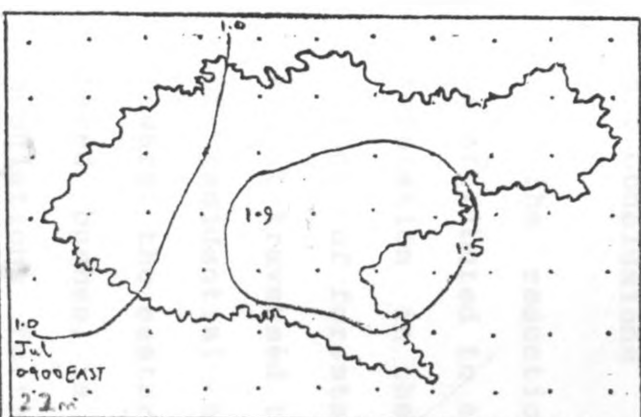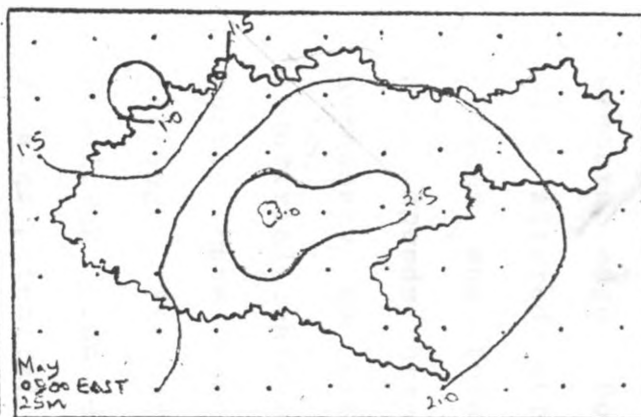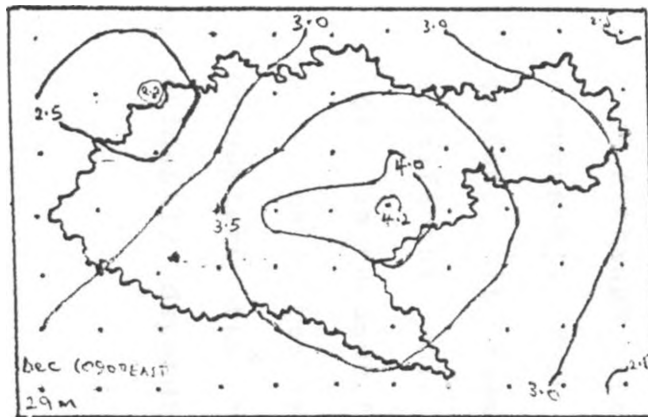6.8: Surface Wind Speeds (September, October, November) (m/s)
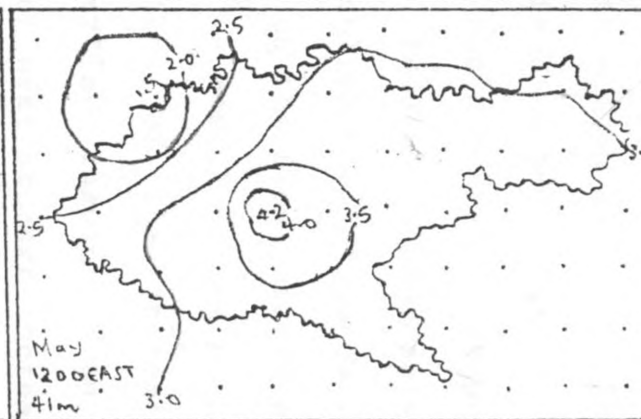
6.9 SBL Wind Speed Regime for December, May and July (m/s)

6.5 Conclusions

The reduction of wind Speed westward of the domain can be attributed to a reasonable degree to the presence of dense vegetation in the westward zone. Apparently, the shielding effect of forests appreciably reduced the speed of the wind as it traversed the region of study; neglecting the effects of residential houses, high wind speeds were noticeable toward the eastern region which, apart from the few, scattered bushes, is a plain land. It is evident that terrain undulations further reduced the wind speeds on the north-western edge. Both Wilson and Jomo Kenyatta are airports with altered surface fabric that can induce heat island effects and this could be partly responsible for the high wind speeds here. Though a denser network of stations is necessary to establish the influence of both the city and industrial centres on the flow, higher speeds at Wilson could partly have been a result of its proximity to the urban setting. The effect of the increase of low pressure resulting from daytime insolation on surfaces that have greater potential of heat storage increased in the afternoon.

Although the town setting could have been partly responsible for the changes in direction close to the surface, it seemed that terrain undulations played a more significant role in the veer in the north-western sector. This is because the veer in the predominantly easterly flow was small, basically because of the angle at which the flow encounters the roughness features - a phenomenon that was evidently dependent on the diurnal changes in the heat

structure. The effects of vegetation and residential zones on the direction veer cannot be utterly ignored owing to the scarcity of observatory stations.

Whereas the magnitude of the influence of the surface roughness features could not be adequately determined, it was clear that the surface features had a significant impact on the direction and speed of flow. Measurements made at the surface at any one of the stations are more likely to indicate local conditions and may not necessarily be representative over the whole domain. Wind field measurements outside the surface boundary layer could probably be more useful in climatological studies. Surface effects were responsible for the difference in the direction of flow between the upper afternoon air and the surface winds at the same time where synoptic disturbances infiltrated the region of study.

Appendix

Suggestions for Further Work

This work was a case study intended to hint on internal changes in the general climatological variations. A truly climatological picture would be obtained if a longer period was considered, say five to ten years, based on the present methodology. A further development could be to use a finer time spacing than that used here. One-hour to 30-minute intervals could considerably improve the planetary boundary layer results, as was done for the morning transition period. This can be achieved by using the available 30-minute data at the airport stations, and interpolating for the other stations based on the observed pattern. The most reliable results could be obtained by using daily (event) data in place of monthly averages in the modelling analyses, a procedure that can aid in establishing model constants. Averaging event results would then be used in establishing a climatological representation. Event analyses would be expected to adequately account for extreme observations thereby eliminating input values such as zero wind speed.

The models used here do not explicitly incorporate the impact of moisture in the atmosphere. Future studies should endeavour to include the effects of condensation and evaporation in changing the heat structure and vertical transport. The influence of precipitation, cumulus convection and cloud cover should be studied in greater detail. The assumption of constant times of sunrise and sunset could be

responsible for a number of errors, a factor that could be corrected by the use of actual observations in future.

Because of limitations in time, data from Eastleigh air port could not be obtained. Being close to the city centre, the station's data can improve the accuracy in studying spatial variations and account for the impact of the city. Though of smaller magnitude than the heat island, terrain effects could be more explicitly accounted for if a finer, more detailed topographic map were obtained.

Acknowledgements

I am most indebted to my supervisors, prof. John K. Ng`ng`a and the late Dr. Andrew E. Okeyo without whose counsel, guidance, interest and continual spurring, this work would not be what it is.

I extend my heartfelt gratitude to the staff of Kenya Meteorological Department (KMD), too many to name, for their assistance in data acquisition and processing. I am particularly grateful to the staff of the Climatological, Radiosonde, Microfilm, DPS, DMC, and the NMC divisions for their generous assistance and for availing computer facilities.

I am thankful to the Survey of Kenya for providing topographical maps of Nairobi.

Of prime importance, I appreciated the funding of the German Academic Exchange Programme (DAAD) who sponsored most of my work, and the University of Nairobi Board of Postgraduate Studies in collaboration with the department of Meteorology for offering the scholarship to me.

My gratitude extends to the entire staff at the department for their concern and contribution in every way. In particular, I am very grateful to Mr. J.R. Mukabana for offering to read through and amend the manuscript while giving invaluable advice before the document was printed.

References

Abu Bakr, E. H.,1988: The boundary layer wind regime in a representative tropical African region - Central Sudan. Research Thesis, Royal Netherlands Meteor. Inst. 154pp

Barr, S and C. W. Kreitzberg, 1975: Horizontal variability and boundary layer modelling. Bound. Layer Meteor., 8, 163-172

Beyrich, F. and B. Klose, 1988: Some aspects of modelling low level jets. Boundary Layer Meteor., 43, 1-14

Bhumralker, C. M., R. L. Mancuso, F. L. Ludwig and D. S. Renne., 1980: A practical and economic method for estimating wind characteristics at potential wind energy conversion sites. Solar Energy, 25, 55-65

Brown R. A., 1974: Analytical Methods in Planetary Boundary Layer Modelling. Adam Hilger. London

Businger J., J. C. Wyngaard, Y. Izumi and E. Bradley, 1971: Flux Profile Relationships in the atmospheric surface layer. J. Atmos. Scie., 28 , 1021-1025

Carson D. J., 1973: The development of a dry inversion layer-capped convectively unstable boundary layer. Quart. J. R. Meteor Soc., 99, 450 - 467

Caughey S. J., J. C. Wyngaard and J. C. Kaimal, 1979: Turbulence in the evolving stable boundary layer. J. Atmos. Scie., 36, 1041-1052

Clarke, R. H., 1970: Observation studies in the atmospheric boundary layer. Quart. J. Roy. Meteor. Soc.,96, 91-94

Cressman, G. P., 1959: An operational objective analysis system. Mon. Wea. Rev., 87, 367-374

Dartt, D. G., 1974: Automated streamline analysis utilising optimum interpolation. J. Appl. Meteor., 11, 901-908

Deardoff, J.W., 1972: parameterisation of the planetary

boundary layer for use in general circulation models. Mon. Wea. Rev.. 100. 93-106

————., 1974: Three-dimensional numerical study of the heated planetary boundary layer. Bound. Layer Meteor.. 7. 81-106

————., 1976: Clear and cloud-capped mixed layer: their numerical simulation, structure and growth and parameterization. Seminar on the treatment of the boundary layer in numerical weather prediction. European Centre for Medium Range Weather Forecasting, Reading, U. K.

EAMD., 1962: Climatic Seasons of East Africa. E. A. Met. Dept.. 8. 4pp

Endlich R. M. and R. L. Mancuso, 1968: Objective analysis of environmental conditions associated with severe thunderstorms and tornadoes. Mon. Wea. Rev.. 96. 342-350

————., F.L. Ludwig and C. M. Bhumralker and M.A. Estoque, 1982: A diagnostic model for estimating winds at potential sites for wind turbines. J. Appl. Meteor.. 21. 1441-1454

Fujita, T.T. and R.M. Wakimoto, 1982: The effect of miso and mesoscale observations on PAM winds obtained during project NIMROD. J. Appl. Meteor.. 21. 840-858

Gandin, L. S.., 1965: Objective Analysis of Meteorological Fields. Israel Program for Scientific Translations, Jerusalem, 242pp

Garrat, J.R., 1982: Surface fluxes and the nocturnal boundary layer height. J. Appl. Meteor.. 21. 725-729

Goodin, W.R., G.J. McRae and G. H. Seinfeld, 1979: A comparison of interpolation methods for sparse data: application to wind and concentration fields. J. Appl. Meteor. 18. 761-771

————., G.J. McRae and G.H. Seinfeld, 1980: An objective analysis technique for constructing three dimensional urban scale wind fields. J. Appl. Meteor.. 19, 98-108

Gord, 1956: Smog, the rate of influx of surrounding cleaner air. Weather. Vol. 11. 230-232

Green P. J. and R. S. Sibson, 1978: Computing Dirichlet tessellations in the plane. Comput. J.. 21. 168-173

Gupta, C. B., 1985: Statistical Methods. Vikas publ. hse. 900pp

Haltiner G. J. and F. L. Martin, 1957: Dynamic and Physical Meteorology. McGraw Hill, 178-243

————., and R. Williams, 1980: Numerical Weather Prediction and Dynamic Meteorology. New York. John Wiley

Harris C. J. , 1979: Mathematical modelling of turbulent diffusion in the environment. Proc. Conference on Mathematical Modelling of Diffusion. Liverpool Univ. Academic Press. 500pp

Heald, R. C. and L. Mahrt, 1981: The dependence of boundary-layer shear on diurnal variation of stability. J. Appl. Meteor.. 19. 859-867

Hjemfelt, M. 1982: Numerical simulation of the effects of St. Louis on Mesoscale boundary airflow and vertical motion: Simulation of urban vs. non-urban effects. J. Appl. Meteor.. 17. 565-577

Holton, J. R.; 1979: An introduction to Dynamic Meteorology. Academic Press. pp102-118

Idso, S. B. and R. D. Jackson, 1969: Thermal radiation from the atmosphere. J. Geophysical Res.. 74. 5397-5403

Junge, C.E., 1973: Air Chemistry and Radioactivity. Academic Press. New York and London, 382pp

Kasahara, A., 1966: The dynamic influence of orography on the

large scale motion of the atmosphere. <u>Mountain Meteor.. 0967. Atm. Sc..</u> Colorado State Univ. Fort Collins.<u>193-220</u>

Kavishe, M. M., 1983: Three-dimensional mean wind flow and thickness patterns over Africa. <u>M.Sc. Thesis.</u> Univ. of Nairobi

Lettau, H., 1969: Note on aerodynamic roughness parameter estimation on the basis of roughness element.

Long, R.R., 1952: The flow of liquid past a rigid barrier in a rotating spherical shell. <u>J. Meteor.. 9.</u> 187-199

Ludwig, F. L. and G. Byrd, 1980: An efficient method for deriving mass-consistent flow fields from observations in rough terrain. <u>Atmos. Environ.. 14.</u> 585-587

Lumley, J.L. and H.A. Panofsky, 1930: <u>The Structure of Atmospheric Turbulence</u>. N. Y. Interscience Publ. 239pp

Lumley, R.G. and J.A. Businger, 1918: <u>An Introduction to Atmospheric Physics</u>. N. Y. Academic Pr.

Munn, R. E., 1966: <u>Descriptive Micrometeorology</u>. Academic Press. N.Y.

Mwingira P. A., 1980: Net radiation over a banana field at Mombasa and its relation to global radiation. <u>Research Report. No.2.</u> EAIMTR (1980)

Nappo, C. J., Jr., 1977: Mesoscale flow over complex terrain during the Eastern Tennessee trajectory experiment (ETTEX) <u>J. Appl. Meteor.. 16.</u> 1186-1196

Ng´ng´a, J.K., 1976: Climatological aspects of air pollution study in Nairobi. <u>Ph.D Thesis</u> Univ. of Nairobi

Ogallo, L.J.A.J., 1980: Time series analysis of rainfall in East Africa. <u>Ph.D Thesis Univ. of Nairobi</u>

Oke, T.R., 1973: City size and urban heat islands. <u>Atmos. Environ.. 7.</u> 769-779

Oke, T. R., 1978: <u>Boundary Layer Climates.</u> Methuen, London.

——., 1987: <u>Boundary Layer Climates</u>. 2nd ed. Methuen London

Okeyo, A. E., 1987: Towards the development of a numerical weather prediction model for Kenya. <u>Ph.D Thesis</u>. Univ. of Nairobi

Okoola, R.E., 1980: The Nairobi heat Island. <u>Kenya J. Sc. and Tech., 1,</u> 53-65

Oludhe, C., 1987: Statistical characteristics of wind power in Kenya. <u>M.Sc. Thesis</u>. Univ. of Nairobi.

Panofsky, H.A., 1949: Objective weather map analysis <u>J. Meteor., 6,</u> 386-392.

——., 1963: Determination of stress from wind and temperature measurements. <u>Quart. J. Roy. Meteor. Soc., 89,</u> 85-94

Pasquill, F., 1974: <u>Atmospheric Diffusion.</u> Wiley, 429pp

——., and F. B. Smith, 1983: <u>Atmospheric Diffusion,</u> 3rd ed. John Wiley

Patnaik, J.K., J.K. Ng'ang'a and P.M.R. Kiangi, 1980: Atmospheric pollution potentials over Africa. <u>Research Report. No.1/80.</u> EAIMTR.

Paulson, C.A., 1970: The mathematical representation of wind speed and temperature profiles in the unstable atmospheric boundary layer. <u>J. Appl. Meteor., 9,</u> 857-861

Pendergast, M.M., 1976: Estimating diffusion coefficients from meteorological data. DP-MS-76-64. Savannah River Laboratory, E. I. du pont de Nemours & Co.

Pielke, R.A., 1984: <u>Meso Meteorology Modelling</u>. Academic Press

Priestley, C.H.B., 1959: <u>Turbulent Transfer in the Lower Atmosphere</u>, Univ. of Chicago Press.

Ramsey, B., 1966: Low level wind flow at Nairobi. *Meteor. Mag. Vol 95.* 47-57

Shepard, D., 1978: A two-dimensional interpolation function for irregularly spaced data. *Proc. 23rd ACM Nat. Conf.,* Las Vegas, 517-524

Sherman, C.A., 1978: A mass consistent model for wind fields over complex terrain. *J. Appl. Meteor., 17, 312-319*

Sutton, O.G., 1953: *Micrometeorolgy.,* Mcgraw Hill

Tennekes, H., 1973: A model for the dynamics of the inversion layer above a convective boundary layer. *J. Atmos. Sc., 30* 558-567.

Thiessen, A.H., 1911: Precipitation averages for large areas. *Mon. Wea. Rev., 39,* 1082-1084

Van Dop, H., B.J. De Haan and C.A. Engeldal, 1982: The KNMI mesoscale air pollution model. *KNMI Sc. Rep.* 82-86.

Venkatram, A., 1980: Estimating the Monin-Obukhov length in a stable boundary layer for dispersion calculations. *Bound. Layer Meteor., 19,* 481-485

Vukovich, F.M., J.W. Dunn III, and B.W. Crissman, 1976: A theoretical study of the St. Louis heat island: The wind and temperature distribution. *J. Appl. Meteor., 15* 417-440

Zilitinkevich, S.S., 1972: On the determination of the height of the Ekman boundary layer. *Bound. Layer. Meteor., 3,* 141-145